

AMERICAN UNIVERSITY OF BEIRUT

INVESTIGATING THE DEREGULATION AND
BIO-FUNCTIONAL RELEVANCE OF CAVEOLIN-1 IN
MUSCULAR LAMINOPATHIES

by
DIMA ABED DIAB EL HARAKEH

A thesis
submitted in partial fulfillment of the requirements
for the degree of Master of Science
to the Department of Biology
of the Faculty of Arts and Sciences
at the American University of Beirut

Beirut, Lebanon
April 2015

AMERICAN UNIVERSITY OF BEIRUT

INVESTIGATING THE Deregulation and
Bio-functional Relevance of Caveolin-1 in
Muscular Laminopathies

by
DIMA ABED DIAB EL HARAKEH

Approved by:

Dr. Diana E. Jaalouk, Assistant Professor
Biology



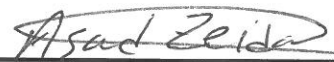
Advisor

Dr. Sawsan Kuraydiyyah, Professor
Biology



Member of Committee

Dr. Asad Zeidan, Assistant Professor
Anatomy, Cell Biology & Physiology



Member of Committee

Date of thesis/dissertation defense: April 20, 2015

AMERICAN UNIVERSITY OF BEIRUT

THESIS, DISSERTATION, PROJECT RELEASE FORM

Student Name: Diab El Harakeh Dima Abed

Last

First

Middle

Master's Thesis Master's Project Doctoral Dissertation

I authorize the American University of Beirut to: (a) reproduce hard or electronic copies of my thesis, dissertation, or project; (b) include such copies in the archives and digital repositories of the University; and (c) make freely available such copies to third parties for research or educational purposes.

I authorize the American University of Beirut, **three years after the date of submitting my thesis, dissertation, or project**, to: (a) reproduce hard or electronic copies of it; (b) include such copies in the archives and digital repositories of the University; and (c) make freely available such copies to third parties for research or educational purposes.

Signature

Date

ACKNOWLEDGEMENT

First and foremost, I would like to express my deep gratitude to my advisor, Dr. Diana Jaalouk, whose expertise, understanding and patience added considerably to my graduate experience. I would like to thank you first for giving me the opportunity to pursue my MSc Thesis in your lab. Thank you for everything we had since day one. Thank you for the trainings, advices and tips that I will carry with me in my coming endeavors. Without exaggeration, you are one of a kind. You taught me how to grow through life instead of going through it. You enlightened my mind and inspired me since day one. Now, I'm confident enough to face my new endeavors strengthened with your professional advices and concepts of life. You taught me the real essence of working and hardships. Words will never express the feeling I have towards you. I am fortunate to have you as my mentor, advisor and teacher. Most importantly, I am lucky to have you as a lifelong friend.

I am sincerely grateful to my thesis committee members, Dr. Sawsan Kuraydiyyah and Dr. Asad Zeidan for their consistent support, encouragement, insightful comments, suggestions and constructive criticism during the course of this thesis.

I am fully indebted to Dr. Noel Ghanem for accepting to serve on my thesis committee as a substitute despite the short notice and last minute request. Your thoughtful comments and questions were valued greatly.

Special thanks go out to Dr. Nisreen Alwan who in addition to providing me with statistical advice was a true friend ever since I joined the MSc Program in the Biology department. Nisreen is a wonderful person in so many ways.

I am very much grateful to my friend Jalal Kazan who provided research support to this study and supported me in so many ways.

I owe my deepest gratitude to the DJ lab members Hind Zahr, Lara Kamand, Ingrid Younes, Sara Assi and Dana Sedki for being a constant source of love and energy ever since. Hind, Ingrid and Sara, I can't thank you enough for sharing with me two years of great friendship and companionship. All the memories and funny moments we had will always stay fresh in my mind. At times of hardship, you were there for me, and you stood right by me, right to the end!

Finally, I would like to express my deepest appreciation to the basic source of my life energy: my family. You have been an outstanding inspiration. Thanks for providing me with unconditional love, support and courage to do my best. More importantly, thanks for believing in me. You are the number one reason I am what I am today. I will always keep you with me as I embark on my life's journey and dreams. I love you so much!

AN ABSTRACT OF THE THESIS OF

Dima Abed Diab El Harakeh for Master of Science
Major: Biology

Title: Investigating the Deregulation and Bio-functional relevance of Caveolin-1 in Muscular Laminopathies

Laminopathies comprise a heterogeneous group of disorders arising from mutations or altered post translational processing of nuclear envelope (NE)/lamina proteins. The majority of these disorders are caused by inherited or *de novo* mutations in the *LMNA* gene and are manifested as diverse pathologies affecting a wide range of tissues including skeletal and cardiac muscle. To date, the molecular mechanisms underlying the phenotypic diversity and disease pathogenesis in laminopathies have not been deciphered. Our objective is to gain a better understanding of the mechanisms by which distinct mutations in the ubiquitously expressed *LMNA* gene contribute to the tissue specific phenotypes that result in muscular laminopathies including Emery-Dreifuss Muscular Dystrophy (EDMD) and Dilated Cardiomyopathy (DCM). We hypothesize that complete loss of or specific mutations in *LMNA* associated with muscular laminopathies exert differential effects on the expression and/or intra-cellular distribution of caveolins which by lieu of their association with the cell membrane caveolae, orchestrate many signaling pathways in response to changes in the cell's biochemical or mechanical environment. Of particular interest to us is caveolin-1, a product of the *Cav-1* mechanosensitive gene (encodes for α & β isoforms of caveolin-1) which has been shown to be implicated in muscle repair and regeneration. In this study, we assessed the transcript and protein expression of *Cav-1* (both α & β isoforms) in mouse embryo fibroblast (MEF) lines derived from mice lacking either A-type lamin (*Lmna*^{-/-}) or emerin (*Emd*^{-Y}) which have the EDMD phenotype or mice homozygous for the N195K mutant (*Lmna*^{N195K/N195K}) which have the DCM phenotype versus wild-type (WT) controls under baseline and oxidative stress conditions. Real-Time PCR quantification of *Cav-1* under baseline conditions showed a reduction in the *Cav-1 α* transcript in *Lmna*^{-/-} MEFs and a significant elevation in the *Cav-1 α* transcript in *Lmna*^{N195K/N195K} and *Emd*^{-Y} MEFs. A similar pattern was obtained upon evaluating the expression of both *Cav-1* isoforms (α & β) in the MEF cell panel. However, Western Blot analysis and densitometry quantification revealed no significant change in Cav-1 α in the three mutant cell lines in comparison to the WT controls. Immunofluorescence staining suggested a marked increase in Cav-1 α expression in *Lmna*^{N195K/N195K} MEFs, yet no change was detected in *Lmna*^{-/-} and *Emd*^{-Y} MEFs. Intriguingly, *Cav-1* gene expression profile was restored upon the expression of *LMNA* WT or *LMNA* E358K mutant (EDMD) in lamin A/C-deficient MEFs by retroviral transfection, but not in *LMNA* L530P mutant that results in EDMD. Additionally, we

noted a significant elevation in the protein levels of Liver Kinase B1 (LKB1), a signaling partner that may plausibly control the activity of Cav-1, in *Lmna*^{-/-} MEFs but not in the *Lmna*^{N195K/N195K} nor in *Emd*^{-/-} MEFs under baseline conditions. In contrast, we noted a significant decline in LKB1 protein levels in lamin A/C-deficient MEFs retrovirally transfected to express *LMNA* L530P mutant form in comparison to their mock control under baseline conditions. Furthermore, under H₂O₂-induced oxidative stress, we examined a differential pattern of induction in Cav-1 (α & β) expression in both *Lmna*^{-/-} and *Lmna*^{N195K/N195K} MEFs in comparison to the WT controls at the transcriptional and translational levels. Taken together, our data provide a possible path toward a mechanistic understanding of the potential contribution of caveolins in the pathogenesis of muscular laminopathies. Future directions will address putative changes in the expression of caveolin-1 and caveolin-3, a product of the muscle-specific *Cav-3* gene *in vitro* in C2C12 myoblasts lacking A-type lamin expression or those expressing the N195K mutant form and in skeletal and/or cardiac muscle tissue derived from an EDMD mouse model and/or a DCM mouse model.

CONTENTS

	Page
ACKNOWLEDGEMENT	v
ABSTRACT.....	vi
LIST OF ILLUSTRATIONS.....	xiv
LIST OF TABLES.....	xvi
LIST OF ABBREVIATIONS.....	xvii
CHAPTER	
I. LITERATURE REVIEW.....	1
A. Nucleus, nuclear structure and organization.....	1
1. Overview.....	1
2. Nuclear lamins and nuclear lamina	
a. Expression of lamins during evolution and differentiation	3
b. Structural organization and assembly of lamins.....	5
c. Functions of lamins.....	9
i. Maintenance of nuclear architecture and cellular integrity	9
ii. Distribution of nuclear pore complexes.....	10
iii. Chromatin remodeling	10
iv. DNA replication, DNA repair and transcription.....	11
v. Cell proliferation and differentiation	12
B. Interactions of lamins with integral proteins of the inner nuclear membrane.....	13
1. Overview.....	13
2. Inner nuclear membrane protein Emerin.....	14
a. Overview.....	14
b. Functions of emerin.....	15
i. Gene regulation.....	15

ii. Actin dynamics	16
C. Lamins and oxidative stress.....	17
D. Laminopathies.....	20
1. Overview.....	20
2. Laminopathies affecting the muscular tissues.....	21
a. Emery-Dreifuss muscular dystrophy	21
b. Dilated cardiomyopathy	23
c. Limb-girdle muscular dystrophy type 1B.....	24
3. Laminopathies affecting the adipose tissues.....	24
a. Dunnigan-type familial partial lipodystrophy.....	24
b. Acquired partial lipodystrophy.....	25
4. Laminopathies affecting the nervous system.....	25
a. Charcot-Marie-Tooth neuropathy type 2	25
b. Autosomal dominant leukodystrophy	26
5. Laminopathies resulting in systemic disorders and premature aging.....	26
a. Hutchinson-Gilford Progeria	26
b. Mandibuloacral dysplasia.....	27
c. Atypical Werner Syndrome	28
d. Restricted Dermopathy.....	29
E. Caveolae and Caveolins.....	30
1. Overview of Caveolae and Caveolins.....	30
2. Caveolin-1.....	32
3. Caveolin-1 in mechanotransduction.....	35
4. Caveolin-1 knockout and mutant mouse models.....	37
F. LKB1.....	38
1. Overview.....	38
2. LKB1 in tumor suppression.....	42
3. LKB1 in cardiovascular physiology and pathophysiology.....	42
G. Gap in Knowledge, Study Rationale and Hypothesis.....	44
H. Objective of the Study and Specific Aims.....	47

I. Significance of the Study.....	48
II. MATERIALS AND METHODS.....	49
A. Cell Lines.....	49
1. Cell Culture.....	51
2. Cell Count.....	52
B. RNA Extraction.....	52
1. Baseline Conditions.....	52
2. H ₂ O ₂ -Induced Oxidative Stress Conditions.....	53
C. Reverse Transcription.....	54
D. Quantitative Real-Time PCR.....	54
E. Protein Extraction, SDS-PAGE & Western Blot Analysis.....	56
1. Protein Extraction.....	56
a. Baseline Conditions.....	56
b. H ₂ O ₂ - Induced Oxidative Stress Conditions.....	57
2. Sample Protein Quantification.....	58
3. SDS-PAGE.....	58
a. Casting & Running the Gel.....	58
b. Preparing & Loading the Samples.....	59
c. Protein Transfer from Gel to Blot.....	60
d. Membrane Blocking, Washing & Antibody Incubations.....	61
e. X-ray Film Imaging of Western Blots.....	63
f. Membrane Stripping & Re-probing.....	63
g. Western Blots Densitometry Analysis.....	64
F. Immunofluorescence Staining.....	66
G. Microscopic Imaging.....	68
H. Statistical Analysis.....	69

III. RESULT.....	70
A. <i>Cav-1</i> (α & β isoforms) transcriptional levels under baseline and oxidative stress conditions in mouse embryo fibroblast (MEF) cell lines derived from mice either lacking A-type lamin expression or emerin expression, homozygous for the N195K mutant form versus wild-type (WT) and in a panel of lamin A/C-deficient MEFs retrovirally transfected to express <i>LMNA</i> WT or mutant forms that result in EDMD (E358K,L530P).....	70
1. <i>Cav-1α</i> and total <i>Cav-1</i> (α + β) are down-regulated in <i>Lmna</i> ^{-/-} MEFs (Lamin A/C null) and significantly upregulated in <i>Lmna</i> ^{N195K/N195K} MEFs and <i>Emd</i> ^{-/-} MEFs (Emd null) under baseline conditions in comparison to <i>Lmna</i> ^{+/+} control MEFs.....	70
2. <i>Cav-1α</i> and total <i>Cav-1</i> (α & β) immediate-early transcripts are induced in <i>Lmna</i> ^{-/-} MEFs and <i>Lmna</i> ^{N195K/N195K} MEFs post exposure to H ₂ O ₂ -induced oxidative stress in comparison to the control <i>Lmna</i> ^{+/+} MEFs.	72
a. <i>Cav-1α</i> and <i>Cav-1</i> (α + β) transcriptional levels are not altered in <i>Lmna</i> ^{+/+} MEF cells following exposure to 0.1 μ M and 0.5 μ M H ₂ O ₂ for 5, 15, 30 and 60min in comparison to mock-treated controls (0.0 μ M H ₂ O ₂).	73
b. <i>Cav-1α</i> and <i>Cav-1</i> (α + β) transcriptional levels are induced in <i>Lmna</i> ^{-/-} MEF cells following exposure to 0.1 μ M and 0.5 μ M H ₂ O ₂ for 5, 15, 30 and 60min in comparison to mock-treated controls (0.0 μ M H ₂ O ₂)	79
c. <i>Cav-1α</i> and <i>Cav-1</i> (α + β) transcriptional levels are induced in <i>Lmna</i> ^{N195K/N195K} MEF cells following exposure to 0.1 μ M and 0.5 μ M H ₂ O ₂ for 5, 15, 30 and 60min in comparison to mock-treated controls (0.0 μ M H ₂ O ₂).....	83
3. <i>Cav-1α</i> and total <i>Cav-1</i> (α & β) immediate-early transcripts are altered in Lamin A/C-deficient MEFs retrovirally transfected to express the <i>LMNA</i> WT or mutant forms that result in EDMD (E358K, L530P) under baseline conditions.....	86
a. <i>Cav-1α</i> immediate-early transcript is induced in Lamin A/C-deficient MEFs retrovirally transfected to express the <i>LMNA</i> WT or the mutant form that result in EDMD (E358K) in comparison to their control Lamin A/C-deficient MEFs expressing the mock retroviral vector without lamin A.	86
b. <i>Cav-1</i> (α + β) immediate-early transcript is induced in Lamin A/C-deficient MEFs retrovirally transfected to express the <i>LMNA</i> WT or the mutant form that result in EDMD (E358K) in comparison to their control Lamin A/C-deficient MEFs expressing the mock retroviral vector without lamin A.	89

B. Protein expression and intracellular distribution of Cav-1 α isoform under baseline and oxidative stress conditions in mouse embryo fibroblast (MEF) cell lines derived from mice either lacking A-type lamin expression or emerin expression, homozygous for the N195K mutant form versus wild-type (WT) and in a panel of lamin A/C-deficient MEFs retrovirally transfected to express <i>LMNA</i> WT or mutant forms that result in EDMD (E358K, L530P).....	91
1. Cav-1 α protein expression is not significantly altered in <i>Lmna</i> ^{-/-} MEFs (Lamin A/C null), <i>Lmna</i> ^{N195K/N195K} MEFs and <i>Emd</i> ^{-/-} MEFs (Emd null) under baseline conditions in comparison to <i>Lmna</i> ^{+/+} control MEFs.....	91
2. Cav-1 α protein expression is deregulated in <i>Lmna</i> ^{-/-} MEFs and <i>Lmna</i> ^{N195K/N195K} MEFs post exposure to H ₂ O ₂ -induced oxidative stress in comparison to the control <i>Lmna</i> ^{+/+} MEFs.....	93
a. Cav-1 α translational levels are not altered in <i>Lmna</i> ^{+/+} MEF cells following exposure to 0.1 μ M and 0.5 μ M H ₂ O ₂ for 5, 15, 30 and 60min in comparison to mock-treated controls (0.0 μ M H ₂ O ₂).	93
b. Cav-1 α translational levels are not altered in <i>Lmna</i> ^{+/+} MEF cells following exposure to 0.1 μ M and 0.5 μ M H ₂ O ₂ for 1.5, 2, 4 and 6hrs in comparison to mock-treated controls (0.0 μ M H ₂ O ₂).	95
c. Cav-1 α translational levels are deregulated in <i>Lmna</i> ^{-/-} MEF cells following exposure to 0.1 μ M and 0.5 μ M H ₂ O ₂ for 5, 15, 30 and 60min in comparison to mock-treated controls (0.0 μ M H ₂ O ₂).	98
d. Cav-1 α translational levels are not altered in <i>Lmna</i> ^{-/-} MEF cells following exposure to 0.1 μ M and 0.5 μ M H ₂ O ₂ for 1.5, 2, 4 and 6hrs in comparison to mock-treated controls (0.0 μ M H ₂ O ₂).	100
e. Cav-1 α translational levels are reduced in <i>Lmna</i> ^{N195K/N195K} MEF cells following exposure to 0.1 μ M and 0.5 μ M H ₂ O ₂ for 5, 15, 30 and 60min.. in comparison to mock-treated controls (0.0 μ M H ₂ O ₂).....	103
f. Cav-1 α translational levels are not altered in <i>Lmna</i> ^{N195K/N195K} MEF cells following exposure to 0.1 μ M and 0.5 μ M H ₂ O ₂ for 1.5, 2, 4 and 6hrs in comparison to mock-treated controls (0.0 μ M H ₂ O ₂).....	105
3. Cav-1 α translational levels are not altered in Lamin A/C-deficient MEFs retrovirally transfected to express the LMNA WT or the mutant form that result in EDMD (E358K) and are significantly reduced in the mutant form (L530P) that results in EDMD in comparison to their control Lamin A/C-deficient MEFs expressing the mock retroviral vector without lamin A....	107
4. Cav-1 α protein expression is differentially expressed in mouse embryo fibroblast (MEF) cell line derived from mice homozygous for the N195K mutant form, but not significantly altered in MEFs derived from mice either lacking A-type lamin expression or emerin expression in comparison to the wild-type (WT) controls under baseline conditions by immunofluorescence staining.....	110

C. Protein expression and intracellular distribution of LKB1 under baseline conditions in mouse embryo fibroblast (MEF) cell lines derived from mice either lacking A-type lamin expression or emerin expression, homozygous for the N195K mutant form versus wild-type (WT) and in a panel of lamin A/C-deficient MEFs retrovirally transfected to express <i>LMNA</i> WT or mutant forms that result in EDMD (E358K, L530P).....	112
1. LKB1 protein expression is significantly elevated in <i>Lmna</i> ^{-/-} MEFs (Lamin A/C null) but unaltered in <i>Lmna</i> ^{N195K/N195K} MEFs and <i>Emd</i> ^{-Y} MEFs (Emd null) under baseline conditions in comparison to <i>Lmna</i> ^{+/+} control MEFs.	112
2. LKB1 translational levels are not altered in Lamin A/C-deficient MEFs retrovirally transfected to express the <i>LMNA</i> WT or the mutant form that result in EDMD (E358K) and are significantly reduced in the mutant form (L530P) that results in EDMD in comparison to their control Lamin A/C-deficient MEFs expressing the mock retroviral vector without lamin A.....	114
 IV. DISCUSSION.....	117
 REFERENCES.....	130

ILLUSTRATIONS

Figure	Page
1. The major architectural components of the mammalian nuclear envelope.	3
2. The structure and carboxy-terminal processing of A-type and B-type lamins..	7
3. Assembly of lamins into filaments.	9
4. A schematic representation of reported mutations in the <i>LMNA</i> gene and the resulting diseases.....	21
5. Electron micrographs showing the ultrastructure of caveolae.....	30
6. Schematic representation showing the domain organization of caveolins.	33
7. Activation of the AMPK-related kinases by LKB1.....	40
8. Posttranslational modification sites of mouse LKB1 protein.	41
9. Mean fold change in <i>Cav-1</i> transcript expression in <i>Lmna</i> ^{-/-} , <i>Lmna</i> ^{N195K/N195K} and <i>Emd</i> ^{-/-} MEF cells in comparison to WT controls at baseline conditions.	71
10. Mean fold change in <i>Cav-1</i> transcript expression in <i>Lmna</i> ^{+/+} MEF cells cultured at 80% confluence under H ₂ O ₂ -induced oxidative stress conditions... ..	75
11. Mean fold change in <i>Cav-1</i> transcript expression in <i>Lmna</i> ^{+/+} MEF cells cultured at full confluence under H ₂ O ₂ -induced oxidative stress conditions.	78
12. Mean fold change in <i>Cav-1</i> transcript expression in <i>Lmna</i> ^{-/-} MEF cells cultured at full confluence under H ₂ O ₂ -induced oxidative stress conditions.....	81
13. Mean fold change in <i>Cav-1</i> transcript expression in <i>Lmna</i> ^{N195K/N195K} MEF cells cultured at full confluence under H ₂ O ₂ -induced oxidative stress conditions.....	84
14. Mean fold change in <i>Cav-1α</i> transcript expression in lamin A/C-deficient MEFs retrovirally transfected to express the <i>LMNA</i> WT or mutant forms (E358K and L530P) that result in EDMD at baseline conditions.	88
15. Mean fold change in <i>Cav-1</i> transcript expression in lamin A/C-deficient MEFs retrovirally transfected to express the <i>LMNA</i> WT or mutant forms (E358K and L530P) that result in EDMD at baseline conditions	90

16. Western Blot analysis of Cav-1 α protein expression in <i>Lmna</i> ^{-/-} , <i>Lmna</i> ^{N195K/N195K} and <i>Emd</i> ^{-Y} mutant MEFs vs. control WT cells cultured at full confluence under baseline conditions.....	92
17. Cav-1 α protein expression in <i>Lmna</i> ^{+/+} MEF cells cultured at full confluence under H ₂ O ₂ -induced oxidative stress conditions for time increments of 5, 15, 30 and 60min..	95
18. Cav-1 α protein expression in <i>Lmna</i> ^{+/+} MEF cells cultured at full confluence under H ₂ O ₂ -induced oxidative stress conditions for time increments of 1.5, 2, 4 and 6hrs.97	
19. Cav-1 α protein expression in <i>Lmna</i> ^{-/-} MEF cells cultured at full confluence under H ₂ O ₂ -induced oxidative stress conditions for time increments of 5, 15, 30 and 60min.	100
20. Cav-1 α protein expression in <i>Lmna</i> ^{-/-} MEF cells cultured at full confluence under H ₂ O ₂ -induced oxidative stress conditions for time increments of 1.5, 2, 4 and 6hrs..	102
21. Cav-1 α protein expression in <i>Lmna</i> ^{N195K/N195K} MEF cells cultured at full confluence under H ₂ O ₂ -induced oxidative stress conditions for time increments of 5, 15, 30 and 60min.....	104
22. Cav-1 α protein expression in <i>Lmna</i> ^{N195K/N195K} MEF cells (DCM model) cultured at full confluence under H ₂ O ₂ -induced oxidative stress conditions for time increments of 1.5, 2, 4 and 6hrs	106
23. Mean fold change in Cav-1 α protein expression in lamin A/C-deficient MEFs retrovirally transfected to express the <i>LMNA</i> WT or mutant forms (E358K and L530P) that result in EDMD cultured at full confluence at baseline conditions.	109
24. Immunofluorescence staining and semi-quantitative analysis of Cav-1 α protein expression in <i>Lmna</i> ^{-/-} , <i>Lmna</i> ^{N195K/N195K} and <i>Emd</i> ^{-Y} mutant MEFs vs. control WT cells cultured at full confluence under baseline conditions.....	111
25. Western Blot analysis of LKB1 protein expression in <i>Lmna</i> ^{-/-} , <i>Lmna</i> ^{N195K/N195K} and <i>Emd</i> ^{-Y} mutant MEFs vs. control WT cells cultured at full confluence under baseline conditions.....	113
26. Mean fold change of LKB1 protein expression in lamin A/C-deficient MEFs retrovirally transfected to express the <i>LMNA</i> WT or mutant forms (E358K and L530P) that result in EDMD cultured at full confluence at baseline conditions.....	116

TABLES

Table	Page
1. A list showing the sequences of the forward and the reverse primers that were employed to quantify the transcript expression of the α isoform of <i>Cav-1</i> , α & β isoforms of <i>Cav-1</i> , and <i>18S</i> reference gene	55

ABBREVIATIONS

%	Percent
/	Per
µg	Micro Gram
µl	Micro Liter
µM	Micro Molar
DAPI	4',6-Diamidino-2-Phenylindole
APLD	Acquired Partial Lipodystrophy
AP-1	Activating Protein-1 Complex
AMPK	AMP-Activated Protein Kinase
APS	Ammonium Persulfate
ATM	Ataxia-Telangiectasia-Mutated
AD-EDMD	Autosomal Dominant EDMD
ADLD	Autosomal Dominant Leukodystrophy
BAF	Barrier-of-Autointegration Factor
BC	Breast Cancer
BTF	BCL2-associated Transcription Factor
BMP	Bone Morphogenetic Protein
BSA	Bovine Serum Albumin
<i>C. elegans</i>	<i>Caenorhabditis elegans</i>
PKA	cAMP-Dependent Protein Kinase
CAT	Catalase
CSD	Caveolar Scaffolding Domain

COD	Caveolin Oligomerization Domain
Cav-1	Caveolin-1
Cav-2	Caveolin-2
Cav-3	Caveolin-3
CNS	Central Nervous System
CMT2	Charcot-Marie-Tooth neuropathy type 2
WRN	Classical Werner's syndrome
Cnx	Connexins
CDK	Cyclin-Dependent Kinase
Cys	Cysteine
°C	Degrees Celsius
ddH ₂ O	Deionized distilled water
DCM	Dilated Cardiomyopathy
DNA	Deoxyribonucleic Acid
DSBs	Double-Strand Breaks
<i>D. melanogaster</i>	<i>Drosophila melanogaster</i>
E2F	Early gene 2 factor
E2F-DP3	Early gene 2 factor-Differentiation regulated transcription factor Polypeptide 3
ESCs	Embryonic Stem Cells
EDMD	Emery–Dreifuss Muscular Dystrophy
ER	Endoplasmic Reticulum
e-NOS	Endothelial Nitric Oxide Synthase
EGFR	Epidermal Growth Factor Receptor

et al.	et alii (and others)
FPLD	Familial partial lipodystrophy
FT	Farnesyl Transferase
FACE2	Farnesylated proteins-Converting Enzyme 2
FBS	Fetal bovine serum
g	Grams
GAPDH	Glyceraldehyde 3-phosphate dehydrogenase
GCL	Germ- Cell-Less
Gln	Glycine
GSH	Glutathione peroxidase
H ₂ O ₂	Hydrogen Peroxide
<i>Hic-5</i>	Hydrogen Peroxide-Inducible Clone 5 Protein
HRP	Horseradish peroxidase
Hrs	Hours
HGPA	Hutchinson-Gilford progeria syndrome
Ig-fold	Immunoglobulin-like fold
INM	Inner Nuclear Membrane
ID	Intercalated discs
IFs	Intermediate Filaments
ICMT	Isoprenylcysteine Carboxymethyltransferase enzyme
Kb	Kilo base pairs
KDa	Kilo Dalton
LADs	Lamina-Associated Domains
LGMD1B	Limb-girdle muscular dystrophy type 1B

LKB1	Liver kinase B1
Lys	Lysine
mTORC1	Mammalian Target of Rapamycin Complex 1
mTOR	Mammalian Target of Rapamycin
MAD	Mandibuloacral dysplasia
MMP-2	Matrix Metalloproteinase-2
MMP-9	Matrix Metalloproteinase-9
mg	Milligram
min	Minute
MAPK	Mitogen Activated Protein Kinase
MKL	Mega Karyoblastic Leukemia
ml	Milliliter
mm	Millimeters
MEF	Mouse Embryo Fibroblast
MO-25	Mouse Protein 25
MyoD	Muscle Differentiation Marker
NOX	NADPH Oxidases
NaOH	Sodium Hydroxide
NE	Nuclear Envelope
NF- κ B	Nuclear Factor Kappa-light-chain-enhancer of activated B cells
NLS	Nuclear Localization Signal
NPC	Nuclear Pore Complex
Nup153	Nucleoporin 153

ONM	Outer Nuclear Membrane
RSK	p90 ribosomal S6 protein kinase
PJS	Peutz-Jeghers syndrome
PFA	Paraformaldehyde
PBS	Phosphate Buffered Saline
PI3K	Phosphatidylinositol 3-Kinase
PVDF	Polyvinylidene Fluoride
PCNA	Proliferating Cell Nuclear Antigen
PKB	Protein Kinase B
ROS	Reactive oxygen species
RD	Restricted Dermopathy
pRb	Retinoblastoma protein
RNA	Ribonucleic Acid
rpm	Rounds per minute
SDS	Sodium Dodecyl Sulfate
Ser	Serine
STK11	Serine/Threonine Kinase 11
SRF	Serum Response Factor
SEM	Standard Error of the Mean
STRAD	STE20-related adaptor
SREBP1	Sterol Response Element –Binding Protein 1
SOD	Superoxide dismutase
TEMED	Tetramethylethylenediamine
Thr	Threonine

TGF- β	Transforming Growth Factor Beta 1 Receptor
Triton [®] X-100	t-Octylphenoxypolyethoxyethanol,
TSC2	Tuberous Sclerosis Complex 2
Tween20	Polyoxyethylene Sorbitol Ester
Y14	Tyrosine residue 14
V	Volts
VEGF	Vascular Endothelial Growth Factor
VSMCs	Vascular Smooth Muscle Cells
WT	Wild Type
ZMPSTE24	Zinc Metalloprotease related to Ste24

CHAPTER I

LITERATURE REVIEW

A. Nucleus, nuclear structure and organization

“We have entered the cell, the Mansion of our birth, and started the inventory of our acquired wealth.”

—Albert Claude

1. Overview

Nearly two billion years ago, an epochal evolutionary event gave rise to eukaryotes through the discovery of a higher-order membrane bound organelle, the nucleus, which separates the genetic material of a cell from other cellular components. Currently, the nucleus is viewed as the most distinctive feature and the chief processing unit of all eukaryotic cells owing to its involvement in fundamental biochemical processes such as, DNA replication, transcription, messenger RNA (mRNA) splicing and chromatin organization. In metazoan cells, the nucleus can be structurally and functionally divided into two regions, the nuclear envelope (NE) lining the interface between the nucleus and the cytoplasm and the nuclear interior where the DNA is condensed and folded into chromosomes occupying nonrandom territories in the nucleoplasm (Dahl et al., 2008). The NE is comprised of two concentric phospholipid bilayer membranes- the outer nuclear membrane (ONM) and the inner nuclear membrane (INM) separated by a 40-50nm perinuclear space which is an extension of the endoplasmic reticulum (ER) lumen. Nevertheless, both membranes are periodically

joined at sites occupied by nuclear pore complexes (NPCs) which represent multiprotein channels involved in bi-directional nucleocytoplasmic transport of macromolecules (Stewart et al., 2007) (Figure 1, see below). While the ONM exhibits numerous connections with the ER membrane, is enriched in ER proteins and associates with ribosomes, it is contiguous with the INM at the borders of each NPC (Grossman et al., 2012). The INM, by contrast, harbors a distinctive set of integral membrane proteins, some of which maintain close associations with chromatin in the interior of the nucleus. The INM does not associate with ribosomes and has not been shown to participate in protein synthesis (Burke & Stewart, 2002). The composition of the INM varies quantitatively and qualitatively between the different cell types as demonstrated by several proteomic analysis studies and even within a single cell type at different stages of differentiation (Datta et al., 2009; Korfali et al., 2010; Liu et al., 2009). Therefore, beyond the classical role of the NE as a physical barrier at the crossroads between the nucleus and the cytoplasm, it is implicated in cellular organization and function.

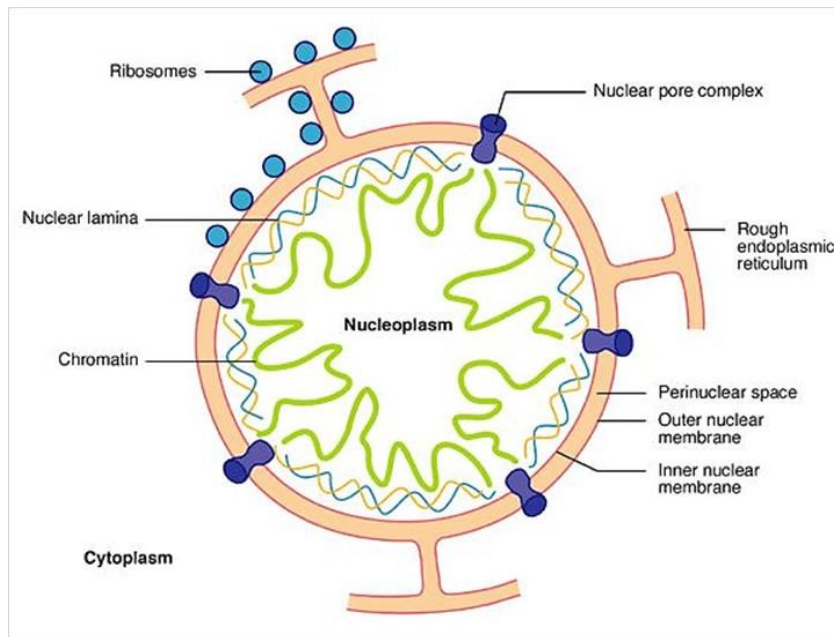


Figure 1| The major architectural components of the mammalian nuclear envelope. (Maidment & Ellis, 2002)

2. Nuclear lamins and nuclear lamina

a. Expression of lamins during evolution and differentiation

In metazoan cells, underlying the INM is a meshwork of type V intermediate filaments (IFs) commonly referred to as the nuclear lamina. The principle components of the nuclear lamina are A-type and B-type nuclear lamins and the lamina associated proteins. The number and the complexity of the lamin coding genes increased with metazoan evolution and seems to be restricted to the Animal Kingdom as comparative DNA sequence analysis revealed no clear homologs in the fully sequenced genomes of lower eukaryotes such as, *Arabidopsis thaliana*, *Saccharomyces cerevisiae* and *Schizosaccharomyces pombe* (Dittmer & Misteli, 2011)(Cohen et al., 2001) (Goldman et al., 2002). *Caenorhabditis elegans* (*C. elegans*) possess one single lamin gene (*Lmn-1*) that is expressed in all the cells except in mature sperms (Liu et al., 2000). The fruit

fly, *Drosophila melanogaster* (*D. melanogaster*), by contrast, has two lamin genes (*Lmn Dm0* and *Lmn C*), the former of which is expressed throughout development when compared to a more specific and delayed lamin C expression during late stages of embryonic development (Bossie & Sanders, 1993)(Gruenbaum et al., 1988). In mammals, nuclear lamins are encoded by three genes namely, *LMNA*, *LMNB1* and *LMNB2*. The *LMNA* gene gives rise to A-type lamins which are abundantly expressed in terminally differentiated cells. Early embryonic cells including embryonic stem cells and undifferentiated embryonal carcinoma cells lack A-type lamin expression (Roerber et al., 1989; Stewart & Burke, 1987). In view of that, it has been reported that mouse and human embryonic stem cells (ESCs) do not express A-type lamins in tissue culture providing ample evidence for the use of A-type lamins as a marker for differentiation (Constantinescu et al., 2006). *Lmna* expression in mice commences during embryogenesis particularly after embryonic day 7-8 initially appearing in the trophectoderm followed by an asynchronous expression of the *Lmna* gene in several other tissues which has led to the speculation that A-type lamins are not important for pre-natal normal cell growth, but are essential for postnatal tissue homeostasis (Burke & Stewart, 2002). Nonetheless, cells of the central nervous system and the lower layer of epidermis express little to no lamin A suggesting that the central nervous system is spared from diseases caused by mutations in the *LMNA* gene. On the contrary, cells of mesenchymal origin express high levels of A-type lamins as elucidated by their frequent involvement in disease associated *LMNA* mutations (Jung et al., 2012). Unlike A-type lamins, B-type lamins are expressed by all somatic cells throughout development and are encoded by two genes, *LMNB1* and *LMNB2* genes. Although thought to be critical for cell viability and survival as shown in previous studies where lamin B1- and lamin

B2-deficient mice die at birth and that knockdown of B-type lamins in human cells is lethal, recent studies performed on mice suggest that B-type lamins are dispensable in many cell types such as, embryonic stem cells (Kim et al., 2011; Kim et al., 2013) and skin cells (Yang et al., 2011). However, it is obvious that B-type lamins are indispensable for organ development as mice lacking B-type lamins expression die shortly after birth from severe defects in the development of the nervous system specifically the brain (Coffinier et al., 2011; Kim et al., 2011).

b. Structural organization and assembly of lamins

Nuclear lamins, as mentioned above, are generally classified as A-type and B-type lamins by virtue of their expression patterns, structural and biochemical features and behavior during mitosis. A-type lamins include two major isoforms namely, lamin A and lamin C, in addition to the two other minor isoforms lamin A Δ 10 and the germ cell specific lamin C2 all of which arise by alternative splicing of one single gene, the *LMNA* gene (Furukawa et al., 1994; Machiels et al., 1996). On the other hand, B-type lamins are encoded by two separate genes, *LMNB1* and *LMNB2*, both of which respectively give rise to the major B-type lamin isoforms particularly lamin B1 and lamin B2. Lamin B3 is the only minor isoform in B-type lamins and is generated by alternative splicing of the *LMNB2* gene (Furukawa & Hotta, 1993). Like lamin C2, the expression of lamin B3 is germ cell specific.

Although structurally similar to cytoplasmic intermediate filaments, lamins possess several distinguishing features. Like other intermediate filament proteins, lamins have a tripartite structure composed of a highly conserved α -helical coiled-coil rod domain spanning more than half of the lamin molecule and comprised of four

heptad repeats denoted 1A, 1B, 2A and 2B connected by flexible linker domains termed L1, L12 and L2 (Figure 2a, see below). Lamins, on the contrary, possess 42 additional amino acids in coil 1B. The α -helical coiled-coil rod domain is flanked by a globular amino-terminal head domain and a carboxy-terminal tail domain (Dittmer & Misteli, 2011). The rod domain is thought to mediate the dimerization of lamins while the head and tail domains are involved in head-to-tail assembly of polymers and higher order polymerization of lamins (Gruenbaum et al., 2005). The amino-terminal head domain in lamins is variable in size but tends to be shorter than the head domain of cytoplasmic intermediate filaments. The tail domain in lamins is characterized by a nuclear localization signal (NLS) required for their transport into the nucleus post synthesis. Adjacent to the NLS, lamins possess an immunoglobulin-like fold domain (Ig-fold) necessary for protein-protein and protein-ligand interactions. Additionally, except for lamin C, the carboxy-terminal tail of lamins A, B1 and B2 contains a CAAX box representing a motif of the amino acid sequence cysteine-aliphatic-aliphatic- any amino acid which serves as a substrate for post-translational modification (Dittmer & Misteli, 2011).

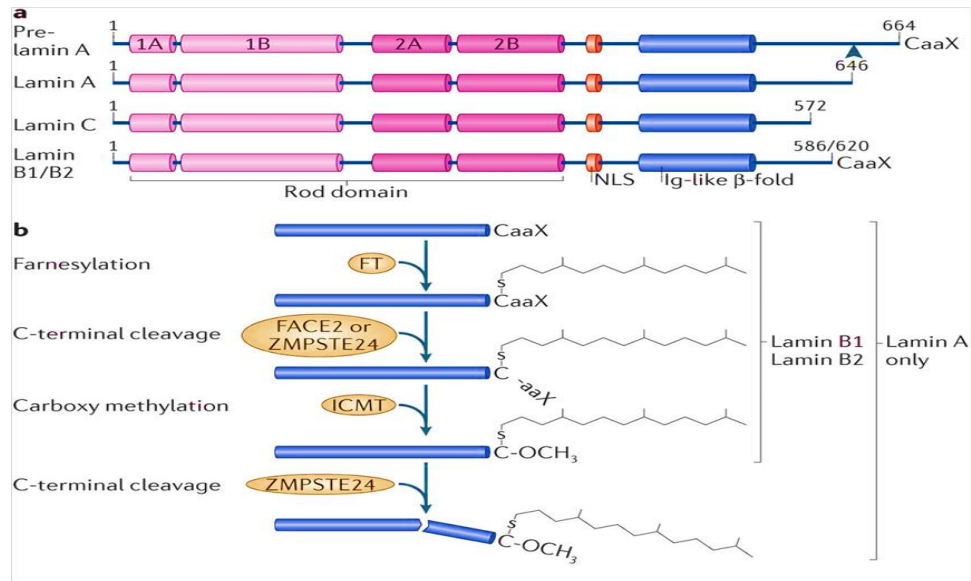


Figure 2 | The structure and carboxy-terminal processing of A-type and B-type lamins. (Modified from Burke & Stewart, 2013).

Initially expressed as pre-lamins, lamins A, B1 and B2 undergo three successive steps of post-translational modifications at the C-terminal tail yielding the mature lamins (Figure 2b, see above). Soon after synthesis, pre-lamins get farnesylated at the cysteine residue of the CAAX box by a farnesyltransferase (FT) enzyme. This is followed by the proteolytic cleavage of the -AAX motif by an endoprotease or endopeptidase, most likely farnesylated proteins-converting enzyme 2 (FACE2) in the case of the B-type lamins, and zinc metalloprotease related to Ste24 (ZMPSTE24) in the case of lamin A. Post-translational processing is then completed by the methylation of the carboxyl group by an isoprenylcysteine carboxymethyltransferase enzyme (ICMT). While the maturation of B-type lamins is terminated at this step demonstrating that mature B-type lamins retain the farnesyl moiety, the farnesylated and carboxymethylated pre-lamin A undergoes further processing to produce the mature lamin A protein. Once incorporated in the NE, it is subjected to the action of the metalloprotease Zmpste24 that removes the last 15 amino acids including the

carboxymethylated and farnesylated cysteine residue (Burke & Stewart, 2013). The modifications achieved at the CAAX box are thought to play a role in the localization and retention of lamins at the nuclear envelope. Despite that, the addition of the farnesyl moiety is dispensable for NE localization as mature lamin C is not farnesylated, and can still localize to the NE. In addition, previous studies pointed out to the fact that the C-terminal tail domain of lamins designate the most variable regions in lamins and contain the binding site for most lamin-binding proteins suggesting that post-translational modifications of lamins may be involved in establishing protein-protein interactions (Schirmer & Foisner, 2007; Wagner & Krohne, 2007; Zastrow et al., 2004).

Two lamin monomers dimerize using their α -helical rod domain in a parallel head-to-head fashion producing a coiled-coil lamin dimer, the basic building block of higher order lamin assemblies (Figure 3, see below). Formation of lamin polymers involves the parallel head-to-tail association between two or more lamin dimers. This feature is unique to lamins as cytoplasmic IFs overlap in an antiparallel side-by-side association of dimers forming the higher order IFs assemblies. It remains unclear, however, if individual lamin filaments *in vivo* interact in a homotypic or a heterotypic manner to generate lamin dimers and polymers. In line with this speculation, a group of researchers have shown that following mitosis, lamin A is targeted and retained on the nuclear face of the INM post incorporation of lamin B1 suggesting that nuclear IFs are homotypic (Moir et al., 2000). Nonetheless, we cannot exclude the possibility of the nascent nuclear lamina undergoing re-organization post recruitment of lamin A.

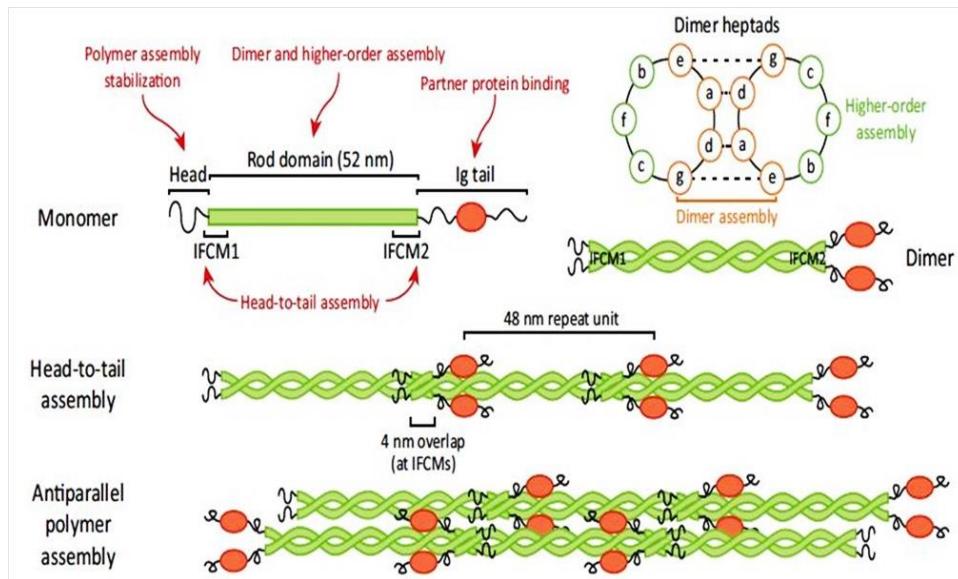


Figure 3 | Assembly of lamins into filaments. (Modified from Davidson & Lammerding, 2013).

c. Functions of lamins

i. Maintenance of nuclear architecture and cellular integrity

Lamins were originally hypothesized to provide structural and mechanical support for the nucleus resisting deformation forces and protecting chromatin from physical damage in an attempt to maintain nuclear and cellular integrity. This hypothesis has been supported by many investigators describing lamins as tensegrity elements involved in resisting deformation forces. In support of this, fibroblasts from *Lmna*^{-/-} mice were reported to undergo nuclear distortions at a faster rate and to a greater extent than those in *Lmna*^{+/+} littermates (Lammerding et al., 2004). Nuclei derived from fibroblasts of these mice were more fragile and less resistant to deformations when compared to nuclei of *Lmna*^{+/+} mice (Broers et al., 2004). This can also partly explain why the nuclei of ESCs, which lack lamin A expression, seem more deformed and malleable (Pajerowski et al., 2007). Noteworthy, the role of B-type lamins in mediating structural and mechanical support to the nucleus remains a matter of further investigation as lamin

B1 deficient mouse embryonic fibroblasts (MEFs) display nuclear blebbings, without any observed alterations in nuclear mechanics. (Lammerding et al., 2006).

ii. Distribution of nuclear pore complexes

One of the crucial functions attributed to lamins is correct positioning of NPCs in the NE. This has been validated in lamin Dm0 deficient *Drosophila* mutants where the absence of lamin Dm0 resulted in the floating of the NPCs around the NE before clustering together. The molecular details of this lamin mediated function emerged later and suggested that the carboxy-terminal tail of a nuclear-pore protein located at the nucleoplasmic ring of the NPCs, namely nucleoporin 153 (Nup153) interacts directly with B-type lamins. This interaction ensures the proper incorporation and distribution of the NPCs in the NE. Accordingly, in *Xenopus* egg extracts with dominant negative lamin mutations, the assembly of the lamina was inhibited and association of Nup153 with the NPCs was not observed. Moreover, the depletion of Nup153 from *Xenopus* egg extracts resulted in increased mobility of NPCs in the NE and their eventual clustering. Therefore, in the absence of either Nup153 or lamin filaments specifically B-type lamins, the positioning of NPCs and their proper incorporation in the NE is impaired (Hutchison, 2002).

iii. Chromatin remodeling

Lamins are perceived as global regulators of chromatin. Genome-wide mapping techniques identified that lamins associate with regions in the genome at sites commonly referred to as the lamina-associated domains (LADs). LADs are generally conceived as gene poor regions residing in repressive chromatin environments despite the fact that

some LADs contain genes that are mostly inactive (Guelen et al., 2008). Although a high percentage of LADs, approximately 75%, is conserved among cell types, a significant proportion is cell type specific providing evidence that different cell types may possess their own LADs as unique “bookmarks”. Conserved LADs, on the contrary, display similar size and genomic positions between mice and humans, yet nucleotide composition may differ (Meuleman et al., 2013). Lamins possess two chromatin binding sites, one located in the C-terminal tail between the end of the rod domain and the Ig-fold like domain and the other lying in the rod domain. In addition, lamin-chromatin interactions are mediated through histones and/or chromatin-associated proteins. Consistent with this, the organization of chromosomes in proliferating *Lmna* mutant fibroblasts was identical to organization of chromosomes in quiescent or senescent cells suggesting that mutations in the *Lmna* gene may result in a structurally impaired nuclear lamina which in turn alters the interaction with chromatin, ultimately leading to a change in the gene expression profile of the cells (Meaburn et al., 2007).

iv. DNA replication, DNA repair and transcription

A significant role for lamins in regulation of DNA replication has been established in multiple studies. Indeed, lamin A was found to associate with sites of early replication in primary fibroblasts and lamin B1 was proposed to colocalize with replication factor proliferating cell nuclear antigen (PCNA) during late S phase in 3T3 cells. DNA replication, for example, was inhibited in *Xenopus* eggs upon the depletion of the major lamin isoform in *Xenopus* (Dechat et al., 2008). In addition, there is increasing evidence that nuclear lamins play a role in DNA repair mainly from studies of premature aging disorders such as HGPS. Numerous studies reported that the accumulation of

farnesylated pre-lamin A or progerin leads to defects in DNA repair. Fibroblasts from patients with HGPS display an enhanced sensitivity to DNA –damaging agents like ultraviolet radiation and chemicals which results in increased occurrence of double-strand breaks (DSBs) while showing a delayed recruitment of p53 binding protein1 (53BP1) (Dechat et al., 2008; Verstraeten et al., 2007) .

Recent studies pointed out to the importance of the interactions of A-type and B-type lamins with integral and non-integral membrane proteins of the NE on gene expression. Several transcription regulators involved in different signal-transduction pathways have been reported to physically interact with nuclear lamins at the nuclear periphery providing ample evidence for a role of the nuclear lamina and nuclear envelope in sequestering transcription factors away from chromatin. For instance, the c-Fos transcription factor is retained at the NE through its association with lamin A/C. This association prevents the heterodimerization of c-Fos with c-Jun, a transcription factor that is required for the formation of the activating protein-1 complex (AP-1). The activity of the AP-1 complex is, therefore, suppressed as its access to its target genes is restricted resulting in growth arrest (Heessen & Fornerod, 2007).

v. Cell proliferation and differentiation

Lamins A/C are involved in regulation of cell cycle progression through interacting with the retinoblastoma protein (pRb). pRb has been identified as a tumor suppressor and a critical cell cycle regulator. When in a hypo phosphorylated state, pRb co-localizes with lamins A/C through its interaction with LAP2 α and binds to the Early gene 2 factor (E2F) family of transcription factors and inhibits their transcriptional activity. However, when pRb is hyper phosphorylated by cyclin/cyclin-dependent kinase

(CDK) complexes, E2F is released and progresses through the restriction point to initiate the S-phase. A role for lamins in regulating differentiation has been supported by the finding that lamins A/C are expressed in terminally differentiated cells. This has been recognized during muscle and adipocyte differentiation. In the case of muscles, differentiation of the myoblasts into myotubes is dependent on lamins A/C interactions with pRB and cyclin D3 which serves as a regulatory subunit of CDK4, CDK6 and CDK2 that is critical for G1 progression. C2C12 myoblast cells with a mutant lamin A were reported to show increased hyper phosphorylation of pRb ultimately leading to inhibition of myoblast differentiation into myotubes (Favreau et al., 2004). Furthermore, the C-terminal tail of lamins A/C interacts with the adipocyte differentiation factor sterol response element –binding protein 1 (SREBP1) leading to the differentiation of adipocytes (Lloyd et al., 2002). This role, however, is affected to varied degrees by mutations in lamin A resulting in a deregulation in adipogenesis.

B. Interactions of lamins with integral proteins of the inner nuclear membrane

1. Overview

The INM harbors an array of integral inner nuclear membrane proteins that maintain close association with chromatin and the nuclear lamina. Indeed, many of the functions attributed to lamins are mediated through their interaction with the lamin binding proteins both at the nuclear periphery and in the nucleoplasm. Proteomic analysis suggests that as many as eighty transmembrane proteins localize to the INM although only a dozen of these have been characterized in detail. Integral INM proteins possess at least one transmembrane segment and an amino-terminal domain facing the nucleoplasm. These include but are not limited to MAN1, LBR, emerin, LAP2, SUN1/2 and smaller

nesprin-1/2 isoforms. Like other proteins, they are synthesized in the ER after which they diffuse towards the INM where they are retained possibly by interacting with the nuclear lamina and/or chromatin. Lamin binding partners have been grouped into architectural partners, chromatin partners, gene regulatory partners and signaling partners despite the fact that some partners fit multiple categories.

2. *Inner nuclear membrane protein Emerin*

a. Overview

Emerin is an integral INM protein of the NE and belongs to a family of nuclear proteins distinguished by a ~ 40 residue motif known as the LEM-domain. The LEM-domain family includes the lamina associated polypeptide-2, LAP2, Emerin and MAN1 (hence its name) INM proteins and was among the first identified family of nuclear membrane proteins. The importance of emerin was highlighted by the discovery of X-linked EDMD, a disease caused by a mutation in the *EMD* gene which codes for emerin back in 1994. Emerin has a nucleoplasmic amino-terminal domain of 220 amino acids, a single transmembrane segment and a short tail in the perinuclear space (Worman & Courvalin, 2005). Emerin contains two distinct functional domains: the LEM-domain located at its amino terminus and mediates its binding to a highly conserved DNA-bridging protein termed, barrier-of-autointegration factor (BAF) which interacts with naked DNA and compacts it, and a central domain involved in interacting with lamin A protein in the nuclear lamina (Lee et al., 2001). Moreover, emerin is expressed in most of the tissues although it is dispensable for cell viability as shown previously in human HeLa cells and *C.elegans* embryo. Nevertheless, emerin is involved in a number of vital functions including cell cycle progression and nuclear assembly (Bengtsson & Wilson,

2004). In spite of its ubiquitous production in most of the tissues, emerin appears to be important for the function of the skeletal and cardiac muscles as mutations in the *EMD* gene resulting in X-linked EDMD were reported to cause muscular dystrophy accompanied with cardiac conduction defects.

b. Functions of emerin

i. Gene regulation

In addition to nuclear lamins, emerin was found to associate with multiple transcriptional regulators through its LEM-domain motif providing a platform for sequestering transcription factors ultimately resulting in the repression of their target genes. The germ cell-less (GCL) is the first transcriptional repressor reported to bind emerin and is conserved from *C.elegans* to humans (Holaska et al., 2003). GCL concentrates at the nuclear envelope where it binds emerin directly. GCL represses the transcriptional capacity of the Early gene 2 factor-Differentiation regulated transcription factor polypeptide 3 (E2F-DP3) by binding to the DP3 subunit of the E2F-DP3 heterodimer. Following a down regulation in the expression of emerin, GCL was found to mislocalize from the NE accompanied by a concomitant increase in the transcriptional activity of the E2F-DP3 transcription factor that is crucial for cell-cycle progression. Biochemical analysis done on emerin complexes provide evidence that BAF and GCL compete to bind to the LEM-domain of emerin suggesting that BAF regulates the activity of GCL (Holaska, 2008). Another transcriptional repressor acting as an emerin-binding partner is the BCL2-associated transcription factor (BTF). BTF is a ubiquitously expressed nuclear protein with the highest expression pattern observed in skeletal muscles. BTF binds to emerin and when overexpressed, it induces apoptosis by inhibiting

the anti-apoptotic BCL2 proteins. Moreover, it has been shown that emerin and BCL2 bind similar regions of BTF. Importantly, EDMD-associated missense mutations disrupt the binding of BTF to emerin indicating an increase in the binding of BCL2 to BTF, the outcome of which is increased apoptosis (Heessen & Fornerod, 2007; Holaska, 2008).

ii. Actin dynamics

One of the chief components of the cytoskeleton in all cell types that is essential for cell integrity, cell division, motility and mechanical resilience is actin. Actin is also abundant in the muscle cells where it is involved in muscle contraction. Noteworthy, actin is also present in the nucleus taking part in chromatin remodeling, the formation of heterogeneous nuclear RNA particles, stress responses, nuclear export and transcription (Pederson & Aebi, 2002). Interestingly, nuclear emerin from mature muscle cells and differentiating myotubes co-immunoprecipitates with lamins A/C, actin and PKA (Lattanzi et al., 2003). Indeed, emerin caps the pointed (minus) ends of F-actin and enhances their polymerization by decreasing their rate of turnover. Emerin, thus, has the potential to stabilize actin polymers at the NE (Bengtsson & Wilson, 2004). The importance of emerin in the regulation of actin dynamics has been highlighted by a recent work reporting a role for emerin and lamin A/C in regulating MKL1-SRF signaling through modulating actin polymerization. Megakaryoblastic leukemia 1 (MKL1) belongs to the myocardin family of mechanosensitive transcription factors with crucial roles in the cardiovascular system. Normally localized in the cytoplasm through binding to G-actin, MKL1 gets translocated to the nucleus in response to mechanical or mitogenic stimulation where it activates serum response factor (SRF) and other genes involved in cellular motility and contractility such as actin and vinculin. This study revealed that

lamin A/C-deficient or mutant mouse embryo fibroblasts (MEFs) have impaired nuclear translocation and defective downstream signaling of the MKL1 transcription factor plausibly caused by the mislocalization of emerin in these cells from the nuclear lamina where it is retained via its interaction with lamins A/C to the endoplasmic reticulum. The altered localization of emerin affects its interaction with nuclear actin ultimately affecting its polymerization which in turn would affect the intracellular localization of MKL1. Interestingly, impaired MKL1/SRF signaling cascade disturbs cytoskeletal actin as numerous cytoskeletal proteins serve as downstream targets of this transcription factor (Ho et al., 2013). This work provides a solid framework in understanding and appreciating the pivotal relationship existing between mutations in lamins A/C of the nuclear lamina, emerin localization, actin dynamics, cytoskeletal organization, intracellular localization of transcription factors and cardiac function.

C. Lamins and oxidative stress

Reactive oxygen species (ROS) are small, short lived natural by-products that mediate several cellular responses including cell proliferation, differentiation, gene expression and migration (Sieprath et al., 2012). Moreover, they are important in promoting homeostasis and cell signaling; however, under stress, they may build up to potentially harmful levels that can cause damage to DNA, proteins and lipids in addition to the accumulation of irreversibly oxidized proteins resulting in defects in proliferation and longevity that have been linked to cardiovascular and neurodegenerative diseases (Shimi & Goldman, 2014). Indeed, the term oxidative stress refers to a state of the cell where the production of ROS is higher than their removal, which is either associated with an increase in the production of ROS or a decrease in their normal elimination by

protective mechanisms involving antioxidant defenses. At the cellular level, there are two major sources of ROS, oxidative phosphorylation occurring in the mitochondria and NADPH oxidases (NOX). Nevertheless, cells are armed with various antioxidant systems to counteract the damaging effects of ROS such as, the ROS defusing enzymes like catalase (CAT), superoxide dismutase (SOD) and glutathione peroxidase (GSH).

Accumulating evidence indicates that laminopathies are often accompanied with altered levels of ROS and increased susceptibility to oxidative stress (Sieprath et al., 2012). In particular, recent data points out to an interdependent relationship between both A-type and B-type lamins and oxidative stress. It was shown that the reduction of mature lamin A or accumulation of aberrant prelamin isoforms alters the levels of antioxidant enzymes (Sieprath et al., 2012). Likewise, when the nuclear lamina is impaired plausibly by disease causing mutations in the *LMNA* gene, the interaction of nuclear lamins with a wide range of transcription factors such as the redox-responsive transcription factors (Rb, SREBP1 and Oct1) is altered (Andres & Gonzalez, 2009; Heessen & Fornerod, 2007). As such, the redox state of the cells will in turn be modified. An intact nuclear lamina is implicated in forming an intact nuclear envelope which elicits proper compartmentalization of the cellular components; however, an impaired nuclear lamina may result in the appearance of transient nuclear envelope disruptions. The latter leads to intermixing of cytoplasmic and nuclear components such as the entry of the mitochondria into the nucleus which may increase the risk of DNA damage due to the close proximity of the generated ROS from the DNA (De Vos et al., 2011). In a similar fashion, oxidative stress was also reported to affect the structure of lamins. This was confirmed by the finding that mammalian lamin A tail contains conserved cysteine residues as targets for irreversible oxidative damage. Furthermore, basal levels of cellular ROS were elevated in

the absence of lamin A or following the loss of the cysteine residues suggesting that the conserved cysteine residues in the tail domain of lamin A are crucial for oxidative stress related functions of lamin A. In response to mild oxidative stress, inter and intramolecular disulfide bonds form between the cysteine residues of different lamin A monomers or within the same monomer respectively. The latter is accompanied with the entry of the cells into a temporary state of cell cycle arrest. Formation of disulfide bonds has been proposed to protect the cysteine residues from irreversible oxidation post exposure to mild oxidative stress in addition to protecting stress responsive partners that interact with the tail of lamin A including, SREBP, PKC α , c-Fos and ERK (Linke & Jakob, 2003; Pekovic et al., 2011) . Noteworthy, the adaptive response to mild oxidative stress is completely abrogated in lamin A/C null fibroblasts. In contrast, high levels of ROS induced oxidative stress are correlated with irreversible oxidation of the cysteine residues and, subsequently, the absence of disulfide bond formation and appearance of dysmorphic nuclei. As such, cells enter into a state of cellular senescence (Pekovic et al., 2011). We can also infer that lamins act as a ROS-sink and buffers that protect the DNA and more critical proteins from oxidative damage up to a certain critical level such that more acute oxidative stress induces irreversible oxidation of the cysteine residues of lamin A leading to a dysfunctional lamina (Sieprath et al., 2012). A change in the cellular redox status influences a number of cellular processes and activities that are generally divided into five broad categories including, (i) modulation of cytokine; growth factor, or hormone action and secretion, (ii) ion transport, (iii) transcription, (iv) neuromodulation, and (v) apoptosis (Lander, 1997). Therefore, the generated ROS act as subcellular messengers, and their mechanisms of action culminate in modulating gene expression and signal transduction (Allen & Tresini, 2000). The signaling pathways that are mostly

known to be redox sensitive are the Mitogen Activated Protein Kinase (MAPK) and Nuclear Factor Kappa-light-chain-enhancer of activated B cells (NF- κ B) signaling pathways. Specifically, in the context of laminopathies, ROS downstream signals include oxidation of proteins as mentioned above, shortening of telomeres and damaging the DNA in the nuclear interior eventually leading to a state of cellular senescence (Hutchison, 2011). Previous work performed on human fibroblasts reported that overexpressing mutant variants of *LMNA* in the aforementioned cells correlated with increased telomere shortening that is in turn very well known to induce premature cell cycle arrest via the activation of the tumor suppressor p53. Furthermore, Farbini et al. claimed the formation of a nuclear shield around the nucleus that is primarily composed of ROS defusing enzymes like CAT, GPX and GST and are seven times higher than those found in the cytosol. The nuclear shield is assembled and maintained via electrostatic interactions and is thought to shield or protect the DNA in the nucleus from the effects of oxidative stress (Fabrini et al., 2010).

D. Laminopathies

1. Overview

Hereditary diseases occasionally result from mutations in a particular gene. Sometimes, mutations in two or more genes are associated with phenotypically similar hereditary diseases. However, rare are those mutations occurring in a single gene and resulting in a panoply of quite unrelated disorders. Over the past few years, a range of exciting findings have been made in the nuclear envelope realm with the discovery that mutations or altered post translational processing of NE/lamina proteins result in a heterogeneous group of disorders collectively known as laminopathies (Maraldi et al.,

2011). The majority of these disorders are caused by mutations in the *LMNA* gene. Inherited or *de novo* mutations spread along the length of the *LMNA* gene and are manifested as diverse pathologies resulting in tissue specific phenotypes (Worman et al., 2009) (Figure 4, see below). More than 400 mutations have been recently identified in the *LMNA* gene making it the most mutated gene known to date (www.umd.be/LMNA/). Laminopathies are grouped into those affecting the muscular tissues and distinguished from each other by the type of muscle tissue involved and the onset of cardiac conduction defects, in addition to adipose tissues and bone. Moreover, they include disorders affecting the nervous system and systemic disorders leading to premature aging.

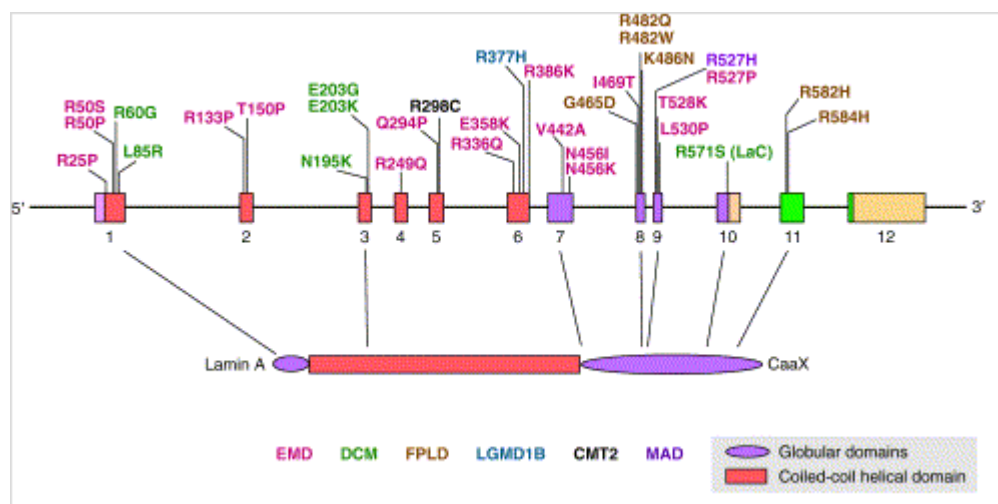


Figure 4 | A schematic representation of reported mutations in the *LMNA* gene (top) and the resulting diseases (bottom) are shown, by color code. (Mounkes et al., 2003)

2. *Laminopathies affecting the muscular tissues*

a. Emery-Dreifuss muscular dystrophy

Emery–Dreifuss muscular dystrophy (EDMD) represents the first indication of an association between the NE and disease. EDMD was initially demonstrated to occur

due to a mutation in an X-linked *EMD* gene which codes for a 29KDa integral inner nuclear membrane protein known as emerin (Bione et al., 1994). X-linked *EMD* mutations are transmitted in a recessive manner and result in either the loss of emerin or its mislocalization to the ER (Fairley et al., 1999). EDMD is classified as the third most common form of muscular dystrophy and is characterized by childhood onset with progressive muscle wasting and weakening accompanied by early contractures as well as joint deformities of the Achilles tendons, spine and elbows. Late-onset defects of EDMD are often associated with abnormal cardiac rhythms and conduction defects which may lead to sudden heart block and cardiac failure (Puckelwartz & McNally, 2011). In 1999, Gisele Bonne and her colleagues identified other mutations mapped to exons of the *LMNA* gene which encode common portions of lamin A and lamin C proteins and result in autosomal dominant EDMD (AD-EDMD). AD-EDMD was also shown to be clinically identical to X-linked EDMD (Bonne et.al, 1999). *LMNA* mutations that give rise to AD-EDMD result in a failure in the folding of the lamin A/C proteins or their assembly often leading to a partial or complete loss of function (Burke & Stewart, 2002). Evidence for interaction between lamin A/C proteins and emerin has been demonstrated in *Lmna* knock-out mice where the absence of lamin A protein from the nuclear lamina resulted in the mislocalization of emerin to the ER (Sullivan et al., 1999). Indeed, these mice provide a unique model for studying AD-EDMD in addition to the fact that they provide insight into the relationship between lamins and INM proteins (Bonne et al., 1999).

b. Dilated cardiomyopathy

Dilated cardiomyopathy (DCM) is a myocardial disorder demarcated by dilation of the left or both ventricles and reduced systolic function resulting in progressive heart failure, thromboembolism, arrhythmia and premature death (Fatkin et al., 2010).

Representing the third most frequent cause of heart failure in the United States after coronary artery disease and hypertension, DCM is marked by significant morbidity and mortality. More than 60 genes have been associated with DCM to date (Tesson et al., 2014). Most of the identified mutations affect sarcomeric proteins and cytoskeleton of the heart muscle like myosin heavy chain, actin, dystrophin and desmin. Of particular relevance to our study are mutations linked to the *LMNA* gene. These mutations occur in the head and rod domains of lamin A/C proteins but are rarely found in the tail domain as opposed to mutations linked to EDMD, familial partial lipodystrophy (FPLD) and Hutchinson-Gilford progeria syndrome (HGPS) (Tesson et al., 2014). Moreover, genetic mutations resulting in DCM are often transmitted in an autosomal dominant manner. Currently, no specific therapy exists for DCM associated *LMNA* mutations which has encouraged researchers to establish both mice and cellular models that may aid in elucidating the mechanisms underlying the disease phenotypes. Accordingly, a missense mutation encoding a Lamin A-N195K variant was introduced into a murine *Lmna* gene by homologous recombination to create a mouse model of dilated cardiomyopathy with conduction system disease (DCM-CD1). These mice, however, did not show any evidence of muscular dystrophy. Indeed, mice homozygous for the *Lmna*-N195K mutation presented signs of DCM by 9 weeks and died at an early age due to arrhythmia. Moreover, *Lmna*^{N195K/N195K} mice showed an abnormal distribution and expression of the main gap junctions in the heart namely connexins (Cnx) that are responsible for impulse

conduction through the myocardium. Interestingly, Cnx 43 was mislocalized in the heart of these mice as immunofluorescence staining of Cnx 43 showed a diffused pattern in the atrial and ventricular chambers as opposed to a sharper and well defined distribution along the junctions found between the cells in wild-type mice. In addition, the localization of the intermediate filament protein desmin found in the Z-lines of the sarcomeres and in the intercalated discs (ID) forming cell-cell junctions between the cardiomyocytes was abnormal suggesting that *Lmna*-N195K mice have defects in the organization of the sarcomeres (Mounkes et al., 2005).

c. Limb-girdle muscular dystrophy type 1B

Limb-girdle muscular dystrophy type 1B (LGMD1B) is an autosomal dominant laminopathy displaying nonsense or missense mutations in the *LMNA* gene. LGMD1B is accompanied by symmetric muscle weakness and progressive muscular dystrophy appearing first in muscles of the proximal leg and pelvic girdle and gradually affecting the humeral arm muscles (Muchir et al., 2000). Unlike EDMD, contractures of the Achilles tendon are rarely observed or develop at a later stage. Cardiac abnormalities are seen in approximately 62% of the patients often depicted by atrioventricular conduction disturbances, arrhythmias and sudden death possibly due to tachyarrhythmia (van Berlo et al., 2005).

3. *Laminopathies affecting the adipose tissues*

a. Dunnigan-type familial partial lipodystrophy

Familial partial lipodystrophy (FPLD) is inherited in an autosomal dominant manner and is caused by mutations in the *LMNA* gene lying specifically in the C-terminal

globular domain of this gene. FPLD is characterized by the loss of subcutaneous fat in the limbs and trunk accompanied by a redistribution of the white fat after puberty (Mounkes et al., 2003). The mutation does not affect the 3D conformation of the protein; instead, it affects its interaction with protein targets. At the cellular level, FPLD results in defects in nuclear architecture, increased fragility of the nucleus and detachment of chromatin from the nuclear lamina (Capell & Collins, 2006).

b. Acquired partial lipodystrophy

Acquired partial lipodystrophy (APLD) is caused by mutations in the *LMNB2* gene which encodes for lamins B2 and B3 proteins. This disorder is accompanied with a decrease in the subcutaneous fat from the head, neck, upper extremities and thorax, but less likely from the lower extremities. APLD is more observed in females and appears before adolescence. Hypertension, dyslipidemia, and diabetes mellitus are commonly associated with this disease (Verstraeten et al., 2007).

4. *Laminopathies affecting the nervous system*

a. Charcot-Marie-Tooth neuropathy type 2

Mutations in the *LMNA* gene have been also linked to Charcot-Marie-Tooth neuropathy type 2 (CMT2), commonly known as autosomal-recessive axonal neuropathy. This syndrome arises from a homozygous missense mutation in the lamin A/C α -helical rod domain resulting in the replacement of arginine at position 298 by cysteine (R298C) (De Sandre-Giovannoli et al., 2002). CMT2 is characterized by early-onset muscular dystrophies. It is also accompanied by muscle wasting and weakening, foot deformities

in addition to axonal degeneration caused by axonal demyelination and reduced axon density.

b. Autosomal dominant leukodystrophy

Autosomal dominant leukodystrophy (ADLD) arises from a duplication of the *LMNB1* gene which encodes lamin B1 protein of the nuclear lamina and results in increased gene dosage in the brain tissue. This disease is an adult onset, slowly progressive neurological disorder characterized by high penetrance and widespread loss of myelin from the central nervous system (CNS). ADLD constitute the first human disease caused by mutations in the *LMNB1* gene. *D. melanogaster* displayed a degenerative phenotype upon overexpression of lamin B1 protein. Likewise, an abnormal nuclear morphology was depicted in *in vitro* cultured cells overexpressing lamin B1 (Padiath et al., 2006; Verstraeten et al., 2007).

5. *Laminopathies resulting in systemic disorders and premature aging*

a. Hutchinson-Gilford Progeria

Hutchinson-Gilford progeria syndrome (HGPS) is a rare and a devastating premature aging disorder affecting children at an early stage of their life with an estimated frequency of 1 per 4-8 million new births. Children affected by this disease show significant phenotypes resembling many aspects of aging. It has been recently demonstrated that progeric children display before 1 year of age diverse symptoms of aging, such as prominent eyes, protruding ears and thin lips accompanied by the appearance of a midline groove in the chin. Those children also exhibit distinct facial appearance, concave nasal ridge, joint stiffness, short clavicles and reduced subcutaneous

fat. Progeric patients die at an average age of 13.5 years as a result of cardiovascular complications due to premature atherosclerosis, myocardial infarction or stroke (Mazereeuw-Hautier et al., 2007). It is now known that progeria arises from a mutation in lamin proteins. A *de novo* point mutation by substitution occurring at codon 608 within exon 11 in the *LMNA* gene leading to the replacement of GGC by GGT has been identified in many subjects of HGPS (Muchir & Worman, 2004). This mutation creates an RNA splice donor site leading to the expression of a truncated prelamin A protein termed progerin lacking 50 amino acids from its carboxyl-terminal tail. This mutant protein termed progerin, lacks a proteolytic cleavage site for removal of the farnesylated group from the carboxyl terminal region of lamin A and is, thus, farnesylated (Mattout et al., 2006). The retained farnesylated group causes the accumulation of progerin in the inner nuclear membrane explaining in part some of the disease phenotypes (Gordon et al., 2012). Progeric patients show evidence of accumulation of progerin thereby increasing the nucleus stiffness leading to the misshapening of the nucleus, one of the hallmark characteristics of progeria at the cellular level. Consequently, the cells become more susceptible to mechanical cell death providing a possible explanation for atherosclerosis in HGPS.

b. Mandibuloacral dysplasia

Initially identified as a rare autosomal recessive disorder, Mandibuloacral dysplasia (MAD) is characterized by premature aging and post-natal growth retardation including delayed closure of the cranial suture and appearance of partial lipodystrophy. Indeed, patients with MAD exhibit a loss of subcutaneous fat from the extremities, and excess fat in the head, neck and trunk, a pattern reminiscent of FPLD patients. Moreover,

patients develop resistance to insulin and display metabolic irregularities such as, diabetes and dyslipidemia. Since patients with MAD frequently develop FPLD, it was postulated that a mutation in the *LMNA* gene may be at the onset of MAD. This was later confirmed when DNA sequencing and analysis of chromosome 1 in MAD patients identified a homozygous missense mutation in the *LMNA* gene (R527H). Further investigation has shown that nuclei from patient skin fibroblasts presented a dysmorphic envelope caused by altered assembly of the nuclear lamina which was attributed to an abnormal lamin A/C distribution; however, this pathogenic effect was not as specific to this disease as it was seen in almost all laminopathic disorders. Interestingly, R527 amino acid resides in the C-terminal tail of lamins A and C and, as mentioned earlier, the C-terminal domain serves as the binding site for several candidate proteins. As such, a mutation in this domain may perturb the 3D-structure of lamins A/C, ultimately disrupting the protein interactions mediated at or in the vicinity of this site like the binding of lamin A to the adipocyte-differentiation factor sterol-response element-binding protein 1 (SREBP1) occurring between residues 227 and 487. One possible outcome to the perturbed interaction between lamins A/C and SREBP1 is the loss of fat observed in FPLD and MAD due to reduced binding of SREBP1 to lamin A (Novelli et al., 2002).

c. Atypical Werner Syndrome

Classical Werner's syndrome (WRN) is a recessively inherited autosomal disease caused by mutations in the *WRN* gene, a member of the *RECQ* family of DNA helicases. This syndrome is associated with short stature, impaired wound healing in addition to premature aging with diabetes mellitus and atherosclerosis. However, DNA

sequencing done on several patients with the aforementioned symptoms did not show any mutations in the *WRN* gene and were accordingly classified as having atypical Werner's syndrome or non-*WRN*. A thorough investigation performed by scientists reported that the so-called atypical WRN arises from a heterozygous missense mutation in the rod domain or in the C-terminal domain of lamin A/C protein (Chen et al., 2003).

d. Restricted Dermopathy

Restricted dermopathy (RD) commonly referred to as, “lethal tight skin contracture syndrome” is a neonatal disorder caused by homozygous and compound heterozygous mutations in *FACE-1* encoding ZMPSTE24. Moreover, heterozygous truncating mutations in the *LMNA* gene have been reported in RD. Features accompanied with this disease include, translucent and partly eroded skin, multiple joint ankyloses, mouth fixed in “O” position, small pinched nose, low-set ears, clavicular hypoplasia, acro-osteolysis and cranial ossification defects. RD affected children die within few hours or days after birth due to respiratory problems particularly, restricted thoracic movements. One of the common heterozygous mutations in *LMNA* gene and resulting in RD is a heterozygous mutation leading to an in-frame skipping of the entire exon 11 of the *LMNA* gene. As such, the synthesized truncated pre-lamin A protein will lack the region that is required for the second cleavage during post-translational modification and remains farnesylated (Verstraeten et al., 2007).

E. Caveolae and Caveolins

1. Overview of Caveolae and Caveolins

Over 50 years ago, caveolae were among the first ultrastructural features of the plasma membranes to be identified by electron microscopy. Despite much progress achieved in the understanding of their composition, structure and functions in health and disease, caveolae remain one of the enigmatic features of plasma membranes. They are defined as non-clathrin coated plasma membrane pits that are 60-80nm wide and are morphologically distinguished by their sphingolipid- cholesterol microdomains (Parton & Simons, 2007). Although they are found in many mammalian cell types, caveolae are primarily abundant in fibroblasts, endothelial cells, adipocytes, and muscle cells (Figure 5, see below).

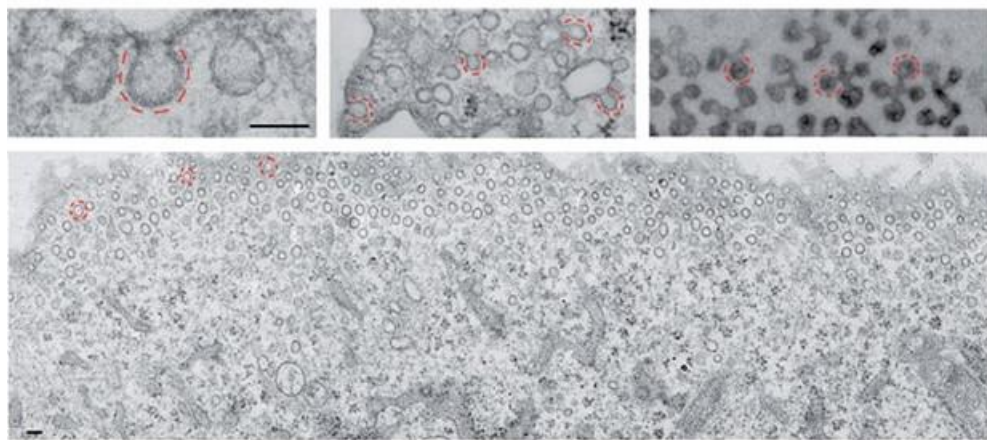


Figure 5 | Electron micrographs showing the ultrastructure of caveolae. The main panel and at high magnification upper left panel represent caveolae in fibroblasts, and the complex arrangements of caveolae in cultured adipocytes (upper middle) and in skeletal muscle (top right). Scale bar 100nm. (Modified from Parton & del Pozo, 2013)

Caveolin proteins act as the defining markers of caveolae formation since their discovery. Caveolins are also found in *C.elegans* suggesting that they are evolutionarily conserved features of metazoan life (Engelman et al., 1998). In vertebrates, the caveolin

gene family is comprised of three members namely, *CAV-1*, *CAV-2* and *CAV-3* genes encoding for caveolin-1 (Cav-1), caveolin-2 (Cav-2) and caveolin-3 (Cav-3) proteins respectively. Among caveolins, Cav-1 serves as a central component of the caveolae where it acts as a scaffolding protein within the caveolar domains of the plasma membrane in most cell types. Moreover, Cav-1 is ubiquitously expressed with particularly high levels in adipocytes, fibroblasts and endothelial cells. Cav-2 is co-expressed and co-localized with Cav-1 and requires Cav-1 for proper membrane targeting. Unlike Cav-1 and Cav-2, the expression of Cav-3 is muscle cell specific (Williams & Lisanti, 2004). In addition, some cell types express the three isoforms including smooth muscle and the zebrafish notochord (Parton & del Pozo, 2013). Noteworthy, Cav-1 and Cav-2 proteins hetero-oligomerize while Cav-1 and Cav-3 form homo-oligomers using their corresponding caveolin oligomerization domain (COD). Caveolin proteins are synthesized in the endoplasmic reticulum (ER) in a signal recognition particle dependent manner after which they begin to oligomerize. Caveolins are then transported to the Golgi complex where their exit is accelerated by cholesterol addition (Monier et al., 1996). Therefore, caveolins are predominantly available at the plasma membrane and may also exist in the endoplasmic reticulum, Golgi apparatus and vesicles as well as in the cytosol (Williams & Lisanti, 2004). All three caveolins are integral membrane proteins inserted in the caveolar membrane with both the amino and carboxyl termini facing the cytoplasm while a hairpin loop remains embedded in the lipid bilayer of the membrane and forms the caveolar scaffolding domain (CSD) which mediates protein-protein interactions and modulation of signal transduction cascades (Figure 6b, see below). In addition to their pivotal role in signal transduction, caveolins are also essential for cholesterol transport, endocytosis and transcytosis.

2. *Caveolin-1*

In vertebrates, there are two isoforms of *CAV-1*, denoted α and β . Cav-1 protein is made up of 178 amino acids and has a molecular weight of 22KDa. Both isoforms are identical except for the region of the first exon. At the protein level, both isoforms are identical except for the presence of 31 additional amino acids in the amino-terminus of Cav-1 α . It was originally believed that both isoforms arise from alternative translation initiation sites of a single mRNA; however, it was later confirmed that both isoforms of Cav-1 arise from two distinct mRNAs possibly generated by alternative splicing suggesting the existence of a transcriptional control over both isoforms (Kogo et al., 2004). Caveolin-1 undergoes post-translational modifications at its amino-terminus and carboxyl-terminus end. Indeed, Src kinase phosphorylates Cav-1 α at the tyrosine residue 14 (Y14) of its N-terminus. Moreover, several cysteine residues in the C-terminal domain of Cav-1 are S-acylated by palmitoylation (Smart et al., 1999). Accordingly, both isoforms share the hydrophobic stretch of amino acids, the caveolin scaffolding domain and the acylated C-terminal domain (Fujimoto et al., 2000) (Figure 6a, see below).

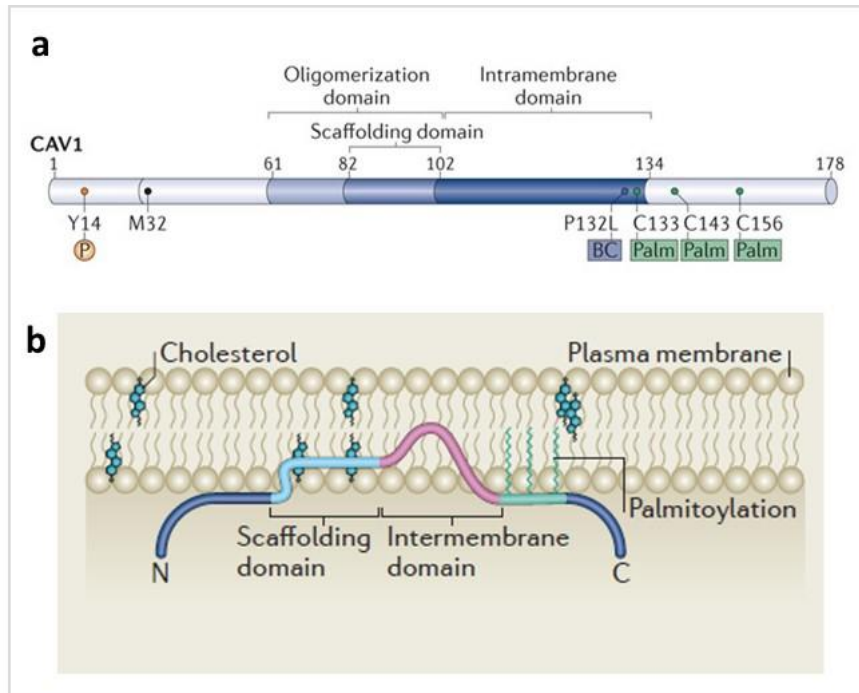


Figure 6 | Schematic representation showing the domain organization of caveolins. a) Structural organization of caveolin 1 (CAV1). Post-translational modifications and disease associated mutations are indicated in the upper panel. Numbers above the lines correspond to the amino acid in mammalian caveolins. Palmitoylation (Palm) sites in CAV1 are indicated in green, a Tyr phosphorylation site in red, and the starting Met of CAV1 β is shown in black. Disease-associated amino acid substitutions in CAV1 are shown in blue. P132L is a common mutation in CAV-1 resulting in breast cancer (BC). b) Caveolins are integral membrane proteins with hairpin loop structures embedded within the membrane and having both the amino-terminus and carboxyl-terminus in the cytoplasm. (Modified from Parton & del Pozo, 2013).

Cav-1 α and Cav-1 β isoforms were functionally characterized in the zebra fish model and were reported to display overlapping but distinct distribution throughout embryonic development (Fang et al., 2006). Their study indicates that the presence of both isoforms is required for proper caveolae formation, actin-cytoskeletal organization and vascular endothelium formation. Zebra fish embryos lacking the expression of the two isoforms showed reduced expression of neural markers and abnormal expression of the muscle differentiation marker MyoD. Interestingly, the two isoforms perform non-redundant functions as deletion of one isoform was not rescued by the heterotypic expression of the alternative isoform of the protein. Evidence for the non-overlapping

functions depicted by both isoforms emanates from the differential partners interacting with the isoforms, such as the bone morphogenetic protein (BMP) receptors that were reported to interact with Cav-1 β only. Nevertheless, the depletion of either isoform of Cav-1 from the embryos disrupted the actin cytoskeleton. Indeed, a more recent study revealed that the F-actin crosslinking protein filamin directly links caveolin-1 ligand to the actin microfilaments in the cytoplasm (Stahlhut & Deurs, 2000). That study also used the yeast-two-hybrid approach to show that Cav-1 β and not Cav-1 α might be the primary ligand for filamin providing additional evidence for the discrete biochemical functions attributed to each Cav-1 isoform. Furthermore, introducing a mutant phosphorylated Cav-1 α at Tyr 14 (pY14-Cav-1 α) into a Cav-1 β depleted embryo did not cause Cav-1 α to mimic the Cav-1 β activity demonstrating that both isoforms exhibit distinct functional roles in signal transduction in cells (Fang et al., 2006). Cav-1 α isoform was exclusively expressed in the intestinal epithelium and in the adult zebra fish endothelial cells providing ample evidence for the specific role of Cav-1 α in this context. Cav-1 was found to localize to the plasma membrane caveolae and Golgi apparatus. It may also exist in a cytoplasmic soluble form and in a secreted form depending on the cell type (Williams & Lisanti, 2004). A study performed on human cultured fibroblasts, endothelial cells and polarized epithelial cells revealed that caveolin-1 is targeted to plasma membrane caveolae domains (Li et al., 2001). The same study reported that the skeletal muscle express Cav-1 protein and specifically, the β isoform of Cav-1 along the Z-lines in the cytosol. Cav-1 is involved in integrin signaling linking integrin subunits to the tyrosine kinase FYN which is considered as an initial step in coupling integrins to the Ras-ERK pathway. Recently, *CAV-1* gene has been classified as a tumor suppressor gene candidate that negatively regulates the Ras-p42/44 mitogen activated kinase pathway

(p42/44 MAPK) (www.genecards.org/cgi-bin/carddisp.pl?gene=CAV1). Moreover, Cav-1 has been implicated in a number of pathways including G-protein beta/gamma signaling cascades, caveolar mediated endocytosis signaling, gap junctions, cell adhesion tight junctions and cytoskeletal remodeling. Likewise, Cav-1 was found to interact with multiple receptors such as the epidermal growth factor receptor (EGFR) and the transforming growth factor beta 1 receptor (TGF- β) (Razani et al., 2001). It has also been shown to play critical roles in muscle repair and regeneration (Volonte et al., 2005). Mutations in the *CAV-1* gene have been associated with a number of diseases among which are muscular dystrophies. In addition, caveolin-1 gene expression is negatively regulated by the activation of the p42/44 MAPK cascade (Smart et al., 1999). Intriguingly, the activation of the PKA pathway by pharmacological agents or its overexpression suppressed the promoter activity of caveolin-1 and was sufficient to down-regulate the Cav-1 protein expression. Accordingly, caveolin-1 can be transcriptionally down-regulated via the p42/44 MAPK and PKA signaling pathways suggesting that there exists a negative reciprocal relation between caveolin-1 and the previously stated signaling cascades such that caveolin-1 appears upstream and downstream them (Smart et al., 1999).

3. Caveolin-1 in mechanotransduction

Numerous studies pointed out to the role of caveolae and caveolin-1 in mechanotransduction particularly because of their abundance in cells exposed to mechanical stress such as the endothelial cells. Acute mechanical stress induced by osmotic swelling or by uniaxial stretching led to the rapid flattening of caveolae at the plasma membrane and a concomitant increase in the free caveolins. Cell flattening which

occurs in an ATP-independent manner provides additional membrane stored within the caveolar invagination to buffer the tension that may build up during mechanical stress (Sinha et al., 2011). Moreover, increasing the transmural pressure in vessel capillaries was accompanied by the disassembly of caveolae and their incorporation in the plasma membrane, a response aiming at regulating the membrane tension (Lee et al., 1995). One direct role for caveolae in mechanotransduction was identified in myotubes of muscular dystrophy patients that were reported to show increased susceptibility to mechanical stress because they lack a functional built up of caveolae (Sinha et al., 2011). In endothelial cells, caveolae have been implicated in transducing changes in the blood flow into biochemical signals controlling vascular function. Direct evidence for the role of caveolin-1 in mechanotransduction and remodeling of the blood vessels came from *Cav-1* knockout mice where a decrease in blood flow did not correlate with reduced lumen diameter; instead it was associated with increased wall thickness and proliferation of cells. Thus, the response of endothelial cells to changes in blood flow was impaired in *Cav-1* knockout mice suggesting that caveolin-1 acts as a mechanosensor that is directly regulated by blood flow (Yu et al., 2006). Another study conducted on smooth muscle cells supported a role for Cav-1 in mechanotransduction. It has been shown that in vascular smooth muscle cells (VSMCs) exposed to cyclic stretch, Cav-1 was rapidly redistributed to focal contacts. In addition, stretch induced cell cycle progression through the activation of the phosphatidylinositol 3-kinase (PI3K)–AKT/protein kinase B (PKB) pathway, the MAPK ERK, c-Src, and integrins providing ample evidence for a role of Cav-1 in this context. This was further validated in *Cav-1* knockout mice where the absence of Cav-1 inhibited the entry of VSMCs into the cell cycle (Sedding et al., 2005).

4. Caveolin-1 knockout and mutant mouse models

One of the remarkable features observed in knockout mice for *Cav-1*, *Cav-2* and/or *Cav-3* is that these mice remain viable and fertile despite the many functions ascribed to caveolins and their wide spread tissue distribution. Noteworthy, *Cav-1*^{-/-} mice display a complete loss of caveolae from all tissues that normally express the Cav-1 protein and from primary cell cultures derived from these mice suggesting a crucial role for Cav-1 in caveolae biogenesis (Drab et al., 2001). *Cav-1*^{-/-} mice suffer from a reduction in the protein expression of Cav-2 to less than 10% of the wild-type levels although the transcriptional levels of *Cav-2* were not affected reinforcing the fact that Cav-1 is essential for the trafficking of Cav-2 to the plasma membrane caveolae (Hnasko & Lisanti, 2003). It was shown that Cav-2 is subjected to proteolytic degradation in *Cav-1*^{-/-} mice except for residual amounts that get trapped in the Golgi apparatus (Hnasko & Lisanti, 2003). Moreover, young mice knockout for Cav-1 and fed on a normal diet become insulin resistant. Interestingly, the system that is mostly affected by the loss of Cav-1 expression is the cardiovascular system. In the heart, Cav-1 is expressed in the endothelial cells and fibroblasts but not in the cardiomyocytes. The deletion of *Cav-1* resulted in an abnormal cardiac function manifested by an enlarged right ventricular cavity and thickened left ventricular wall, a phenotype that is often associated with systolic dysfunction and myocyte hypertrophy as well as increased fibrosis in the perivascular spaces. Nevertheless, the p42/44 MAPK cascade was over activated in the cardiac tissue and fibroblasts of these mice accompanied by elevated endothelial nitric oxide synthase (eNOS) activity (Cohen et al., 2003). In addition, mice knocked out for Cav-1 develop dilated cardiomyopathy and pulmonary hypertension (Zhao et al., 2002). *Cav-2*^{-/-} mice demonstrate a normal expression and localization of Cav-1 as well as a

normal formation of caveolae; however, these mice suffered from severe pulmonary dysfunction (Razani et al., 2002). Indeed, Cav-2 deficient mouse models revealed that Cav-2 suppresses the proliferation of the lung endothelial cells (Xie et al., 2010). Mice deficient of Cav-3 lack muscle cell caveolae but maintain normal expression levels of Cav-1 and Cav-2 as well as normal caveolae domains in other tissues expressing caveolins. Deficiency of Cav-3 results in a group of muscle diseases commonly referred to as caveolinopathies (Bruno et al., 2007). Indeed, defects in Cav-3 were reported to cause four distinct skeletal muscle diseases that may be phenotypically categorized into limb girdle muscular dystrophy, rippling muscle disease, distal myopathy, and hyperCKemia. In addition, one caveolin-3 mutation has been identified in a case of hypertrophic cardiomyopathy (Gazzerro et al., 2010). Cav-3 knockout mice develop myocardial hypertrophy, dilatation and reduced fractional shortening at 4 months of age accompanied by cellular infiltration and perivascular fibrosis (Gazzerro et al., 2010). Nonetheless, Cav-3 knock-out mice show degeneration of the skeletal muscle and disorganization of the T-tubule network (Hnasko & Lisanti, 2003).

F. LKB1

I. Overview

Liver kinase B1 (LKB1), also known as serine/threonine kinase 11 (STK11), is a 50KDa tumor suppressor protein that was first found mutated in Peutz-Jeghers syndrome (PJS). Patients with PJS develop marked cutaneous pigmentation of the mucous membranes and show an increased risk of hamartomatous polyposis (outgrowth of differentiated tissues) particularly in the gastrointestinal tract. Intracellular LKB1 is implicated in regulating cell metabolism, cell polarity, cell differentiation and

proliferation, apoptosis and DNA damage response (Vaahtomeri & Mäkelä, 2011). In addition to its role in regulating cellular metabolism, LKB1 was found to be crucial for the normal embryonic development as global knockout of *Lkb1* in mice results in embryonic lethality due to defects in neural tube closure, mesenchymal cell death and abnormal vascular development. Extraembryonic development is also severely affected in these mouse models (Ylikorkala et al., 2001). In humans, the *LKB1* gene maps to chromosome 19 and is composed of 10 exons spanning 23kb (Mehenni et al., 1998). Mouse *Lkb1* gene is homologous to human *LKB1* yet it is located on chromosome 10 and spans 15kb only (Smith et al., 1999). At the transcriptional level, human *LKB1* and mouse *Lkb1* genes exist in the form of two splice variants generated by alternative splicing of the last coding exon of the *LKB1* gene in human and mouse *Lkb1*. In mammals, the splice variants are designated as LKB1_L in humans (Lkb1_L in mouse) and LKB1_S (Lkb1_S in mouse) and give rise to a 50 kDa LKB1_L or Lkb1_L protein (long form) and a 48 kDa LKB1_S or Lkb1_S protein (short form) respectively. Both isoforms differ in their C-terminal tail and their expression patterns. The short isoform is predominantly expressed in the testis with minimal expression levels in other tissues suggesting that the latter may be involved in male fertility. On the contrary, the long isoform of LKB1 or Lkb1 is ubiquitously expressed in mammalian cells (Denison et al., 2009). LKB1 serves as a master serine/threonine kinase upstream of the AMP-activated protein kinase (AMPK) family which comprises 14 members (Figure 7, see below).

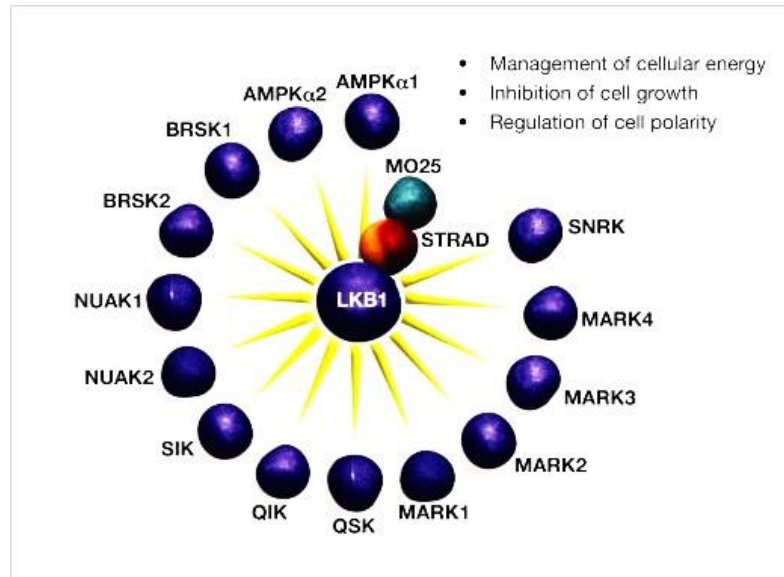


Figure 7 | Activation of the AMPK-related kinases by LKB1. Diagram representing the activation of the two isoforms of AMPK and the 12 AMPK-related kinases by the LKB1:STRAD:MO25 complex. (Amended from Alessi et al., 2006)

Mouse LKB1 is comprised of 436 residues divided into an N-terminal and C-terminal non-catalytic regions and a central catalytic domain extending from residues 44 to 309 (Figure 8, see below). The N-terminal domain contains a nuclear localization signal (NLS) while the C-terminal domain contains a conserved prenylation motif (Cys₄₃₃–Lys–Gln–Gln₄₃₆) at the carboxyl-terminus downstream of a consensus cAMP-dependent protein kinase (PKA) phosphorylation site (Alessi et al., 2006; Gan & Li, 2014). LKB1 is subjected to post-translational processing by phosphorylation and prenylation as stated above. Previous work done on LKB1 suggests that it can be phosphorylated at 8 residues. As shown in Figure 8, LKB1 is phosphorylated at Ser31, Ser325, Thr366 and Ser431 by upstream kinases. It can also be auto phosphorylated at Thr185, Thr189 and Thr336 and Ser404. At Ser431, LKB1 may be phosphorylated by PKA and p90 ribosomal S6 protein kinase (RSK) in response to agonists which trigger the activation of these kinases in an attempt to regulate cell growth through the phosphorylation of LKB1 (Collins et al., 2000; Sapkota et al., 2001). Moreover, it is

likely that *in vivo*, LKB1 is phosphorylated on Thr366 by ataxia-telangiectasia-mutated (ATM) kinase triggered by exposure of cells to radiation (Sapkota et al., 2002). In mammalian cells, LKB1 exists in a heterotrimeric complex with two other proteins, namely STE20-related adaptor (STRAD) and mouse protein 25 (MO25) (Figure 7, see above). STRAD is homologous to other protein kinases; however, it lacks several residues required for its kinase activity and was thus termed a pseudokinase. It has been shown that STRAD induces the translocation of LKB1 from the nucleus where it is initially located to the cytoplasm and enhances its catalytic activity by changing the conformation of the protein to an active form. Binding of the scaffolding protein MO25 is thought to stabilize the interaction and binding of STRAD to LKB1 (Gan & Li, 2014). The cytosolic localization of LKB1 seems to be important for its tumor suppression function as LKB1 mutants that lose their ability to enter the nucleus retain a full capacity of the tumor suppressor activity (Tiainen et al., 2002).

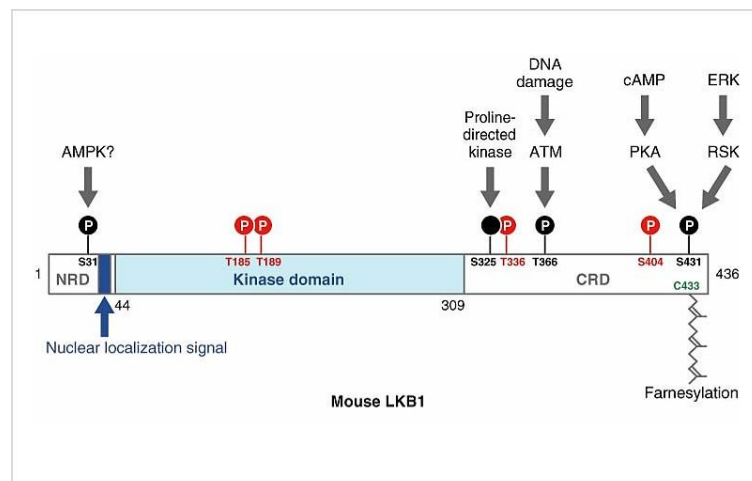


Figure 8 | Posttranslational modification sites of mouse LKB1 protein. Autophosphorylation sites are shown in red, and the sites phosphorylated by other kinases are depicted in black. The noncatalytic domains are in white and the kinase domain is in light blue. The Cys433 farnesylation site is shown in green. The upstream kinases and agonists postulated to phosphorylate each site are also indicated. (Amended from Alessi et al., 2006.)

2. LKB1 in tumor suppression

The first evidence supporting a role for LKB1 in tumor suppression came out when the overexpression of wild-type LKB1 resulted in G1 cell cycle arrest in HeLa and G361 cells which do not express LKB1 (Tiainen et al., 1999). LKB1 not only inhibits cancer cell growth or promotes death of cancer cells, but it also impedes cancer cell metastasis. This is plausibly mediated directly by LKB1 or indirectly via its downstream signaling partners. For instance, LKB1 is capable of inducing cell cycle arrest and cell death in a p53 dependent manner through AMPK signaling. Upon phosphorylation of AMPK by LKB1, the former can phosphorylate p53 activating its ability to induce cellular senescence (Jones et al., 2005). Besides, LKB1 can promote G1-induced cell cycle arrest by upregulating the expression of the CDK inhibitor p21^{WAF1/CIP1} or by physically binding to p53 in the nucleus to stabilize it and phosphorylate it directly or indirectly. LKB1 has been reported to induce apoptosis in a p53-dependent manner. It can also activate autophagy through the activation of tuberous sclerosis complex 2 (TSC2) which in turn inhibits mammalian target of rapamycin complex 1 (mTORC1) resulting in autophagy induction. Likewise, a role for LKB1 in inhibition of cancer cell invasion and metastasis has also been extensively studied and reported in *in vitro* and *in vivo* studies where the overexpression of LKB1 led to a drastic down regulation in matrix metalloproteinase-2 and -9 (MMP-2 and MMP-9) (Gan & Li, 2014).

3. LKB1 in cardiovascular physiology and pathophysiology

The role of LKB1 in the heart has been comprehensively investigated in several studies, a couple of which proposed that LKB1 signaling in the cardiac myocytes is essential for the normal atrial and ventricular development. This function has been

supported by a large body of evidence specifically upon the cardiac specific deletion of Lkb1 in mice. Indeed, these mice suffered from atrial enlargement and fibrillation 4 weeks after the deletion of Lkb1 (Ikeda et al., 2009). The cardiac phenotype was further exacerbated by the appearance of left ventricular hypertrophy 12 weeks post Lkb1 deletion from the cardiac myocytes hinting at a role for Lkb1 in the inhibition of proteins involved in cardiac hypertrophy (Noga et al., 2007). Additionally, impaired cardiac function was accompanied by a reduction in the fractional shortening, left ventricular diastolic dilation and cardiac systolic dysfunction (Ikeda et al., 2009). Aiming at elucidating the molecular mechanisms underlying the hypertrophic phenotype observed in these mice, signaling cascades downstream of Lkb1 have been investigated thoroughly. It was, thus, established that in cardiac specific Lkb1 deficient mice, the phosphorylated levels of p-AMPK were reduced. It is worth noting here that activated AMPK acts as a negative regulator of protein synthesis in normal cardiac myocytes. Consequent to the decrease observed in p-AMPK levels, the activity of the mTOR complex and its downstream kinase p70S6 increased triggering a hypertrophic response (Dolinsky et al., 2009). Lkb1-deficient cardiac myocytes were also reported to display lowered levels of the vascular endothelial growth factor (VEGF) in both the atria and ventricles. In line with this finding, previous work suggested that AMPK activation promotes VEGF expression and angiogenesis in the skeletal muscle (Ouchi, Shibata, & Walsh, 2005). One plausible explanation for the reduction in VEGF revealed upon cardiac specific deletion of Lkb1 in the heart may be that Lkb1 promotes angiogenesis through the activation of the AMPK/VEGF signaling axis in the cardiac myocytes. Other studies reported that endothelial cell specific deletion of Lkb1 led to a marked reduction in the VSMCs suggesting a defect in signal transduction between the endothelial cells

and the VSMCs (Londesborough et al., 2008). One of the main tasks prompted by VSMCs is to surround the nascent endothelial tubing and to promote maturation and stability to the blood vessels (Armulik, Abramsson, & Betsholtz, 2005). Interestingly, this process is regulated by the endothelial cells in the vasculature through the initiation of a signaling cascade towards the surrounding VSMCs. However, in the absence of VSMCs, blood vessels become fragile and more susceptible to disruption. One of the important mediators of the signaling between endothelial cells and adjacent differentiating VSMCs is TGF β that was found defective in Lkb1 deficient endothelial cells providing evidence for a role of Lkb1 in TGF β -mediated VSMC recruitment during angiogenesis in mammalian development (Londesborough et al., 2008). Nevertheless, the regulatory effect of Lkb1 on TGF β in endothelial cells warrants further investigation to elucidate the signaling cascade linking Lkb1 to TGF β .

G. Gap in Knowledge, Study Rationale and Hypothesis

The last decade was demarcated by several quantum leaps in the field of laminopathies. This holds true as the amount of research performed in this domain is dramatically rising day after day. Despite much progress, the molecular mechanisms underlying the disease pathogenesis remain to be deciphered, in particular, how mutations in a near ubiquitously expressed gene such as the *LMNA* gene, result in a diverse array of tissue specific phenotypes. Many hypotheses have been postulated to explain the tissue specific aspects of laminopathies, two of which stand out the most; namely the “structural hypothesis” and the “gene regulation hypothesis”. The structural hypothesis suggests that mutations in the *LMNA* gene in which a weakening of the lamina occurs render the nucleus more fragile and susceptible to mechanical stress

eventually leading to cell death and disease progression in mechanically stressed tissues, such as the cardiac and skeletal muscles (Broers et al., 2004; Burke & Stewart, 2002; Hutchison & Worman, 2004). Nevertheless, a clear relationship between the structural defects and the associated severe muscular phenotypes observed in laminopathies has not been yet established (Ho & Lammerding, 2012). Our interest falls on the gene regulation hypothesis which proposes that perturbed gene regulation and altered interaction with tissue specific transcription factors underlie the tissue specific phenotypes observed in laminopathies. In concordance with the gene regulation hypothesis, numerous signaling pathways directing proliferation, apoptosis and differentiation have been implicated in laminopathies, such as the Wnt- β -catenin, Notch, transforming growth factor beta (TGF- β) and the mitogen activated protein kinase (MAPK) signaling pathways (Ho & Lammerding, 2012). Our focus will be on the gene regulation theory with particular emphasis on select mechanosensitive genes; genes that respond to mechanical stress and translate the physical/mechanical force into a biochemical signal (Jaalouk & Lammerding, 2009; Nowlan et al., 2008). This interest stems out from the fact that both muscular laminopathies to be investigated are manifested in mechanically stressed tissues.

A pilot study in our laboratory investigated two mechanosensitive genes namely *Cav-1* and *Hic-5* in the context of laminopathies based on several criteria on top of which is their involvement in mechanotransduction. Additionally, we narrowed down the scope of mechanosensitive genes to those reported to respond to oxidative stress, are key players in muscle biology and myogenesis and whose knockout/mutant models display phenotypes similar to those of *Lmna* knockout/mutant models. To date, however, the role of caveolins in muscular laminopathies remains to be elucidated. Of particular

significance to this study is the identification of *Cav-1* as a mechanosensitive gene in that a large number of studies have reported its role in mechanotransduction responses particularly in the context of vascular smooth muscle cells and endothelial cells as stated earlier. Accordingly, in view of the recognized role of Cav-1 in mechanotransduction in response to changes in the stiffness of the extracellular matrix and modulations in cell-generated tension, both of which are altered in muscular laminopathies, we hereby rationalize that there is a deregulation in Cav-1 in muscular laminopathies, particularly in DCM and EDMD in terms of its expression levels and/or intracellular localization. Today, the role of Cav-1 in mechanotransduction, however, is mainly viewed as a downstream signaling platform, but little is known about its function in primary mechanosensing. Nevertheless, it remains obscure whether Cav-1 function is regulated by upstream signaling molecules. Therefore, in an attempt to investigate some of the putative upstream signaling molecules that may plausibly control the activity of Cav-1, we decided to assess in this study possible deregulations in the expression level of LKB1 in laminopathic cell lines available in our laboratory. The interest in LKB1 stems out from the fact that a very recent work done by a group of scientists reported an up-regulation in Cav-1 expression levels in endothelial cell specific deletion of LKB1 in mice *in vivo*. The same study suggested that the activity of eNOS that is maintained inactive upon the binding of Cav-1 was reduced providing better insight into the regulation of Cav-1-eNOS signaling axis by LKB1 and possibly some of its downstream targets (Zhang et al., 2014).

H. Objective of the Study and Specific Aims

Our long term objective is to gain a better understanding of the mechanisms by which distinct mutations in the *LMNA* gene contribute to the tissue specific phenotypes that result in muscular laminopathies. To this end, delineating the function mediated by *Cav-1* through studying its expression levels may provide adequate evidence regarding its biofunctional relevance in muscular laminopathies. Accordingly, for the purpose of this study (short-to-midterm), our specific aims are:

Specific Aim 1: To quantify putative deregulation in *Cav-1* (both α and β isoforms) transcriptional levels under baseline and oxidative stress conditions in mouse embryo fibroblast (MEF) cell lines derived from mice either lacking A-type lamin or emerin expression (EDMD phenotype), homozygous for the N195K mutant form (DCM phenotype) versus wild-type (WT) and in a panel of lamin A/C-deficient MEFs expressing *LMNA* WT or mutant forms that result in EDMD (E358K, L530P) by retroviral transfection.

Specific Aim 2: To assess potential alterations in Cav-1 (both α and β isoforms) protein expression and intracellular distribution under baseline and oxidative stress conditions in MEF cell lines derived from mice either lacking A-type lamin or emerin expression, homozygous for the N195K mutant form versus WT and in a panel of lamin A/C-deficient MEFs genetically altered to express the *LMNA* WT or mutant forms that result in EDMD (E358K, L530P).

Specific Aim 3: To investigate putative modulations in the translational level of LKB1 under baseline conditions in mouse embryo fibroblast (MEF) cell lines derived from

mice either lacking A-type lamin or emerin expression (EDMD phenotype), homozygous for the N195K mutant form (DCM phenotype) versus wild-type (WT) and in a panel of lamin A/C-deficient MEFs genetically modified to express the *LMNA* WT or mutant forms that result in EDMD (E358K, L530P).

I. Significance of the Study

Investigating the effects of specific lamin A/C mutations on the differential expression and distribution of the mechanosensitive gene *Cav-1* will offer new insights into the molecular mechanisms responsible for the tissue specific phenotypes observed in muscular laminopathies. Insight gained from this work would provide multiple cues to an emerging puzzle that would be pieced together by future studies. By that time, feasible therapies targeting the pathogenic consequences of lamin A/C mutations in muscular laminopathies will start to emerge.

CHAPTER II

MATERIALS AND METHODS

A. Cell Lines

Given the technical hurdles and high costs that are associated with the isolation, culturing, and maintenance of cardiac myocytes (be it neonatal or adult), all experiments in this pilot study were performed using immortalized mouse embryo fibroblast (MEF) lines as surrogate models for preliminary testing of our hypotheses. MEF lines were derived from two mouse models of EDMD; one that is lamin A/C – deficient (*Lmna*^{-/-}) and another one that is emerin – deficient (*Emd*^{-Y}). Furthermore, we tested our hypotheses in MEFs derived from the *Lmna*^{N195K/N195K} mouse model of DCM. MEFs derived from wild-type (WT) littermates (*Lmna*^{+/+}) served as controls. These cell lines were generously provided to us by Dr. Jan Lammerding (Cornell, NY).

Lmna^{-/-} mouse model was generated by removing exons 8 to part of exon 11 of the *Lmna* gene. Loss of full length transcripts and stable lamin A/C proteins was validated by Northern Blot and Western Blot analysis respectively (T Sullivan et al., 1999). At birth these mice are indistinguishable from their wild-type littermates, but their postnatal development is retarded and characterized by the appearance of muscular dystrophy. The loss of lamin A/C proteins from the nuclear envelope of MEFs derived from this model did not affect the distribution of lamins B1 and B2. However, the integrity of the nuclear envelope was compromised accompanied by mislocalization of emerin from the nuclear envelope. In addition, these cells had an irregular nuclear

morphology often highly elongated in comparison to the circular, slightly ovoid nuclei of their WT controls (Lammerding et al., 2004; Lombardi & Lammerding, 2011; Sullivan et al., 1999).

Lmnd^{N195K/N195K} represents a knock out/knock in mouse model with a missense mutation in the *Lmna* gene leading to the substitution of asparagine by lysine at amino acid 195 (Mounkes et al., 2005). Defects in the nuclear envelope of MEFs derived from these mice were routinely observed accompanied with apparent nuclear herniations, clustering of NPCs and loss of heterochromatin from the nuclear periphery. The nuclei of these cells are irregular in shape and elongated as opposed to their wild-type controls (Lammerding et al., 2004; Lombardi & Lammerding, 2011; Zwerger et al., 2013).

Emd^Y mouse model was generated by the targeted deletion of exons 2-6 in the X-linked *Emd* gene. Complete loss of the *Emd* transcript and emerin protein was confirmed by Northern Blot, Western Blot and immunofluorescence staining (Melcon et al., 2006). The nuclei of MEFs derived from this mouse model are overtly normal without any morphological alterations or any changes in the distribution of other nuclear envelope proteins including lamin A (Melcon et al., 2006).

Additionally, a panel of lamin A/C-deficient MEF cell lines retrovirally transfected to express the *LMNA* WT or mutant forms that result in EDMD (E358K, L530P) were kindly provided by the laboratory of Dr. Jan Lammerding (Cornell, NY) and have been used for further validation of the hypotheses tested under the three aims. It is worth noting that this panel of MEF lines has been widely and successfully used in other research studies aiming at answering a broad array of biochemical and biomechanical questions relevant to these disease models. Wild-type (WT) or mutant lamin A variants possessing a point mutation at amino acid 358 resulting in the

replacement of glutamic acid by lysine and at amino acid 530 leading to the replacement of leucine by proline, E358K and L530P respectively were cloned into a bicistronic retroviral vector (pRetroX-IRES-ZsGreen1, Clontech). The expression vectors were then transfected into 293GPG retroviral packaging cell line (kind gift from Richard C. Mulligan, Harvard Medical School, Massachusetts) based on the manufacturer specifications. ZsGreen1 retrovector without lamin A insert was used to generate the mock control cells. Afterwards, viral supernatants were filtered and retrovirally infected into lamin A/C – deficient MEFs. The efficiency of gene transfer was assayed 5 days after retroviral infection by flow cytometry probing ZsGreen1 levels (Rowat et al., 2013). Following sorting of MEFs, genetically modified cells that expressed the *LMNA* WT were labelled *Lmna*^{-/-} DJ1-WT-S and those that expressed the mutant forms of lamin A were termed *Lmna*^{-/-} DJ1-E358K-S and *Lmna*^{-/-} DJ1-L530P-S in comparison to their mock control *Lmna*^{-/-} DJ1-mock-S.

1. Cell Culture

Adherent MEF cells were propagated in tissue culture using specialized media consisting of Dulbecco's Modified Eagle's Medium DMEM-AQ media (Cat.# D0819, Sigma-Aldrich), supplemented with 1% penicillin–streptomycin (Cat.# DE17-602E, Lonza), 10% Fetal bovine serum (FBS) (Cat.# F9665, Sigma-Aldrich) and 1% sodium pyruvate (Cat.# S8636, Sigma-Aldrich). When monolayer cells reached 80% confluence, they were rinsed once with 5ml of 1X Phosphate Buffered Saline without Ca and Mg (PBS) (Cat.# 17-517Q, Lonza). This was followed by the addition of 1.5ml of 1X Trypsin (Lonza) to detach the cells from the surface of the 10cm plate post incubation at 37°C and 5% CO₂ for 5min. Cells were then resuspended in 6.5ml of

serum supplemented media to inactivate trypsin and centrifuged at 600xg at 4°C for 5min. Cell pellet was resuspended in 1ml of complete growth medium. Afterwards, an appropriate volume of cells depending on the split ratio was pipetted into new cell culture plates pre-filled with 10ml of complete growth medium.

2. Cell Count

Trypan blue vital exclusion stain and a hemacytometer were used to accurately determine the number of viable cells from the total population of cells in a 10cm plate. Post resuspension of the cell pellet in 1ml of complete growth medium, a sample of the cells was removed and diluted 1:10 for counting. An appropriate volume of cells (depending on seeding density) was then taken and mixed with the required volume of complete media to be distributed to cell culture plates.

B. RNA Extraction

RNA samples were isolated from *Lmna*^{+/+}, *Lmna*^{-/-}, *Lmna*^{N195K/N195K}, *Emd*^{-Y} MEFs and from *Lmna*^{-/-} DJ1-mock-S, *Lmna*^{-/-} DJ1-WT-S, *Lmna*^{-/-} DJ1-E358K-S and *Lmna*^{-/-} DJ1-L530P-S MEFs under the following conditions:

1. Baseline Conditions

Emd^{-Y} MEFs and *Lmna*^{-/-} DJ1-mock-S, *Lmna*^{-/-} DJ1-WT-S, *Lmna*^{-/-} DJ1-E358K-S and *Lmna*^{-/-} DJ1-L530P-S MEFs were seeded in 6cm plates at 13x10⁴ cells/ml in specialized serum supplemented media. When the cells reached 100% confluence, they were rinsed once with PBS(1X) and RNA was extracted from the corresponding panel of MEF cells using the TRI Reagent (TRIZol, Cat.# T9424, Sigma-Aldrich)

according to the manufacturer's specifications. RNA samples were then stored at -70°C . Extracted RNA samples were then quantified and assessed for purity and integrity using the Nanodrop Spectrophotometer (Thermonanodrop 2000C, Central Research Science Lab (CRSL) facility, AUB).

2. H_2O_2 -Induced Oxidative Stress Conditions

Lmna^{+/+} and *Lmna*^{N195K/N195K} MEFs were seeded in 12 well plates at 6.5×10^4 cells/ml while the lamin A/C knock-out MEFs were seeded in 12 well plates at 8×10^4 cells/ml in serum supplemented media. When the cells attained 100% confluence, they were treated with either 0.1-0.5 μM H_2O_2 (Hydrogen Peroxide Solution-34.5-36.5%, Cat.# 18304-L, Sigma-Aldrich) for increments of 5, 15, 30 and 60min. Hydrogen peroxide was freshly prepared at each time of use by serially diluting a sample of the stock of concentration 15.14 mol/L into 1mol/L then 0.1mol/L. This intermediate dilution was further diluted to 1mmol/L then into 50 $\mu\text{mol/L}$. A specific volume of the final dilution (50 $\mu\text{mol/L}$) was added to each well of the 12 well plate containing 2ml of complete media so that the final concentration of H_2O_2 was 0.1 μM or 0.5 μM . The final concentrations of H_2O_2 were previously optimized by Ms. Lara Kamand and were reported to stress the MEF cells without causing apoptosis (Lara Kamand, MSc Thesis 2013). Post treatment, cells were rinsed once with PBS (1X) and RNA extraction from *Lmna*^{+/+} MEFs was performed using the RNeasy Kit (QUAIGEN) based on the manufacturer's specifications. Extraction of RNA from *Lmna*^{N195K/N195K} and *Lmna*^{-/-} MEFs was done using TRI Reagent (TRIzol, Cat.# T9424, Sigma-Aldrich) according to the manufacturer's specifications. Untreated cells within each cell line and corresponding to each time point were used as controls.

C. Reverse Transcription

0.5µg or 1µg of each total input RNA sample was reverse transcribed into cDNA using the iScript cDNA Synthesis Kit (Cat.# 170-8891, Bio-Rad). Briefly, each RNA sample was mixed with 4µl of the 5X iScript Reaction Mix in addition to 1µl of the iScript reverse transcriptase enzyme and adjusted to a total volume of 20µl with nuclease free sterile water (Amresco) in a labeled pre-cooled RNase free PCR tube using barrier tips. Reverse transcription of RNA into cDNA was initiated in the DNA engine machine (Peltier thermal cycler, Bio-Rad) based on a protocol consisting of 5min at 25°C to ensure proper annealing of the random primers, followed by a 30min extension step of the cDNA strands at 42°C and eventually for 5min at 85°C to heat inactivate the iScript reverse transcriptase. All cDNA samples were stored at -20°C.

D. Quantitative Real-Time PCR

Real-Time PCR quantification of gene expression was performed using the iQ SYBR Green Supermix (Cat.# S4438, Sigma-Aldrich) with specific primer pairs for each gene (Table 1). The primer sequences pertaining to select mechanosensitive genes were previously validated and computationally derived from the MGH/Harvard Medical School Primer Bank Database (www.pga.mgh.harvard.edu/primerbank).

Table 1: A list showing the sequences of the forward and the reverse primers that were employed to quantify the transcript expression of the α isoform of <i>Cav-1</i> , α & β isoforms of <i>Cav-1</i> , and <i>18s</i> reference gene		
Gene (species)	Primer	Sequence
<i>Cav-1α</i> (mouse)	Forward	5'-GCGACCCTAAACACCTCAAC -3'
<i>Cav-1α</i> (mouse)	Reverse	5'-ATGCCGTCAAAACTGTGTGTC-3'
<i>Cav-1α+β</i> (mouse)	Forward	5'-GGCACTCATCTGGGGCATTTA-3'
<i>Cav-1α+β</i> (mouse)	Reverse	5'-CTCTTGATGCACGGTACAACC-3'
<i>18s</i> (mouse)	Forward	5'-TCAAGAACGAAAGTCGGAGG-3'
<i>18s</i> (mouse)	Reverse	5'-GGACATCTAAGG GCATCACA-3'

Each reverse transcribed cDNA sample was diluted into 1:20 to prepare a cDNA working stock by adding 5 μ l of cDNA to 95 μ l of nuclease free sterile water into a pre-cooled and autoclaved 1.5ml microfuge tube using barrier tips. Subsequently, for each 4 μ l of the diluted cDNA (1:20) derived from the different samples, 6.5 μ l of the nuclease free sterile water was added followed by 1 μ l of the 1:10 diluted forward primer and 1 μ l of the 1:10 diluted reverse primer for each gene in addition to 12.5 μ l of the Supermix so that the final volume was 25 μ l. Samples were prepared in duplicates and were kept on ice throughout the experiment. The reaction was performed using a Real-Time PCR machine (c-1000 Touch thermal cycler, Bio-Rad, CRSL facility, AUB). The protocol used consisted of the following steps: an initial heating step to 50°C for 2min followed by an increase to 95°C to melt open the double-stranded DNA helix into two single stranded DNA templates. The reaction was then allowed to cool to 60°C for 1min to ensure proper annealing of primers to their complementary single-stranded DNA templates. Afterwards, the temperature was slightly raised to 72°C for 30sec. During this extension phase, the Taq DNA polymerase extends the sequence-specific primer by incorporating complementary nucleotides to the DNA template yielding a double-

stranded DNA complex. This process was repeated for 40 cycles. The final extension step was for 10min at 72°C. Experimental results were recorded and analyzed using the Bio-Rad CFX Manager Software. In addition, expression levels for the reference gene *18s* coding for the mouse 18s ribosomal subunit were quantified to serve as internal controls for normalization within each experiment and between the independent repeats.

E. Protein Extraction, SDS-PAGE & Western Blot Analysis

I. Protein Extraction

Proteins were extracted from *Lmna*^{+/+}, *Lmna*^{-/-}, *Lmna*^{N195K/N195K}, *Emd*^{-/-} MEFs and from Lamin A/C-deficient MEFs genetically altered to express the *LMNA* WT, DJ1-WT-S, or the mutant forms that result in EDMD, DJ1-E358K-S and DJ1-L530P-S in addition to their mock control, DJ1-mock-S, under the following conditions:

a. Baseline Conditions

Lmna^{+/+}, *Lmna*^{-/-}, *Lmna*^{N195K/N195K}, *Emd*^{-/-} MEFs and *Lmna*^{-/-} DJ1-mock-S, *Lmna*^{-/-} DJ1-WT-S, *Lmna*^{-/-} DJ1-E358K-S and *Lmna*^{-/-} DJ1-L530P-S MEFs were seeded in 6cc plates at 13x10⁴ cells/ml in complete media. When the cells reached 100% confluence in culture, they were rinsed twice with pre-cooled PBS (1X) using 1.5ml /6cc dish depending on cell density. Cells were then lysed using 150µl/6cc plate of standard RIPA lysis buffer (Cat.# R-0278, Sigma-Aldrich) supplemented with Protease Inhibitor Cocktail (Cat.# P-8340, Sigma-Aldrich) at 1:1000 freshly added at the time of use. Samples were then incubated in the cold room ProBlot™ Rocker 25 for 20min. Afterwards, lysate clusters were lodged off the 6cc plates using a cell scraper and/or micropipette tip. Lysate clusters corresponding to the above mentioned MEF cells were transferred to pre-cooled sterile microfuge tubes and placed in a vertical rotator in the

cold room to allow efficient mixing for 10min. Cell lysates were then centrifuged at 12000xg at 4°C for 10min. Following centrifugation, supernatants containing protein extracts from different samples were transferred to new pre-labeled, sterile and pre-cooled microfuge tubes. Samples were then stored at -20°C. Protein extracts from *Lmna*^{+/+} MEFs served as controls for comparison between the *Lmna*^{+/+}, *Lmna*^{-/-}, *Lmna*^{N195K/N195K}, *Emd*^{-/-} panel of MEFs. Furthermore, protein extracts from *Lmna*^{+/+}, *Lmna*^{-/-}, and *Lmna*^{-/-} DJ1-mock-S were used as controls for comparison between *Lmna*^{+/+}, *Lmna*^{-/-}, *Lmna*^{-/-} DJ1-mock-S, *Lmna*^{-/-} DJ1-WT-S, *Lmna*^{-/-} DJ1-E358K-S and *Lmna*^{-/-} DJ1-L530P-S panel of mutant MEFs.

b. H₂O₂- Induced Oxidative Stress Conditions

Lmna^{+/+} and *Lmna*^{N195K/N195K} MEF cells were seeded in 12 well plates at 6.5x10⁴ cells/ml while *Lmna*^{-/-} MEFs were seeded in 12 well plates at 8x10⁴ cells/ml in serum supplemented media. When the cells reached 100% confluence, they were treated with either 0.1-0.5μM H₂O₂ for increments of 5, 15, 30 and 60min and for 1.5hrs, 2, 4 and 6hrs successively. Post exposure to H₂O₂, cells were rinsed twice with pre-cooled PBS (1X) using 1ml /well in a 12 well plate. Cells were then lysed using 100μl/well of standard RIPA lysis buffer supplemented with Phosphatase Inhibitor Cocktail III at 1:5 occasionally (Cat.# 41600096, BioWorld) and Protease Inhibitor Cocktail regularly at 1:1000 freshly added at the time of use. Samples were then processed as mentioned above. Protein extracts from mock treated control cells within each cell line and corresponding to each time point were pooled together and were used to serve as controls for comparison.

2. Sample Protein Quantification

Protein quantification was done in 96 well plates. The first two lanes were used for standardization using specific dilutions of 1mg/ml of BSA (Bovine Serum Albumin, Cat.# 0332, Amresco) in deionized distilled water (ddH₂O). The standards were prepared in duplicates with the following BSA content (µg): 0.0, 2.0, 4.0, 6.0, 8.0, and 10.0. 5µl of each sample was placed in duplicate in the subsequent lanes. Afterwards, 200µl of the Optiblot Bradford Reagent (Cat.# ab119216, Abcam) was added to each well and measurement of protein contents was performed using the SpectraMax ascent software (Multiskan EX, Thermo lab Systems).

3. SDS-PAGE: Sodium Dodecyl Sulfate-Polyacrylamide Gel Electrophoresis

a. Casting & Running the Gel

Whole cell lysates from each cell line cultured *in vitro* under baseline and H₂O₂-induced oxidative stress conditions were resolved by a 4-12% Tris-HCl buffer providing an optimal separation of the small- to medium- sized proteins. The resolving and the stacking gels were hand casted using short plates and spacer plates with 0.75mm, 1mm and 1.5mm integrated spacers. Each short plate and spacer plate of a particular thickness were evenly aligned and slid into the casting frame. The casting frame was then placed into the casting stand while ensuring its proper alignment to prevent leakage. To prepare 0.75mm thick resolving or lower gel, we mixed 1.6ml of 30% Acrylamide/Bis (Cat.# 161-0158, Bio-Rad) with 1ml of 1.5M Tris-HCl pH 8.8 (Cat.# 161-0798, Bio-Rad) and 1.4ml of deionized distilled water. We then added to the resolving gel solution 70µl of APS (Ammonium Persulfate, Cat.# 161-0700, Bio-Rad) and 10µl of TEMED (Tetramethylethylenediamine, Cat.# 0761, Ultra-pure grade,

Amresco). The mixture was smoothly poured to the lower green mark of the casting frame using a glass or a disposable plastic pipette after which we immediately overlaid the top of the resolving gel with isobutanol to prevent it from drying. The resolving gel was left for 45min to polymerize. Similarly, a 0.75mm thick stacking or upper gel was prepared by mixing 375 μ l of 30% Acrylamide/Bis with 625 μ l of 0.5M Tris-HCl pH 6.8 (Cat.# 161-0799, Bio-Rad) and 1.5ml of deionized distilled water. 70 μ l of APS and 10 μ l of TEMED were then mixed with the stacking gel solution and poured between the glass plates until the top of the short plate was reached. The comb was seated between the glass plates by securely aligning the comb ridge with the top of the short plate, and the stacking gel was left to polymerize and solidify for 15-20min. Meanwhile, 1X MOPS running buffer was prepared by measuring 14.4g of glycine (Cat.# 161-0724, Bio-Rad), 2.5g of Tris-base (Cat.# 161-0719, Bio-Rad) and 1g of SDS (Sodium Dodecyl Sulfate, Cat.# 161-0302, Bio-Rad). The mixture was dissolved in 1L of deionized distilled water on a stirrer at room temperature. Casted gels were placed into the clamping frame in the electrophoresis cell or running chamber with the short plate facing inward while sliding both arms of the clamping chamber over the gels, locking them into place. Subsequently, the chamber was filled with 1X running buffer, the combs were removed slowly and the formed wells were rinsed thoroughly with the running buffer.

b. Preparing & Loading the Samples

10-20 μ g of total protein per sample was prepared by adding to each pre-cooled sterile microfuge tube the appropriate volume of the protein sample, deionized distilled water and 5X sample buffer (composed of glycerol, SDS, 0.5M Tris-HCl pH 6.8 and

traces of bromophenol blue). Pre-made 5X sample buffer stored at -20°C was freshly mixed with 10% β -mercaptoethanol prior to each use. Samples were then denatured at 95°C for 5min using a thermobloc and placed directly on ice to prevent protein refolding. Afterwards, samples were loaded slowly using gel loading tips allowing them to evenly settle on the bottom of the wells. Precision Plus Protein standard (Cat.# 161-0373, Bio-Rad) used as a molecular weight marker for the determination of the protein size was also loaded (10 μ l). The electrophoretic cell was covered with a lid in an orientation that matches the color coded plugs on the electrode assembly and electrical leads were inserted into the power supply. SDS-PAGE was then run at 200V for 45min until the tracking dye in the sample buffer reached the bottom of the gel. Ice-buckets surrounded the running chamber shortly after the beginning of the run to prevent overheating.

c. Protein Transfer from Gel to Blot

Subsequent to the molecular weight-based migration of proteins through the gel, proteins were transferred from the gel onto a polyvinylidene fluoride (PVDF) transfer membrane (Immuno-Blot™ PVDF Membrane, Cat.# 162-0177, Bio-Rad). The PVDF membrane was cut to the desired size of the gel using a blotting paper as a reference. In brief, the membrane was activated by soaking it in 100% methanol (Sigma-Aldrich) for 1min under the fume hood. Then, the membrane was incubated in ice cold transfer buffer (1X). The standard buffer for wet transfer is the same as the (1X) Tris-glycine buffer used for the running buffer; however, instead of adding SDS, methanol was added to a final concentration of 20%. The buffer was left to completely dissolve in an Erlenmeyer flask on a stirrer and was later stored at 4°C. Sponges

(two/gel) and blotting papers (two/gel) cut to the same size of the gel were also soaked in the transfer buffer. The running buffer was poured-off the running chamber and the gel was released from the clamping frame. Meanwhile, a gel releaser was used to remove the gel and submerge it in the transfer buffer. The gel and membrane sandwich was tightly assembled by placing the membrane and the gel between the buffer-soaked blotting papers in this order: white cassette→ sponge→ blotting paper→ PVDF membrane→ gel→ blotting paper→ sponge→ black cassette ensuring that no air bubbles were trapped between the membrane and the gel. Then, the assembled gel and membrane sandwich was placed in the transfer unit with the black side of the unit facing the black cassette and the red side facing the white cassette of the sandwich. Transfer buffer (1X) was then poured into the transfer cell and a cooling unit was added. The transfer cell was then placed in a Styrofoam box covered in ice. We connected the transfer cell to the power supply and started the run at 100V for 2hrs. Later, the blotting papers and the gel were discarded in polyacrylamide waste containers and the membrane was soaked in 10ml of the 0.1% PBS-T (Phosphate Buffer Saline Tween20) washing buffer for few minutes on the ProBlot™ Rocker 25 at room temperature prior to membrane blocking.

d. Membrane Blocking, Washing & Antibody Incubations

Each membrane was incubated in 20ml of 5% non-fat dry milk (Regilait) prepared in 0.1% PBS-T to block the non-specific sites on the membrane. Incubation was performed at room temperature on the ProBlot™ Rocker 25 at 60 rpm for 1-2hrs. The blocking solution was prepared by weighing 5g of non-fat dry milk and adding it to 100ml of 0.1% PBS-T. The solution was vortexed for few minutes until the powdered

milk completely dissolved in the washing buffer. The washing buffer (0.1% PBS-T) was prepared by adding to 100ml of 10X non-sterile PBS without Ca and Mg, 900ml of deionized distilled water and adjusted to a pH of 7.2. We then added 1ml of Tween20 (Polyoxyethylene sorbitol ester, Cat.# P1379, Sigma-Aldrich) to the 1L of PBS-T (1X) at a final concentration of 0.1%. Following blocking, each membrane was incubated in a plastic pouch with 25ml of 5% non-fat dry milk prepared in 0.1% PBS-T. Each membrane was incubated with the primary antibody diluted in 3-5ml of 5% non-fat dry milk prepared in 0.1% PBS-T at 4°C on a ProBlot™ Rocker 25 at 60 rpm overnight. The primary antibodies that we probed for in this study are: Cav-1 α (N-20) used at 1:200. Cav-1 α (N-20) is a rabbit polyclonal IgG provided at 200 μ g/ml (sc-894, Santa Cruz Inc.). In addition, we probed for LKB1 (Ley37D/G6), a primary mouse monoclonal IgG provided at 1mg/ml and used at a dilution of 1:100 (ab15095, Abcam). GAPDH primary antibody was employed as a loading control for normalization within each experiment. The former is a rabbit polyclonal IgG provided at 200 μ g/ml (FL-335-sc-25778, Santa Cruz Inc.). The antibody was used at a dilution of 1:200. The next day, each membrane was placed in a plastic case and washed thrice in 20ml of the 0.1% PBS-T washing buffer at room temperature on a ProBlot™ Rocker 25 at 90 rpm, 10min each. We then proceeded by incubating each membrane with a Horseradish peroxidase (HRP)-conjugated secondary antibody directed against the species of the primary antibody. The HRP-conjugated secondary antibodies used in this study were: Goat anti rabbit IgG, 0.8 μ g/ μ l, used at 1:2500 and obtained from Jackson Immunoresearch and Goat Anti-mouse IgG H&L used at 1:2000. The Goat Anti-mouse IgG H&L was provided at 1mg/ml (ab97023, Abcam). Each membrane was incubated with the specific secondary antibody diluted as mentioned above in 5ml of 5% non-fat dry milk prepared

in 0.1% PBS-T. Incubation was done in a plastic pouch on a ProBlot™ Rocker 25 at 60 rpm for 1hr at room temperature. Post incubation with the secondary antibody, each membrane was washed in 20ml of 0.1% PBS-T washing buffer at room temperature for three times 10min each on a ProBlot™ Rocker 25 at 90 rpm.

e. X-ray Film Imaging of Western Blots

Western Lightening Chemiluminescence Reagent (ECL Western Blotting Substrate Kit, Abcam) composed of Reagent A (ab65628) and Reagent B (ab65629) were used to develop the signal using autoradiography X-ray film (AGFA) and XOMAT X-ray film processor (Optimax). In brief, 1ml of each reagent was added to the probed membrane placed in a plastic case in the dark. The membrane was left for 1min for the chemical reaction to occur while gently agitating the plastic case. Afterwards, the membrane was transferred to a cassette (Spectroline Monotec Cassette, Spectronics Corp.) and covered with a plastic pouch. The chemiluminescent signal was detected and recorded by exposure of the membrane to a light-sensitive autoradiography X-ray film inserted into the cassette in the dark room. The films were exposed for 45sec, 1min and 1.5min when the membrane was probed for Cav-1 α (N-20). In addition, films were exposed for 20sec, 30sec and 45sec when membranes were probed for LKB1 (Ley37D/G6) and for 30sec, 1min and 1.5min when probing for GAPDH primary antibody.

f. Membrane Stripping & Re-probing with a Different Primary Antibody

Membrane-bound antibody-protein complex were stripped using 15ml of 0.1M NaOH (Sodium hydroxide) prepared by diluting 1M NaOH in deionized distilled water

at room temperature for 45min. Post stripping, each membrane was washed for few minutes with 10ml of 0.1% PBS-T washing buffer. Subsequently, each membrane was blocked in 5% non-fat dry milk prepared in 0.1% PBS-T as mentioned earlier at room temperature on a ProBlot™ Rocker 25 at 60 rpm for 1hr. This was followed by incubation with 3-5ml of primary antibody such as GAPDH prepared in 5% non-fat dry milk in 0.1% PBS-T washing buffer on a ProBlot™ Rocker 25 at 60 rpm for 1hr. We then proceeded as mentioned previously by washing the membrane thrice in 0.1% PBS-T washing buffer for 10min each and incubating the membrane with the HRP-conjugated secondary antibody directed against the species of the primary antibody. Western Blot experiment was completed thereafter by washing the membrane with 0.1% PBS-T for three times 10min each and developing a chemiluminescent signal using an autoradiography X-ray film (AGFA) as stated previously.

g. Western Blots Densitometry Analysis

Protein expression levels were quantified by densitometry normalized to GAPDH loading controls using Image J 1.49 free Java image processing program software. The software was downloaded from an online application source that is made available for the public: <http://imagej.nih.gov/ij/download.html>. Developed X-ray films pertaining to the protein of interest such as, Cav-1 α or LKB1 and GAPDH loading controls were scanned on a flatbed scanner in .tif format at 1200 dpi. Densitometry analysis using Image J software was done by converting the scanned X-ray film image to an 8-bit type gray-scale image. We then proceeded by outlining the left most lane using the rectangular selection tool in the Image J toolbar. Outlined rectangles should be tall and narrow to enclose band(s) in one single lane. The outlined lane was then

highlighted and labelled. The rectangular selection was dragged over right to the next lane, highlighted and labelled. This step was repeated for each subsequent lane. A lane profile plot was later generated for each lane showing peaks corresponding to the relative density of the contents of the rectangle covering each lane. To decrease the background noise that occasionally accompanies Western Blot, drop lines were used to close off the peaks of interest so that each peak defines a closed area using the Straight Line selection tool from Image J toolbar. This step requires some subjective judgment on the behalf of the user to determine where the peaks ends and where the background noise starts. The Wand tool was then utilized to measure the area of each peak. After highlighting all of the peaks with the Wand tool available in the Image J toolbar, each measured peak was labelled with its size as a percent of the total size of the measured peaks. Results were then pasted into an Excel spreadsheet where the Relative density of the previously measured peaks was calculated in comparison to a standard by dividing the percent value of each lane by the percent value of the standard lane. Under baseline conditions, the density of each selected sample corresponding to *Lmna*^{-/-}, *Lmna*^{N195K/N195K} and *Emd*^{+/Y} MEFs was measured relative to the protein expression levels in *Lmna*^{+/+} MEFs. Moreover, the density of the selected samples pertaining to *Lmna*^{-/-} DJ1-mock-S was measured relative to the protein expression levels of *Lmna*^{-/-} MEFs, and the density of the selected samples corresponding to *Lmna*^{-/-} DJ1-WT-S, *Lmna*^{-/-} DJ1-E358K-S and *Lmna*^{-/-} DJ1-L530P-S was measured relative to the protein expression levels of *Lmna*^{-/-} DJ1-mock-S. However, under oxidative stress conditions, the densities of the selected samples were calculated relative to the protein expression level in the mock treated control MEFs within each cell line. The relative density of each protein of interest in each sample was then adjusted to the relative density of GAPDH loading

control by dividing relative density of each sample by the loading control relative density for that same sample.

F. Immunofluorescence Staining

MEF cells were seeded at 13×10^4 cells/ml in 6- well plates on 22 x 22 mm wide and 0.17-0.25mm thick square cover glass (Corning) using 4ml of complete media per well. Cells were left to adhere overnight to two days at 37°C and 5% CO₂ until they reached 80-85% confluence. At that time, cells were rinsed twice in 2ml of 1X PBS, 5min each. Before proceeding with the experiment, cells were checked for overall confluence, spreading and integrity using a phase contrast microscope (Olympus IX 71 microscope, Biology Department, AUB). Cells were then fixed using 2ml of freshly prepared 4% PFA in 1X PBS at room temperature for 20min. The 4% PFA was prepared by diluting the 16% PFA solution (Paraformaldehyde, Cat.# 15710, Electron Microscopy Sciences) in 1X PBS. Cells were washed three times in 2ml of 1X PBS; a quick first wash followed by two washes, 5min each. Next, cells were permeabilized with 1.5ml of freshly prepared 0.2% Triton X-100 in 1X PBS at room temperature for 10min. The 0.2% Triton X-100 was prepared by diluting a working stock of 10% Triton-X in 1X PBS. The latter was also prepared by diluting the original stock of Triton[®] X-100 (t-Octylphenoxy polyethoxy ethanol, Cat.# T8787, Sigma-Aldrich) in 1X PBS. Following permeabilization, cells were rinsed three times in 2ml of 1X PBS as mentioned above and blocked in 2ml of 2% BSA in 1X PBS at room temperature for 2hrs. The 2% BSA in 1X PBS was prepared by diluting the -20°C stored working stock of 10% BSA in 1X PBS depending on the number of samples. After 2hrs of blocking, the blocking media was removed and the wells were rinsed once in 2ml of 1X PBS for

5min. The coverslips were then transferred using fine tip forceps to a humidified tray and flipped onto 0.5ml of the primary antibody of interest added over a piece of parafilm. Incubation with the primary antibody was performed at room temperature for 2hrs. All primary antibodies were used at recommended dilutions according to the manufacturer's specifications and were prepared in 1% BSA in 1X PBS. Cells were incubated with Cav-1 α (N-20), a rabbit polyclonal IgG provided at 200 μ g/ml and used at 1:200 (sc-894, Santa Cruz Inc.). Following incubation with the primary antibody, coverslips were returned to the 6-well plate(s) while ensuring that the cells were properly oriented right side up for washing. Cells were then washed for three times in 2ml of 1X PBS for 5min each on the ProBlot™ Rocker 25 at 30 rpm at room temperature. Afterwards, cells were incubated with 1ml of the Alexa Fluor-conjugated secondary antibody prepared in PBS only at room temperature on a ProBlot™ Rocker 25 at 30 rpm for 1hr. The secondary antibody used in this study is Alexa Fluor® 488 conjugated goat anti-rabbit IgG (H&L) provided at 1.5 μ g/ μ l and used at 1:200 (Jackson ImmunoResearch). Cells were next washed three times in 2ml of 1X PBS, 5min each at room temperature and on a ProBlot™ Rocker 25 at 30 rpm. Secondary only incubated coverslips corresponding to each tested cell line were used as negative controls to demonstrate low non-specific binding of the secondary antibody. Finally, we mounted the coverslips on glass slides that were previously cleaned with deionized distilled water. This step was carried out by dispensing one drop of the UltraCruz™ Hard-set Mounting Medium provided as a 10ml solution containing 1.5 μ g/ml of 4',6-diamidino-2-phenylindole (DAPI) as a DNA counterstain onto the glass slides and placing the coverslip cell side down in a forward motion after removing excess of 1X PBS remaining on the coverslip due to the washing steps by simply holding the coverslip

vertically against a kim wipe. Excess mounting medium flowing out from under the coverslips and spilling on the sides were removed using the tip of a folded kim wipe. This was followed by sealing the edges of the coverslips with nail polish and placing the slides in a slide box in the dark at room temperature overnight for microscopic imaging. The next day, stained cells were imaged then placed at 4°C for long-term storage.

G. Microscopic Imaging

Image acquisition was performed within 24 to 48hrs of staining using the fluorescence Olympus microscope (Axiovert 200, Zeiss, CRSL facility). Stained cells were first examined with a standard phase-contrast microscope (Olympus microscope, Axiovert 200, Zeiss, CRSL facility) to assess overall confluence, integrity and spreading of cells. Fluorescence image acquisition was done with 20x and 40x objective magnification for quantification of fluorescence intensity. We acquired nine frames per slide with the 20x objective magnification and four frames per slide with the 40x objective magnification. As for the negative control slides, three frames per slide were imaged.

Cells stained for Cav-1 α primary antibody were examined using the FS14 fluorescence filter of the fluorescence microscope as the excitation wavelength of Alexa 488 fluorophore is 495nm and its emission wavelength is 519nm. Acquisition of images pertaining to Cav-1 α protein was done at an exposure of 3000ms. Acquisition of images for DAPI DNA counterstain was done with the FS02 fluorescence filter using one exposure time point for each slide.

Confocal microscopy images were acquired using the LSM710 Confocal Microscope (Carl Zeiss, DTS facility) for representative images of both caveolin-1 α and

DAPI using the 63x/ 1.40 oil DIC M27 objective magnification. As for the negative control slides, three frames per slide were imaged.

H. Statistical Analysis

In all experiments performed, data are expressed as mean \pm standard error of the mean (SEM) derived from 3 to 5 independent experiments per group and in some assays as in Real-Time PCR, they were done in duplicates. Statistical analysis was carried out using Microsoft Excel Program and IBM SPSS Statistics 20. Data were analyzed either with two-tailed student t-test for comparison between two groups or using one-way ANOVA followed by the 2-sided Dunnett post hoc test for comparisons of several groups with a control. Groups were considered significantly different at values of $P \leq 0.05$, with the symbols ‘*’ for $P \leq 0.05$, ‘**’ for $P \leq 0.01$ and ‘***’ for $P \leq 0.001$.

CHAPTER III

RESULTS

A. Assess putative deregulations in *Cav-1* (α & β isoforms) transcriptional levels under baseline and oxidative stress conditions in mouse embryo fibroblast (MEF) cell lines derived from mice either lacking A-type lamin expression or emerin expression (EDMD phenotype), homozygous for the N195K mutant form (DCM phenotype) versus wild-type (WT) and in a panel of lamin A/C-deficient MEFs retrovirally transfected to express *LMNA* WT or mutant forms that result in EDMD (E358K, L530P).

1. *Cav-1 α* and total *Cav-1* (α + β) are down-regulated in *Lmna*^{-/-} MEFs (Lamin A/C null) and significantly upregulated in *Lmna*^{N195K/N195K} MEFs and *Emd*^{-Y} MEFs (*Emd* null) under baseline conditions in comparison to *Lmna*^{+/+} control MEFs.

We aimed to determine transcriptional expression levels of *Cav-1* (α & β isoforms) in *Lmna*^{-/-} MEFs, *Lmna*^{N195K/N195K} MEFs and *Emd*^{-Y} MEFs under baseline conditions. For this purpose, quantitative Real-Time PCR (qRT-PCR) experiments were performed on the aforementioned MEF cells post RNA extraction and cDNA synthesis while ensuring consistency in cell density, spreading and confluency across tested samples and in independent repeats. Under baseline conditions and when normalized to the transcriptional levels of *18s* reference gene, Real-Time PCR quantification data revealed that the expression of *Cav-1 α* in *Lmna*^{-/-} MEFs was down-regulated with a 0.68-fold (± 0.2) of that of the control *Lmna*^{+/+} MEFs reflecting an approximately 30% reduction in transcript expression. This reduction, however, was not statistically significant from that of the *Lmna*^{+/+} MEFs (P -value > 0.05). In *Lmna*^{N195K/N195K} MEFs, *Cav-1 α* transcript expression was significantly up-regulated with a 1.98-fold (± 0.35) change when compared to that of the control *Lmna*^{+/+} MEFs (P -value < 0.05). A similar significant up-regulation in the *Cav-1 α* transcript expression was observed in the *Emd*^{-Y}

MEFs with a 2.03-fold (± 0.21) of that of the control *Lmna*^{+/+} MEFs (P -value <0.05).

Data represent mean fold difference \pm SEM of four independent experiments, each done in duplicates. (Figure 9A, see below).

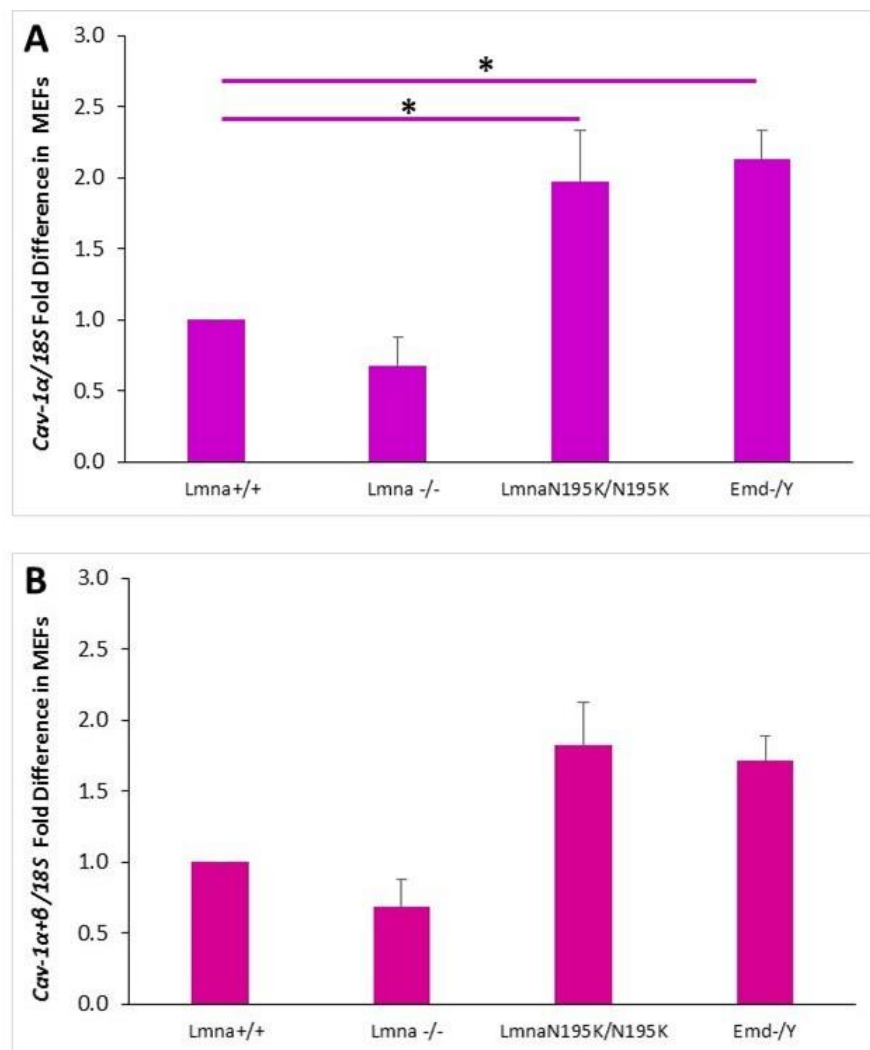


Figure 9 | Mean fold change in *Cav-1* transcript expression in *Lmna*^{-/-}, *Lmna*^{N195K/N195K} and *Emd*^{-Y} MEF cells in comparison to WT controls at baseline conditions. Real-Time PCR quantification data suggest that the *Cav-1α* (panel A) and total *Cav-1* (panel B) transcript expression is down-regulated in MEFs deficient in A-type lamins and is up-regulated in MEF cells expressing the *Lmna* N195K mutant form and in the *Emd*-deficient MEFs. *Cav-1* transcript expression was normalized to that of the *18s* reference gene. Data represent mean fold difference \pm SEM in comparison to WT controls derived from 4 independent experiments; each performed in duplicates. One asterisk represents a statistical significance ($P < 0.05$).

Quantification of the total pool of *Cav-1* ($\alpha+\beta$ isoforms) transcript by Real-Time PCR suggests that the total pool of *Cav-1* follows a similar expression pattern as that of the α isoform of *Cav-1* (Figure 9B, see above). Indeed, our quantification results normalized to the transcriptional levels of *18s* reference gene indicate that *Cav-1*($\alpha+\beta$) transcript level in the lamin A/C-deficient MEFs is lower relative to the control *Lmna*^{+/+} MEFs with a 0.69-fold (± 0.19). The obtained reduction was not statistically significant (P -value > 0.05) reflecting a similar 30% reduction in the β isoform as observed in the *Cav-1* α transcript. On the contrary, *Cav-1*($\alpha+\beta$) transcript level was up-regulated in both *Lmna*^{N195K/N195K} and *Emd*^{-Y} MEFs with a 1.82-fold (± 0.3) and 1.71-fold (± 0.17) difference in comparison to their wild-type controls under baseline conditions respectively. Nevertheless, the observed increase in *Cav-1*($\alpha+\beta$) transcriptional levels was not determined to be statistically significant (P -value > 0.05). Quantification data represented as mean fold difference \pm SEM was generated from four independent experiments, each done in duplicates (Figure 9B, see above). The marked up-regulation seen in both N195K MEFs and *Emd* null MEFs was more pronounced in *Cav-1* α with slight differences from the expression of *Cav-1*($\alpha+\beta$) suggesting that the β isoform was slightly lower than the α isoform particularly in the *Emd*^{-Y} MEFs.

2. *Cav-1* α and total *Cav-1* (α & β) immediate-early transcripts are induced in *Lmna*^{-/-} MEFs and *Lmna*^{N195K/N195K} MEFs post exposure to H₂O₂-induced oxidative stress in comparison to the control *Lmna*^{+/+} MEFs.

To assess the response of *Cav-1* (both isoforms α & β) to H₂O₂-induced oxidative stress, cells from *Lmna*^{+/+}, *Lmna*^{-/-} and *Lmna*^{N195K/N195K} MEFs were seeded to full confluence while ensuring consistency in cell-cell contact profiles across tested samples and in independent repeats. Cells from the different lines were exposed to

0.1 μ M and 0.5 μ M of H₂O₂ for time increments of 5, 15, 30 and 60min, followed by RNA extraction, reverse transcription and Real-Time PCR assessment.

- a. *Cav-1 α* and *Cav-1 (α + β)* transcriptional levels are not altered in *Lmna*^{+/+} MEF cells following exposure to 0.1 μ M and 0.5 μ M H₂O₂ for 5, 15, 30 and 60min in comparison to mock-treated controls (0.0 μ M H₂O₂).

We intended to determine any alterations in the transcriptional levels of the immediate-early transcript *Cav-1 α* and *Cav-1 (α & β)* in response to H₂O₂-induced oxidative stress when *Lmna*^{+/+} MEF cells reached 80% confluence in addition to full confluence in an attempt to study the differential response of wild-type cells cultured at different densities to oxidative stress. Our Real-Time PCR data suggest that in wild-type MEF cells cultured at both densities, the transcriptional levels of *Cav-1 α* and *Cav-1 (α & β)* were not altered following exposure to 0.1 μ M and 0.5 μ M of H₂O₂ for 5, 15, 30, and 60min in comparison to mock-treated controls (0.0 μ M H₂O₂). At 80% confluence, we obtained a 1.35- and 1.31-fold (\pm 0.19 and \pm 0.43) increase in the *Cav-1 α* immediate-early transcript in response to a 5min exposure to 0.1 μ M and 0.5 μ M of H₂O₂ respectively (Figure 10A, see below). This increase was not noted to be statistically significant in comparison to the mock-treated *Lmna*^{+/+} MEFs (0.0 μ M H₂O₂) (*P*-value>0.05). At 15min post exposure to 0.1 μ M and 0.5 μ M of H₂O₂, *Cav-1 α* transcript levels nearly normalized with 1.12- and 1.18-fold (\pm 0.05 and \pm 0.12) change respectively and were not statistically different from their mock control (*P*-value>0.05). Moreover, in response to a 30min treatment with 0.1 μ M of H₂O₂, the *Cav-1 α* transcriptional levels remained steady at 1.08-fold (\pm 0.19) without showing any significant difference from the mock control at the same time point (*P*-value>0.05). On the contrary, the α isoform of *Cav-1* increased to 1.61-fold (\pm 0.46) following a 30min

treatment with 0.5 μ M of H₂O₂, but the increase was statistically insignificant in comparison to the mock-treated controls (P -value>0.05). Following 60min of exposure to 0.1 μ M and 0.5 μ M of H₂O₂, the *Cav-1 α* transcript levels in *Lmna*^{+/+} MEFs reached a 1.21- and 1.73-fold change (\pm 0.15 and \pm 0.0) when compared to the mock *Lmna*^{+/+} MEF controls suggesting that the α isoform of *Cav-1* remained nearly steady when exposed to 0.1 μ M of H₂O₂ whereas a minimal rise in the expression of *Cav-1 α* was detected in response to 0.5 μ M of H₂O₂. In both cases, we were not capable of detecting a significant difference in the transcriptional levels of the α isoform of *Cav-1* in comparison to the mock-treated control *Lmna*^{+/+} MEFs. Data represent mean fold difference \pm SEM of three independent experiments, each done in duplicates.

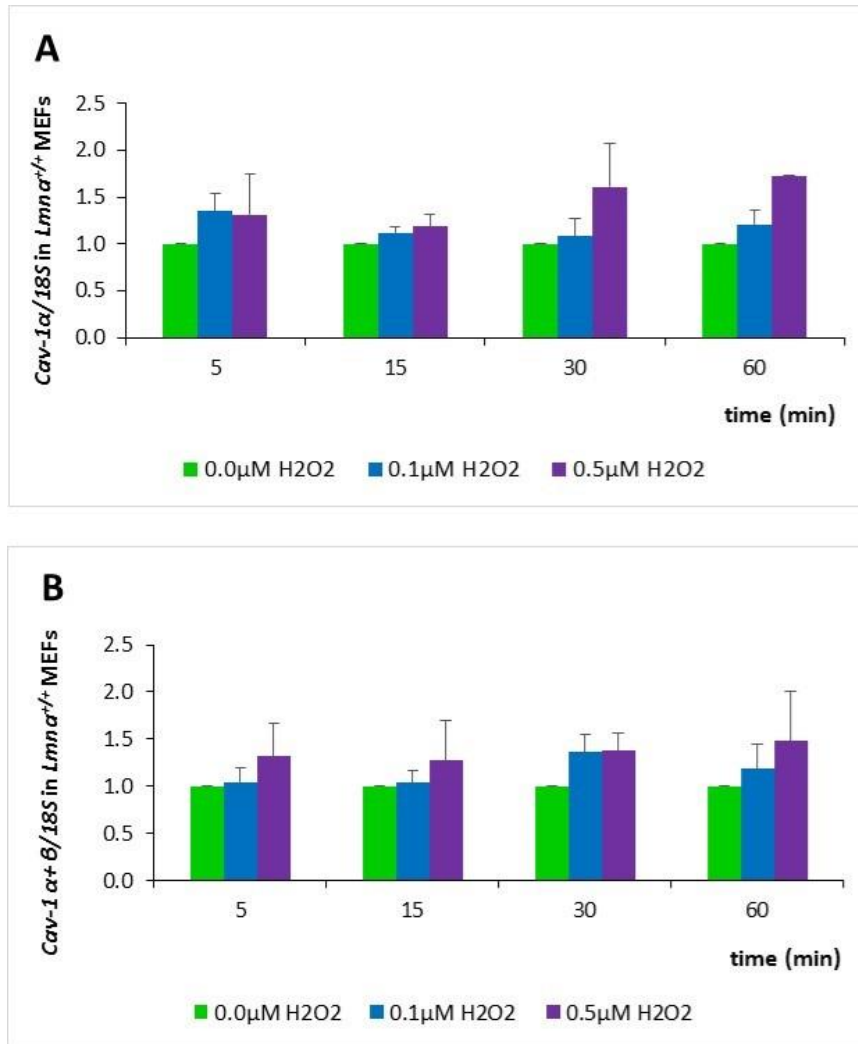


Figure 10 | Mean fold change in *Cav-1* transcript expression in *Lmna*^{+/+} MEF cells (wild-type model) cultured at 80% confluence under H₂O₂-induced oxidative stress conditions. Data from Real-Time PCR quantification indicate that immediate-early transcript expression of *Cav-1α* (panel A) and total ($\alpha+\beta$) *Cav-1* (panel B) normalized to that of *18s* reference gene is not significantly altered in *Lmna*^{+/+} MEF cells following exposure to 0.1μM or 0.5μM of H₂O₂ for 5, 15, 30, and 60min in comparison to mock-treated controls (0.0μM H₂O₂). Data represent mean fold change \pm SEM derived from 3 independent experiments; each performed in duplicates.

In *Lmna*^{+/+} MEF cells cultured at 80% sub-confluence, the total *Cav-1* pool was not significantly altered in response to both doses of H₂O₂ at any of the four studied time points (P -value>0.05) (Figure 10B, see above). At 5min post exposure to 0.1μM and 0.5μM of H₂O₂, the transcriptional levels of *Cav-1*($\alpha+\beta$) normalized to *18s*

reference gene were not statistically significant with a 1.05- and 1.32-fold (± 0.16 and ± 0.35) change in comparison to the mock-treated control *Lmna*^{+/+} MEFs respectively (P -value >0.05). The response of the wild-type cells to both doses of H₂O₂ after 15min of exposure was similar to their response at 5min with a 1.04- and 1.28-fold (± 0.13 and ± 0.42) change which was also not statistically different from the mock-treated cells (0.0 μ M H₂O₂). Following 30min of exposure to 0.1 μ M of H₂O₂, the total *Cav-1* transcript levels increased to 1.36-fold (± 0.19). This value was roughly identical to the total *Cav-1* transcriptional levels obtained at the same time point but in response to 0.5 μ M of H₂O₂ (1.38-fold ± 0.18). The attained transcriptional levels were not noted to be different when compared to the mock-treated control cells. A similar insignificant difference in the expression of the *Cav-1*($\alpha+\beta$) was observed 60min post exposure to 0.1 μ M and 0.5 μ M of H₂O₂ with a respective 1.18- and 1.48-fold- (± 0.26 and ± 0.53) difference relative to the mock-treated control wild-type cells (P -value >0.05). Data represent mean fold difference \pm SEM of three independent experiments, each done in duplicates.

Quantification of the *Cav-1* α transcriptional levels normalized to *18s* reference gene in wild-type MEFs at full confluence proposes that the exposure of these cells to 0.1 μ M and 0.5 μ M of H₂O₂ for the four depicted time points did not induce a significant modulation in the expression of the *Cav-1* α transcript (Figure 11A, see below). *Lmna*^{+/+} MEFs exposed for 5min to both doses of H₂O₂ remained near baseline levels with a 1.21- and 1.05-fold (± 0.47 and ± 0.15) in response to 0.1 μ M and 0.5 μ M respectively. No significant difference in the transcript levels of *Cav-1* α was detected in comparison to the mock-treated wild-type controls at this time point (P -value >0.05). A comparable pattern of *Cav-1* α transcript expression was seen 15min post treatment with H₂O₂ with a

1.26- and 0.91-fold (± 0.32 and ± 0.23) change relative to the control treated cells. The expression levels of *Cav-1 α* transcript in response to 0.1 μ M H₂O₂ remained stable even after 30min of exposure to H₂O₂ followed by a slight insignificant decrease to 0.87-fold (± 0.17) 60min post exposure to 0.1 μ M H₂O₂ (P -value >0.05) in comparison to the mock-treated control cells. In contrast, *Cav-1 α* transcript levels in response to 0.5 μ M H₂O₂ increased to 1.29-fold (± 0.32) change relative to the *Lmna*^{+/+} mock-treated control MEFs 30min post exposure to H₂O₂, but the increase was not determined to be significant. After 60min of exposure to 0.5 μ M H₂O₂, the transcriptional levels of *Cav-1 α* normalized to *18s* reference gene was 1.66-fold (± 0.72) change in comparison to the mock-treated cells. The detected increase was not significant (P -value >0.05).

Quantification of the Real-Time PCR data represent mean fold difference \pm SEM of three independent experiments, each done in duplicates.

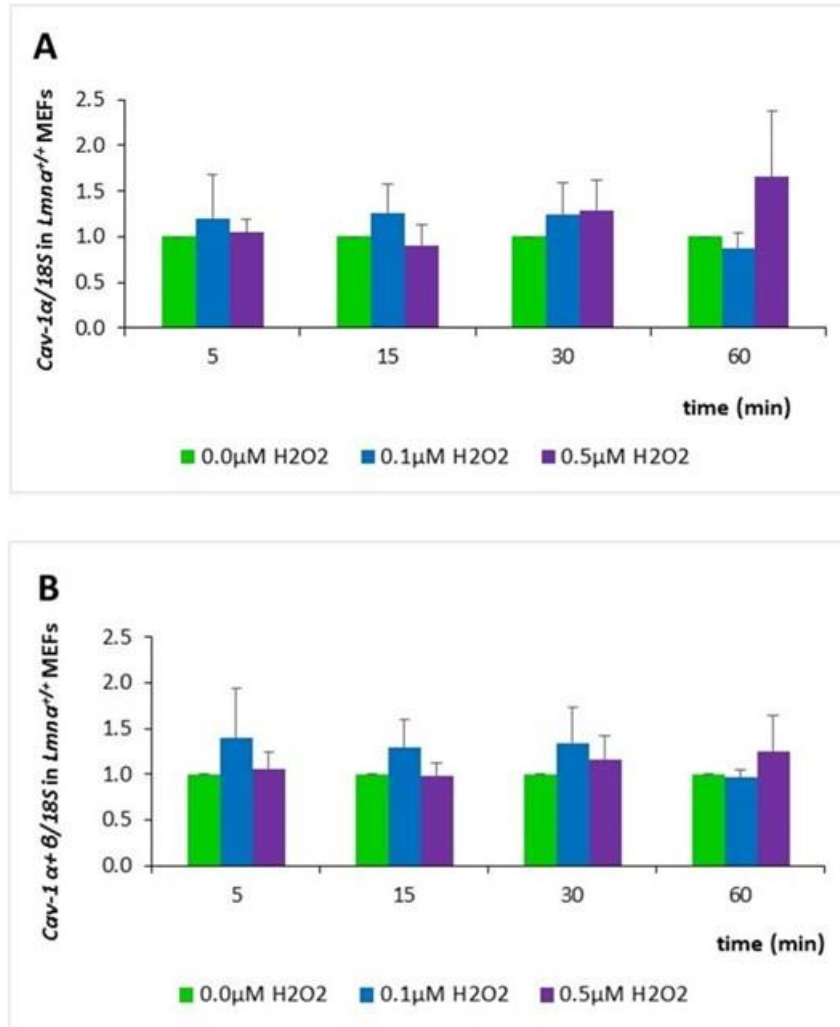


Figure 11| Mean fold change in *Cav-1* transcript expression in *Lmna*^{+/+} MEF cells (wild-type model) cultured at full confluence under H₂O₂-induced oxidative stress conditions. Data from Real-Time PCR quantification indicate that immediate-early transcript expression of *Cav-1α* (panel A) and total ($\alpha+\beta$) *Cav-1* (panel B) normalized to that of *18s* reference gene is not significantly altered in *Lmna*^{+/+} MEF cells following exposure to 0.1 μM or 0.5 μM of H₂O₂ for 5, 15, 30, and 60min in comparison to mock-treated controls (0.0 μM H₂O₂). Data represent mean fold change \pm SEM derived from 3 independent experiments; each performed in duplicates.

We also aimed at studying any alteration in the total pool of *Cav-1* ($\alpha+\beta$) normalized to *18s* reference gene in wild-type cells at full confluence. As shown in Figure 11B, the expression of the total pool of *Cav-1* was unaltered in response to the two applied doses of H₂O₂ and within the expected 60min duration (P -value>0.05).

Indeed, in response to 5min of exposure to 0.1 μ M and 0.5 μ M of H₂O₂, we noticed a 1.40- and 1.05-fold change (± 0.54 and ± 0.19) in the total pool of *Cav-1* in comparison to the mock-treated cells. After 15min of exposure to H₂O₂, a similar pattern of transcriptional expression was observed with a 1.30- and 0.99-fold change (± 0.30 and ± 0.14) in response to 0.1 μ M and 0.5 μ M of H₂O₂ without showing any significant difference in comparison to the wild-type control cells. The *Cav-1*($\alpha+\beta$) transcriptional levels in response to 0.1 μ M of H₂O₂ for 30min became constant at 1.34-fold (± 0.39), yet it was not determined to be statistically significant relative to the mock-treated control wild-type cells. Moreover, the total pool of *Cav-1* transcription levels increased slightly to reach 1.17-fold (± 0.25) upon exposing the cells to 0.5 μ M of H₂O₂ without showing any statistical significance when compared to the mock-treated control wild-type cells. Following 60min of exposure to both doses of H₂O₂, total *Cav-1* pool normalized in response to 0.1 μ M H₂O₂ with a 0.96-fold (± 0.09). In response to 0.5 μ M of H₂O₂, the total *Cav-1* pool remained nearly stable with a 1.26-fold (± 0.39), both of which were not statistically different from the mock-treated control *Lmna*^{+/+} MEFs. Data represent mean fold difference \pm SEM of three independent experiments, each done in duplicates.

- b. *Cav-1* α and *Cav-1* ($\alpha+\beta$) transcriptional levels are induced in *Lmna*^{-/-} MEF cells following exposure to 0.1 μ M and 0.5 μ M H₂O₂ for 5, 15, 30 and 60min in comparison to mock-treated controls (0.0 μ M H₂O₂).

A rapid response to 0.1 μ M and 0.5 μ M of H₂O₂ was obtained upon the quantification of the *Cav-1* α transcriptional levels normalized to *18s* reference gene in lamin A/C-deficient MEFs (Figure 12A). Real-Time PCR data suggest a 1.74- and 2.26-fold (± 0.23 and ± 0.38) increase in the *Cav-1* α transcript 5min post exposure to 0.1 μ M and 0.5 μ M of H₂O₂ respectively. The marked elevation of *Cav-1* α transcript in response

to 0.5 μ M of H₂O₂ was determined to be statistically significant in comparison to the mock-treated control *Lmna*^{-/-} MEFs (*P*-value \leq 0.01); however, we were not capable of detecting a statistical significance in the *Cav-1 α* transcript post exposure to 0.1 μ M of H₂O₂. Following 15min of exposure to both doses of H₂O₂, the transcriptional levels of the α isoform of *Cav-1* were up-regulated to approximately equal levels in response to 0.1 μ M and 0.5 μ M of H₂O₂ whereby a 2.12- and 2.17-fold increase (\pm 0.52 and \pm 0.49) was measured respectively. Nevertheless, both responses in the *Cav-1 α* transcript were not noted to be statistically significant which may likely be explained by the large standard error obtained between the independent repeats (*P*-value $>$ 0.05). A slight drop in the *Cav-1 α* transcriptional levels was detected after 30min of exposure to 0.1 μ M and 0.5 μ M of H₂O₂ in that a 1.46- and 1.55-fold (\pm 0.41 and \pm 0.26) decrease was measured neither of which was considered statistically different from the mock-treated control *Lmna*^{-/-} MEFs (*P*-value $>$ 0.05). The expression of the *Cav-1 α* transcript increased and reached equal levels following a 60min exposure to 0.1 μ M and 0.5 μ M of H₂O₂ in that a 2.03- and 2.03-fold (\pm 0.35 and \pm 0.31) change was quantified respectively suggesting that *Cav-1 α* transcript elicited a similar response to both concentrations of H₂O₂ after 15, 30 and 60min of treatment. Notably, *Cav-1 α* transcript levels were statistically different from the mock-treated control cells in response to both doses of H₂O₂ (*P*-value \leq 0.05) at 60min post exposure. Results represent mean fold difference \pm SEM of four independent experiment, each performed in duplicates.

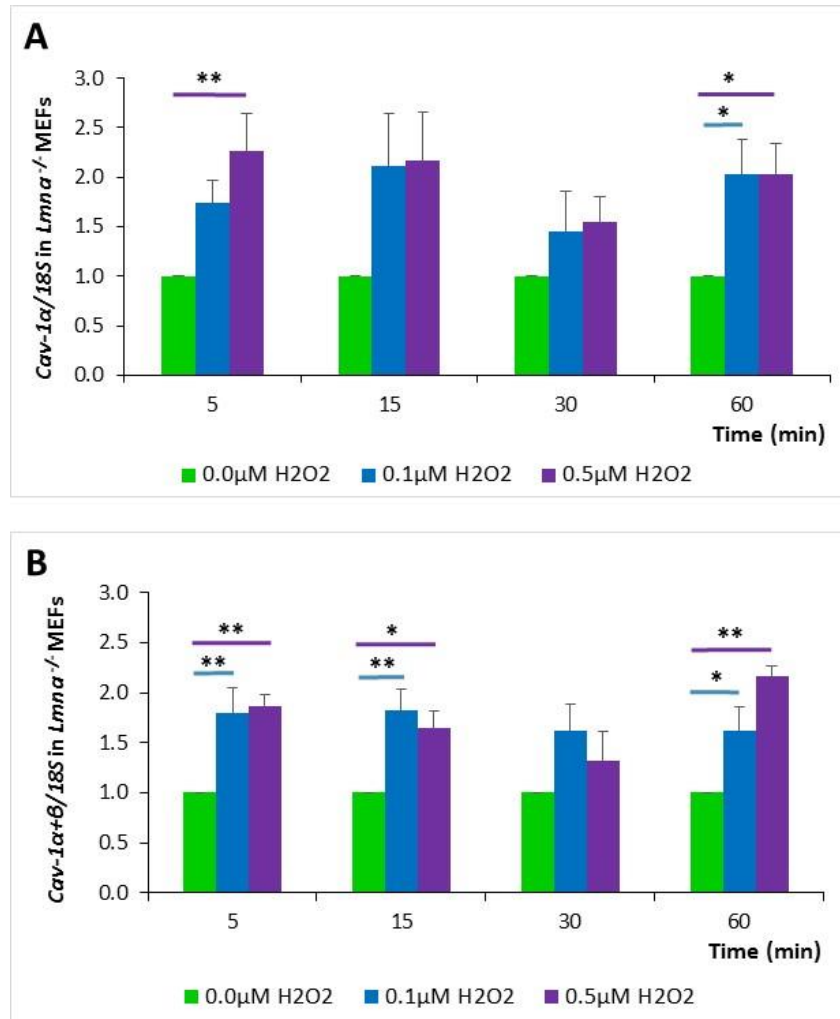


Figure 12 | Mean fold change in *Cav-1* transcript expression in *Lmna*^{-/-} MEF cells (EDMD model) cultured at full confluence under H₂O₂-induced oxidative stress conditions. Data from Real-Time PCR quantification show that immediate-early transcript expression of *Cav-1α* (panel A) normalized to that of *18s* reference gene is significantly up-regulated in *Lmna*^{-/-} MEF cells following exposure to 0.5μM of H₂O₂ for 5min and post exposure to 0.1μM or 0.5μM of H₂O₂ for 60min. Likewise, immediate-early transcript expression of total ($\alpha+\beta$) *Cav-1* (panel B) normalized to that of *18s* reference gene is significantly up-regulated in *Lmna*^{-/-} MEF cells following exposure to 0.1μM or 0.5μM of H₂O₂ for 5, 15, or 60min in comparison to mock-treated controls (0.0μM H₂O₂). Data represent mean fold change \pm SEM derived from 4 independent experiments; each performed in duplicates. One asterisk represents a statistical significance ($P<0.05$). Two asterisks represent a statistical significance ($P<0.01$).

In *Lmna*^{-/-} MEFs, we also noted an early induction in the transcriptional levels of the total pool of *Cav-1* (both $\alpha+\beta$) at 5min post exposure to 0.1μM and 0.5μM of

H₂O₂ with a 1.8- and 1.86-fold increase (± 0.25 and ± 0.12) respectively (Figure 12B, see above). The detected induction in response to both concentrations of H₂O₂ in *Cav-1*($\alpha+\beta$) was statistically significant when compared to the mock-treated control lamin A/C deficient MEFs ($P\text{-value} \leq 0.01$). After 15min of exposure to 0.1 μ M of H₂O₂, the total pool of *Cav-1* was steady at 1.82-fold (± 0.22) that was considered statistically different from the mock-treated control cells ($P\text{-value} \leq 0.01$); however, a minimal decrease was measured in the total pool of *Cav-1* in response to 0.5 μ M of H₂O₂ with a 1.64-fold (± 0.17) change that was determined to be statistically significant relative to the mock-treated control lamin A/C-deficient MEFs ($P\text{-value} \leq 0.05$). The transcript levels of the total pool of *Cav-1* were reduced in response to a 30min exposure to 0.1 μ M and 0.5 μ M of H₂O₂, whereby a 1.62- and 1.33-fold (± 0.26 and ± 0.28) decrease was quantified and noted not to be statistically different from the mock-treated control cells. We obtained another stabilization in the transcript levels of the total pool of *Cav-1* after 60min of treatment with 0.1 μ M of H₂O₂ with a 1.62-fold (± 0.23) that was detected to be significant relative to their mock-treated control cells ($P\text{-value} \leq 0.05$). Nevertheless, the transcriptional levels of *Cav-1*($\alpha+\beta$) peaked at 60min post exposure to 0.5 μ M of H₂O₂ in that a 2.16-fold (± 0.11) increase was quantified and determined to be statistically significant in comparison to the mock-treated control *Lmna*^{-/-} MEFs ($P\text{-value} \leq 0.01$). Quantification data represent mean fold difference \pm SEM generated from four independent repeats, each performed in duplicates.

- c. *Cav-1 α* and *Cav-1* ($\alpha+\beta$) transcriptional levels are induced in *Lmna*^{N195K/N195K} MEF cells following exposure to 0.1 μ M and 0.5 μ M H₂O₂ for 5, 15, 30 and 60min in comparison to mock-treated controls (0.0 μ M H₂O₂).

In *Lmna*^{N195K/N195K} MEFs, a marked elevation in the levels of *Cav-1 α* transcript was observed as early as 15min post exposure to 0.1 μ M and 0.5 μ M of H₂O₂ in that a 2.20-fold (± 0.15) and 2.70-fold (± 0.09) increase was measured respectively (Figure 13A, see below). The pronounced increase in the *Cav-1 α* transcript levels was statistically significant when compared to the mock-treated N195K MEFs (*P*-value <0.001). After the peak expression obtained at 15min post treatment with 0.1 μ M and 0.5 μ M of H₂O₂, the transcriptional levels of *Cav-1 α* dropped to 1.77-fold (± 0.26) and 1.88-fold (± 0.58) when compared to the mock-treated control N195K MEFs in response to 0.1 μ M and 0.5 μ M of H₂O₂ for 30min respectively. Another peak in the expression of *Cav-1 α* was statistically measured after 1hr of treatment with 0.1 μ M of H₂O₂ whereby a 2.09-fold (± 0.30) increase was obtained (*P*-value <0.01). However, the expression levels of *Cav-1 α* leveled down to 1.61-fold (± 0.25) after 1hr of treatment with 0.5 μ M of H₂O₂. Results represent mean fold difference \pm SEM of three independent experiments, each performed in duplicates.

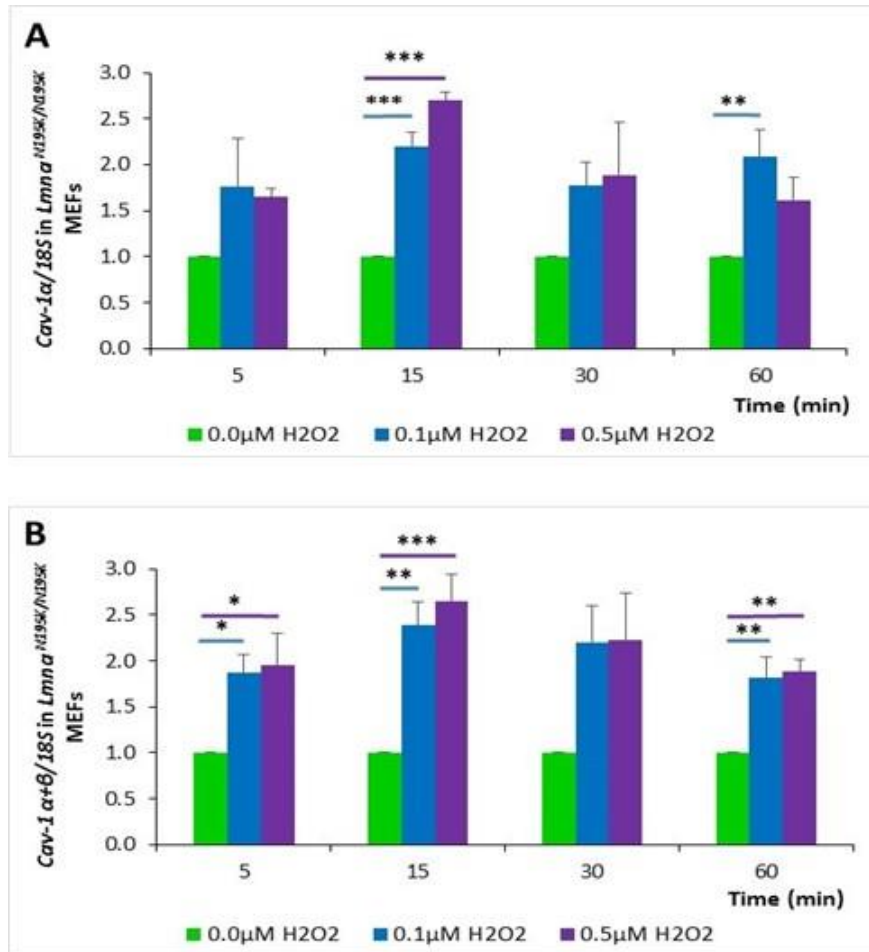


Figure 13| Mean fold change in *Cav-1* transcript expression in *Lmna*^{N195K/N195K} MEF cells (DCM model) cultured at full confluence under H₂O₂-induced oxidative stress conditions. Data from Real-Time PCR quantification show that immediate-early transcript expression of *Cav-1 α* (panel A) normalized to that of *18s* reference gene is significantly up-regulated in *Lmna*^{N195K/N195K} MEF cells following exposure to 0.1 μ M or 0.5 μ M of H₂O₂ for 15min and post exposure to 0.1 μ M of H₂O₂ for 60min. Likewise, immediate-early transcript expression of total (α + β) *Cav-1* (panel B) normalized to that of *18s* reference gene is significantly up-regulated in *Lmna*^{N195K/N195K} MEF cells following exposure to 0.1 μ M or 0.5 μ M of H₂O₂ for 5, 15, or 60min in comparison to mock-treated controls (0.0 μ M H₂O₂). Data represent mean fold change \pm SEM derived from 3 independent experiments; each performed in duplicates. One asterisk represents a statistical significance ($P < 0.05$). Two asterisks represent a statistical significance ($P < 0.01$). Three asterisks represent a statistical significance ($P < 0.001$).

Cav-1(α + β) gene induction was observed as early as 5min post treatment with 0.1 μ M and 0.5 μ M of H₂O₂ with a respective 1.87-fold (± 0.20) and a 1.95-fold (± 0.35) increase when compared to the mock-treated N195K MEFs (Figure 13B, see above).

This induction was statistically significant with a P -value < 0.05 suggesting a rapid induction in the *Cav-1 β* transcript. The maximum induction in total *Cav-1* response was obtained at 15min post exposure to 0.1 μ M and 0.5 μ M of H₂O₂ with a 2.40-fold (± 0.24) and a 2.65-fold (± 0.29) increase respectively. The rise in the *Cav-1*($\alpha + \beta$) transcript expression at 15min post exposure to 0.1 μ M and 0.5 μ M of H₂O₂ was statistically significant in comparison to the mock-treated control N195K MEFs (P -value < 0.01 and P -value < 0.001 respectively). At 30min post treatment, the expression of *Cav-1* ($\alpha + \beta$) transcripts leveled down and was steady at 2.21-fold (± 0.40) and 2.22-fold (± 0.51) in response to 0.1 μ M and 0.5 μ M of H₂O₂ respectively. However, this decrease was not statistically different from the mock-treated N195K control MEFs. Following 60min of exposure to H₂O₂, the expression of the *Cav-1*($\alpha + \beta$) transcripts revealed a smaller increase in response to 0.1 μ M of H₂O₂ with a 1.82-fold (± 0.22) change in the total *Cav-1* transcript which was statistically significant when compared to the control mock-treated N195K MEFs (P -value < 0.01). Moreover, a rise in the expression levels of *Cav-1*($\alpha + \beta$) transcripts was measured after 60min of exposure to 0.5 μ M of H₂O₂ with a 1.88-fold (± 0.14) suggesting an increase in the *Cav-1 β* transcript levels. The increase in the *Cav-1*($\alpha + \beta$) transcripts was statistically significant in comparison to the mock-treated N195K MEFs with a P -value less than 0.01. Quantification of the Real-Time PCR data represent mean fold difference \pm SEM of three independent experiments, each done in duplicates.

3. ***Cav-1 α and total Cav-1 (α & β) immediate-early transcripts are altered in Lamin A/C-deficient MEFs retrovirally transfected to express the LMNA WT or mutant forms that result in EDMD (E358K, L530P) under baseline conditions.***

To further validate our hypothesis, our next aim was to test whether the retroviral expression of WT *LMNA* or mutant forms that result in EDMD in lamin A/C-deficient MEFs would affect the transcriptional levels of *Cav-1* (α & β) under baseline conditions. Accordingly, Real-Time PCR experiments were performed on *Lmna*^{-/-} MEFs genetically altered to express the *LMNA* WT (DJ1-WT-S) or mutant forms that result in EDMD (DJ1-E358K-S and DJ1-L530P-S) in comparison to their mock control (DJ1-mock-S) cells post RNA extraction and cDNA synthesis while ensuring consistency in cell density, spreading and confluence profiles in 2-D culture across tested samples and in between independent repeats.

a. *Cav-1 α immediate-early transcript is induced in Lamin A/C-deficient MEFs retrovirally transfected to express the LMNA WT or the mutant form that result in EDMD (E358K) in comparison to their control Lamin A/C-deficient MEFs expressing the mock retroviral vector without lamin A.*

Prior to analyzing the effect of re-introducing via retroviral expression WT lamin A or mutant forms that result in EDMD on the expression of *Cav-1 α* , we intended to compare at first any difference in the *Cav-1 α* expression levels between the lamin A/C-deficient MEFs expressing the mock retroviral vector without lamin A and their control lamin A/C-deficient MEFs while anticipating that no difference should be obtained between both of them. Notably, under baseline conditions and when normalized to the transcriptional levels of *18s* reference gene, Real-Time PCR quantification data show that the expression of *Cav-1 α* is markedly induced in lamin A/C-deficient MEFs expressing the mock retroviral vector without lamin A in

comparison to their control lamin A/C-deficient MEFs whereby a 4.58-fold (± 0.86) increase was detected in the transcriptional level of *Cav-1 α* in *Lmna*^{-/-} MEFs DJ1-mock-S when compared to their control *Lmna*^{-/-} MEFs (Figure 14A, see below). The induction was determined to be statistically significant as indicated by the 2-tailed student t-test (*P*-value < 0.05).

Real-Time PCR data indicate a significant elevation in the *Cav-1 α* expression levels normalized to *18s* in *Lmna*^{-/-} MEFs genetically modified to express the *LMNA* WT (DJ1-WT-S) or the mutant form that results in EDMD (DJ1-E358K-S) (Figure 14B). Indeed, we obtained a 3.56-fold (± 0.2) and a 2.98-fold (± 0.43) increase in the *Cav-1 α* immediate-early transcript in *Lmna*^{-/-} MEFs DJ1-WT-S and *Lmna*^{-/-} MEFs DJ1-E358K-S respectively which was statistically different from the *Lmna*^{-/-} MEFs DJ1-mock-S (*P*-value ≤ 0.001). Nevertheless, we did not detect any significant difference between the *Lmna*^{-/-} MEFs genetically modified to express the mutant form that results in EDMD (DJ1-L530P-S) and their mock control (DJ1-mock-S) in that a 0.37-fold (± 0.07) difference was measured (*P*-value > 0.05) (Figure 14B). Quantification of the Real-Time PCR data represent mean fold difference \pm SEM of three independent experiments, each done in duplicates.

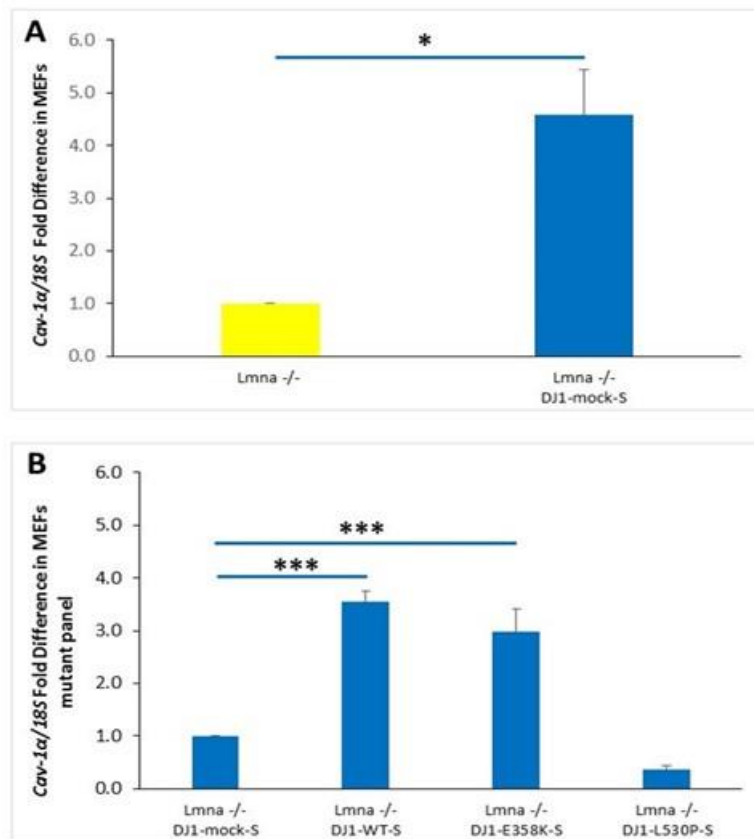


Figure 14| Mean fold change in *Cav-1α* transcript expression in lamin A/C-deficient MEFs retrovirally transfected to express the *LMNA* WT or mutant forms (E358K and L530P) that result in EDMD at baseline conditions. Real-Time PCR quantification data suggest that *Cav-1α* is significantly elevated in lamin A/C-deficient MEFs expressing the mock vector without lamin A (*Lmna*^{-/-} MEFs DJ1-mock-S) in comparison to its control *Lmna*^{-/-} MEFs (panel A) and in lamin A/C-deficient MEFs retrovirally transfected to express the *LMNA* WT or mutant form (E358K) that results in EDMD in comparison to their control lamin A/C-deficient MEFs expressing the mock vector without lamin A (*Lmna*^{-/-} MEFs DJ1-mock-S) (panel B). *Cav-1α* transcriptional levels are not altered in lamin A/C-deficient MEFs retrovirally transfected to express the mutant form (L530P) that results in EDMD. *Cav-1α* transcript expression was normalized to that of the *18s* reference gene. Data represent mean fold difference ± SEM in comparison to the controls *Lmna*^{-/-} MEFs (panel A) and *Lmna*^{-/-} MEFs (DJ1-mock-S) (panel B) derived from 3 independent experiments; each performed in duplicates. One asterisk represents a statistical significance ($P < 0.05$) and three asterisks represent a statistical significance ($P \leq 0.001$).

- b. *Cav-1*($\alpha+\beta$) immediate-early transcript is induced in Lamin A/C-deficient MEFs retrovirally transfected to express the *LMNA* WT or the mutant form that result in EDMD (E358K) in comparison to their control Lamin A/C-deficient MEFs expressing the mock retroviral vector without lamin A.

As stated earlier, we compared the transcriptional levels of total *Cav-1*($\alpha+\beta$) in lamin A/C-deficient MEFs expressing the mock retroviral vector without lamin A in comparison to their control lamin A/C-deficient MEFs. Real-Time PCR data suggest that there is a significant induction in the expression of *Cav-1*($\alpha+\beta$) under baseline conditions and when normalized to *18s* reference gene in *Lmna*^{-/-} MEFs DJ1-mock-S with a 3.38-fold (± 0.74) difference when compared to their control *Lmna*^{-/-} MEFs (*P*-value < 0.05) (Figure 15A).

Real-Time PCR data indicate a significant increase in the *Cav-1*($\alpha+\beta$) expression levels normalized to *18s* in *Lmna*^{-/-} MEFs retrovirally transfected to express the *LMNA* WT (DJ1-WT-S) or the mutant form that results in EDMD (DJ1-E358K-S) (Figure 15B). Indeed, we obtained a 3.02-fold (± 0.6) and a 2.81-fold (± 0.45) increase in the *Cav-1 α* immediate-early transcript in *Lmna*^{-/-} MEFs DJ1-WT-S and *Lmna*^{-/-} MEFs DJ1-E358K-S respectively which was statistically different from the *Lmna*^{-/-} MEFs DJ1-mock-S (*P*-value < 0.05). Nevertheless, we did not detect any significant difference between the *Lmna*^{-/-} MEFs retrovirally transfected to express the mutant form that results in EDMD (DJ1-L530P-S) and their mock control (DJ1-mock-S) in that a 0.34-fold (± 0.08) difference was measured (*P*-value > 0.05) (Figure 15B). Quantification of the Real-Time PCR data represent mean fold difference \pm SEM of three independent experiments, each done in duplicates.

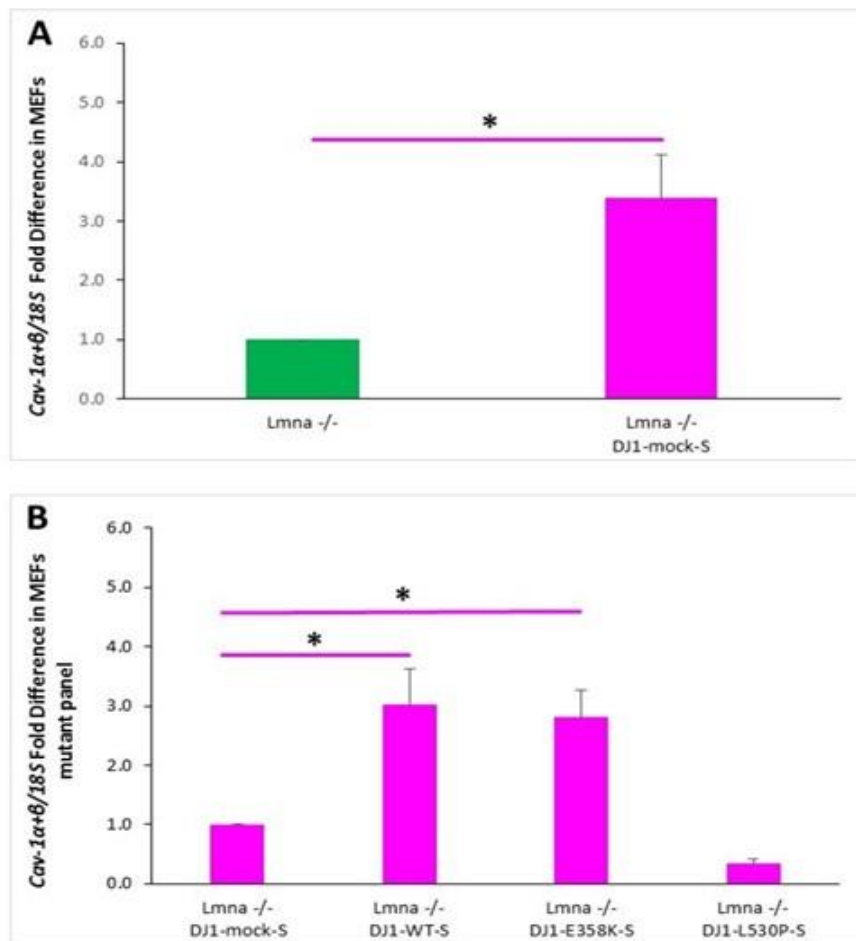


Figure 15| Mean fold change in *Cav-1* transcript expression in lamin A/C-deficient MEFs retrovirally transfected to express the *LMNA* WT or mutant forms (E358K and L530P) that result in EDMD at baseline conditions. Real-Time PCR quantification data suggest that *Cav-1* transcript is significantly elevated in lamin A/C-deficient MEFs expressing the mock vector without lamin A (*Lmna*^{-/-} MEFs DJ1-mock-S) in comparison to its control *Lmna*^{-/-} MEFs (panel A) and in lamin A/C-deficient MEFs retrovirally transfected to express the *LMNA* WT or mutant form (E358K) that results in EDMD in comparison to their control lamin A/C-deficient MEFs expressing the mock vector without lamin A (*Lmna*^{-/-} MEFs DJ1-mock-S) (panel B). *Cav-1α* transcriptional levels are not altered in lamin A/C-deficient MEFs retrovirally transfected to express the mutant form (L530P) that results in EDMD. *Cav-1α* transcript expression was normalized to that of the *18s* reference gene. Data represent mean fold difference ± SEM in comparison to the controls *Lmna*^{-/-} MEFs (panel A) and *Lmna*^{-/-} MEFs (DJ1-mock-S) (panel B) derived from 3 independent experiments; each performed in duplicates. One asterisk represents a statistical significance ($P < 0.05$).

B. Investigate potential alterations in protein expression and intracellular distribution of Cav-1 α isoform under baseline and oxidative stress conditions in mouse embryo fibroblast (MEF) cell lines derived from mice either lacking A-type lamin expression or emerin expression (EDMD phenotype), homozygous for the N195K mutant form (DCM phenotype) versus wild-type (WT) and in a panel of lamin A/C-deficient MEFs retrovirally transfected to express *LMNA* WT or mutant forms that result in EDMD (E358K, L530P).

1. *Cav-1 α protein expression is not significantly altered in *Lmna*^{-/-} MEFs (Lamin A/C null), *Lmna*^{N195K/N195K} MEFs and *Emd*^{-Y} MEFs (*Emd* null) under baseline conditions in comparison to *Lmna*^{+/+} control MEFs.*

In the second aim of this study, we intended to determine any modulation in the Cav-1 α protein expression under baseline conditions by Western Blot analysis using a Cav-1 α specific antibody. Accordingly, protein extraction from total cell lysates was performed when cells were cultured at full confluence under baseline conditions while ensuring consistency in cell density, spreading and confluence profiles across tested samples and in between independent repeats.

Qualitative analysis was done by observing and comparing densitometry signals on autoradiography films between the various samples. This was followed by a semi-quantitative densitometry analysis using Image J software. Image J analysis of the Cav-1 α densitometry signals normalized to that of the GAPDH loading control suggests that there exists no significant difference in the steady state protein expression of Cav-1 α between *Lmna*^{-/-}, *Lmna*^{N195K/N195K} and *Emd*^{-Y} mutant MEFs in comparison to the control WT cells cultured under baseline conditions (Figure 16A, see below). A 1.09-fold change (± 0.07) in the Cav-1 α protein expression was detected in the *Lmna*^{-/-} MEFs and was not determined to be statistically significant in comparison to the WT controls (P -value >0.05) (Figure 16B). Likewise, a 0.61-fold (± 0.06) decrease was obtained in the N195K mutant MEFs without showing any statistical significance when compared to the WT control MEFs (P -value >0.05). The protein expression of Cav-1 α in *Emd*^{-Y}

MEFs was also not statistically different from the WT control MEFs with a 0.66-fold change (± 0.22) ($P\text{-value} > 0.05$) (Figure 16B). Data represent mean fold change \pm SEM of four independent repeats.

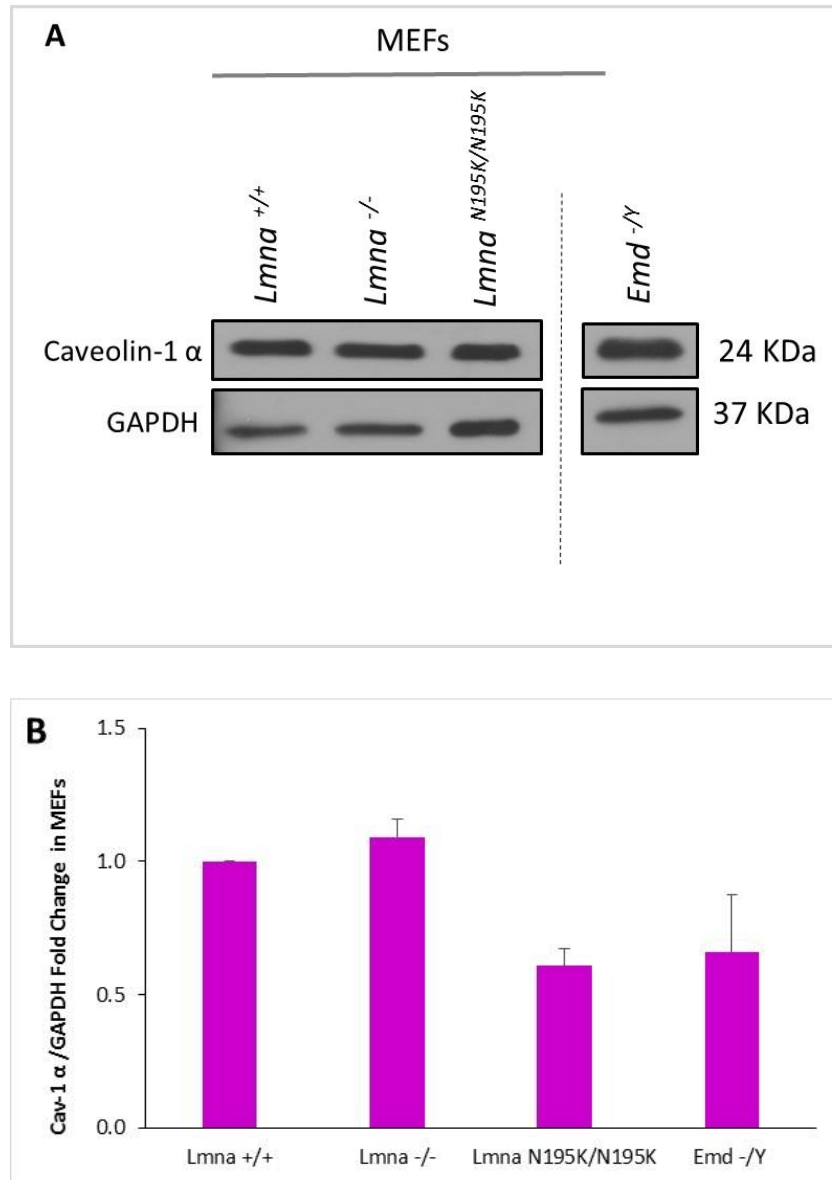


Figure 16| Western Blot analysis of Cav-1 α protein expression in *Lmna* ^{-/-}, *Lmna* ^{N195K/N195K} and *Emd* ^{-/Y} mutant MEFs vs. control WT cells cultured at full confluence under baseline conditions. Panel A; representative blot. Image J quantification and analysis of the Cav-1 α densitometry signal normalized to that of the GAPDH loading control shows that there is no statistically significant difference in the Cav-1 α protein expression levels between *Lmna* ^{-/-}, *Lmna* ^{N195K/N195K} and *Emd* ^{-/Y} mutant MEFs in comparison to the control WT cells cultured under baseline conditions (panel B). Data represent mean fold change \pm SEM derived from 4 independent experiments.

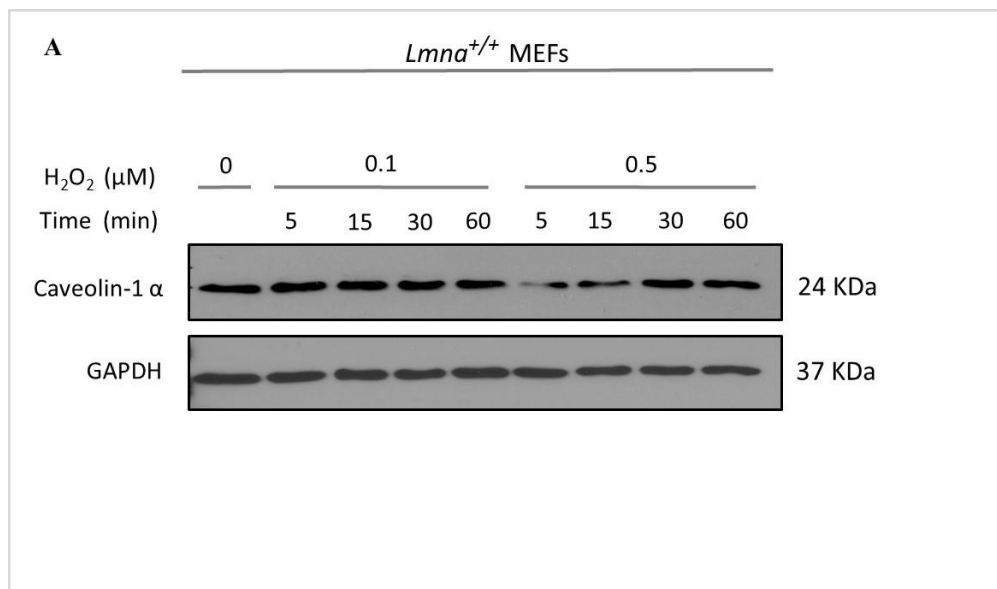
2. *Cav-1α* protein expression is deregulated in *Lmna*^{-/-} MEFs and *Lmna*^{N195K/N195K} MEFs post exposure to H₂O₂-induced oxidative stress in comparison to the control *Lmna*^{+/+} MEFs.

To assess the response of the Cav-1α isoform to H₂O₂-induced oxidative stress, cells from *Lmna*^{+/+}, *Lmna*^{-/-} and *Lmna*^{N195K/N195K} MEFs were seeded until full confluence while ensuring consistency in cell-cell contact profiles across tested samples and in independent repeats. Cells from the different lines were exposed to 0.1μM and 0.5μM of H₂O₂ for time increments of 5, 15, 30 and 60min, followed by protein extraction, SDS-PAGE and Western Blot densitometry quantification and analysis. We also tested for putative alterations in the protein expression of Cav-1α post exposure to both concentrations of H₂O₂ for the following time points: 1.5, 2, 4 and 6hrs.

a. Cav-1α translational levels are not altered in *Lmna*^{+/+} MEF cells following exposure to 0.1μM and 0.5μM H₂O₂ for 5, 15, 30 and 60min in comparison to mock-treated controls (0.0μM H₂O₂).

Qualitative assessment of autoradiography Western Blot films generated from wild-type MEFs suggests no change in the protein expression of Cav-1α normalized to GAPDH loading control following exposure to 0.1μM and 0.5μM of H₂O₂ along the 60min duration of the experiment (Figure 17A). As depicted in Figure 17B, densitometry quantification and analysis using Image J indicates that after 5min of exposure to 0.1μM and 0.5μM of H₂O₂ respectively, a 1.14-fold and 0.89-fold (± 0.06 and ± 0.18) change was obtained that was not statistically different from the mock-treated *Lmna*^{+/+} controls (0.0μM H₂O₂) (*P*-value>0.05). Following 15min of exposure to 0.1μM and 0.5μM of H₂O₂, Cav-1α translational levels normalized back to baseline levels with a respective 1.04- and 0.96-fold (± 0.21 and ± 0.3) change which was also insignificant in comparison to the mock-treated *Lmna*^{+/+} controls (*P*-value>0.05). Cav-

1 α protein expression level was not affected by exposing the WT cells to 0.1 μ M of H₂O₂ for 30min, in that the Cav-1 α translational levels remained constant and not significantly different from their corresponding mock-treated controls with a 0.91-fold (\pm 0.14) as shown by densitometry analysis (P -value $>$ 0.05). On the contrary, we noted an elevation in the protein expression of Cav-1 α isoform in response to 0.1 μ M of H₂O₂ for 30min whereby a 1.46-fold (\pm 0.25) increase was depicted, yet the increase was not determined to be statistically significant relative to the mock-treated controls (P -value $>$ 0.05). One hour post treatment with both doses of H₂O₂, Cav-1 α protein levels remained steady in response to 0.1 μ M of H₂O₂ with a 0.86-fold (\pm 0.13). In response to 0.5 μ M of H₂O₂, however, we noted a slight drop in the protein expression of Cav-1 α isoform with a 1.32-fold (\pm 0.26). In both cases, we were not capable of detecting a statistical significance (P -value $>$ 0.05). Densitometry semi-quantitative data is represented as mean fold change \pm SEM of four independent repeats.



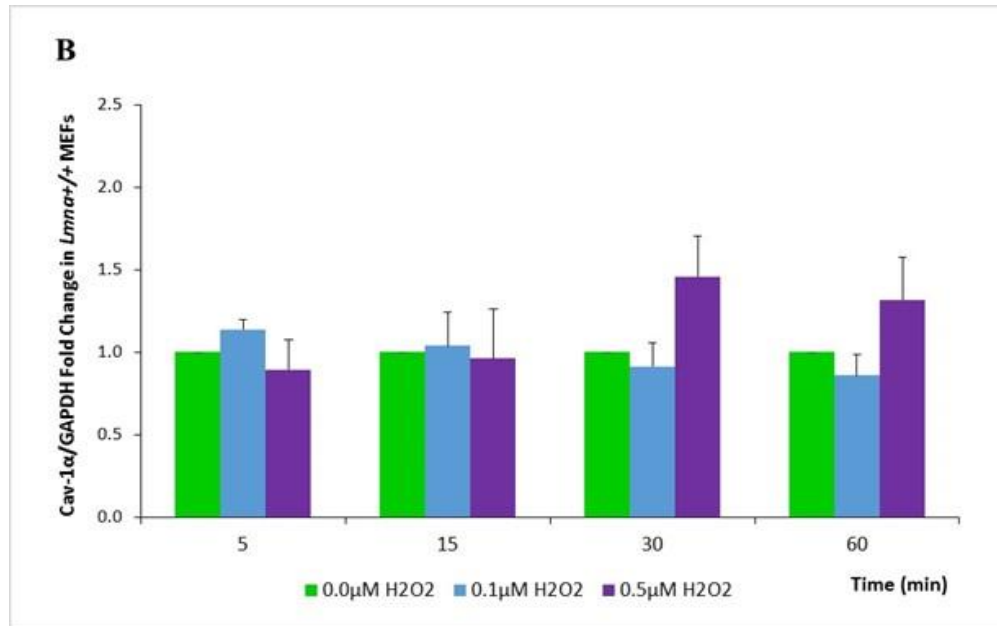


Figure 17| Cav-1 α protein expression in *Lmna*^{+/+} MEF cells (wild-type model) cultured at full confluence under H₂O₂-induced oxidative stress conditions for time increments of 5, 15, 30 and 60min. Data from Western Blot analysis (panel A; representative blot) show that immediate-early protein expression of Cav-1 α is not altered in *Lmna*^{+/+} MEF cells following exposure to 0.1 μ M or 0.5 μ M H₂O₂ for 5, 15, 30, and 60min in comparison to mock-treated controls (0.0 μ M H₂O₂). Image J quantification and analysis of the Cav-1 α densitometry signal normalized to that of the GAPDH loading control shows that there is no statistically significant difference in Cav-1 α protein expression in cells treated with the two different concentrations of H₂O₂ at the four different time points in comparison to the mock-treated control *Lmna*^{+/+} MEF cells (panel B). Data represent mean fold change \pm SEM derived from 4 independent experiments.

- b. Cav-1 α translational levels are not altered in *Lmna*^{+/+} MEF cells following exposure to 0.1 μ M and 0.5 μ M H₂O₂ for 1.5, 2, 4 and 6hrs in comparison to mock-treated controls (0.0 μ M H₂O₂).

Under the same conditions used above and by exposing the lamin A/C wild-type MEFs to 0.1 μ M and 0.5 μ M of H₂O₂ for 1.5, 2, 4 and 6hrs, we did not observe any change in the protein expression levels of Cav-1 α normalized to GAPDH loading controls following a qualitative assessment of the autoradiography films (Figure 18A). Densitometry quantification data revealed no significant modulations in the translational levels of the α isoform of Cav-1 despite exposing those cells to the same doses of H₂O₂ but for a longer duration (Figure 18B). Following exposure to 1.5hrs of H₂O₂, we

detected a 0.96- and 1.27-fold (± 0.17 and ± 0.24) change in the expression of Cav-1 α that was not considered significant in comparison to the mock-treated *Lmna*^{+/+} controls (0.0 μ M H₂O₂) (P -value >0.05). Moreover, data suggests a slight increase in the Cav-1 α expression levels after 2hrs of treatment with 0.1 μ M of H₂O₂ indicated by a 1.22-fold (± 0.12) relative to the mock-treated controls. However, this slight change was not noted to be statistically significant (P -value >0.05). At the same time point, we report that Cav-1 α expression levels in response to 0.5 μ M of H₂O₂ were maintained at a steady state with a 1.26-fold (± 0.12) which was also not statistically different from the mock-treated control WT MEFs (P -value >0.05). Cav-1 α translational levels remained constant at 1.18- and 1.25-fold (± 0.27 and ± 0.1) change following exposure to 0.1 μ M and 0.5 μ M of H₂O₂ for 4hrs. Both quantified values were not determined to be statistically different from their corresponding mock control (P -value >0.05). After 6hrs of exposure to both concentrations of H₂O₂, we detected an insignificant decrease in the Cav-1 α translational levels designated by a 0.84- and 1.15-fold (± 0.34 and ± 0.3) decrease in comparison to the mock-treated controls (P -value >0.05). Densitometry semi-quantitative data is represented as mean fold change \pm SEM of four independent repeats.

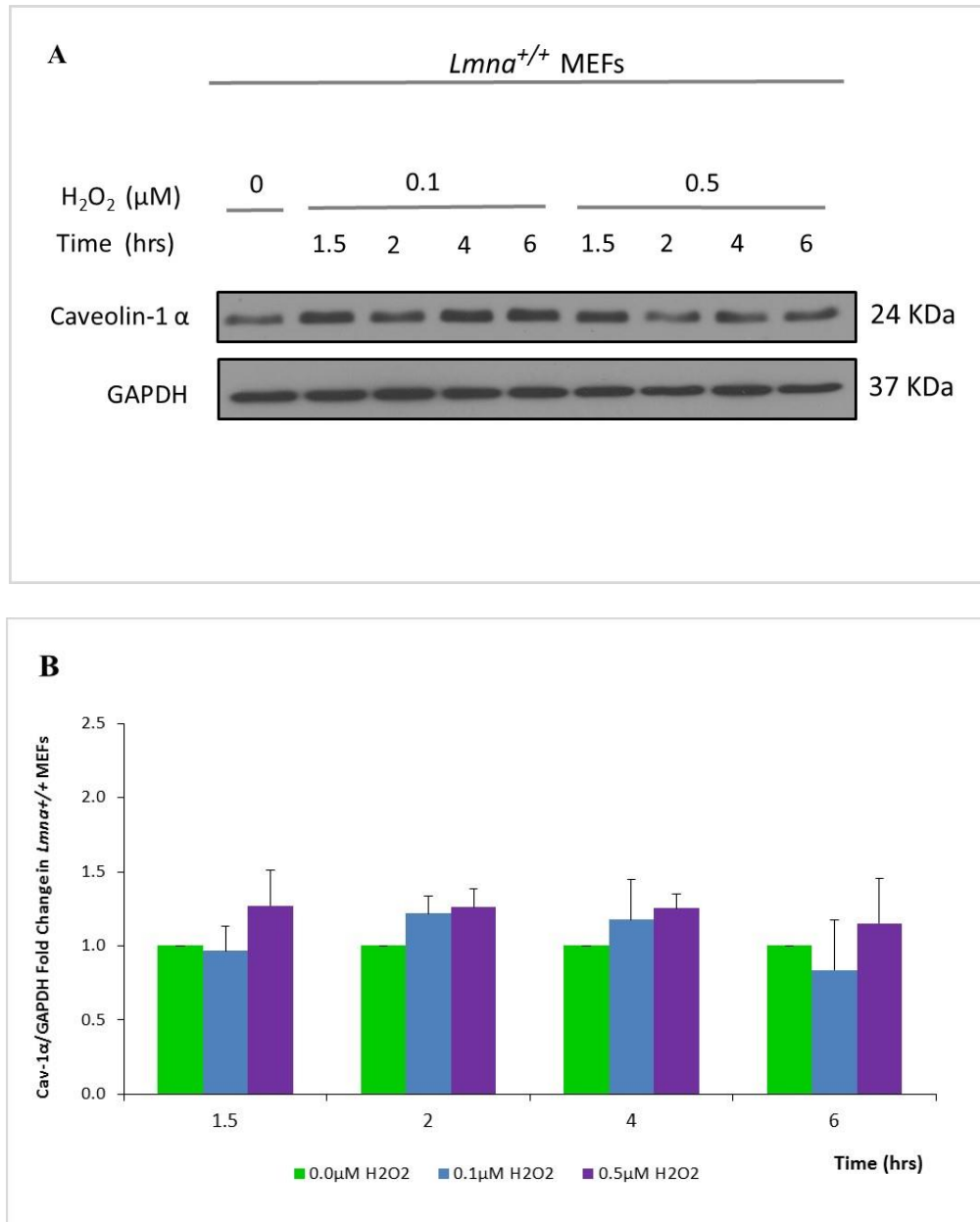
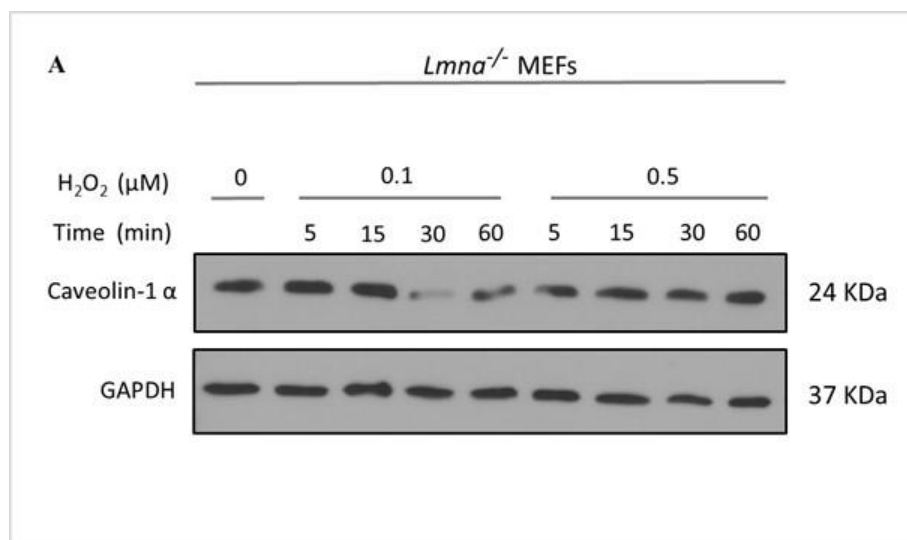


Figure 18| Cav-1 α protein expression in *Lmna*^{+/+} MEF cells (wild-type model) cultured at full confluence under H₂O₂-induced oxidative stress conditions for time increments of 1.5, 2, 4 and 6hrs. Data from Western Blot analysis (panel A; representative blot) show that immediate-early protein expression of Cav-1 α is not altered in *Lmna*^{+/+} MEF cells following exposure to 0.1 μ M or 0.5 μ M H₂O₂ for 1.5, 2, 4, and 6hrs in comparison to mock-treated controls (0.0 μ M H₂O₂). Image J quantification and analysis of the Cav-1 α densitometry signal normalized to that of the GAPDH loading control shows that there is no statistically significant difference in Cav-1 α protein expression in cells treated with the two different concentrations of H₂O₂ at the four different time points in comparison to the mock-treated control *Lmna*^{+/+} MEF cells (panel B). Data represent mean fold change \pm SEM derived from 4 independent experiments.

- c. Cav-1 α translational levels are deregulated in *Lmna*^{-/-} MEF cells following exposure to 0.1 μ M and 0.5 μ M H₂O₂ for 5, 15, 30 and 60min in comparison to mock-treated controls (0.0 μ M H₂O₂).

Immediate-early protein expression of the Cav-1 α isoform normalized to GAPDH loading control shows a down-regulation in the translational level of Cav-1 α post exposure to 0.1 μ M of H₂O₂ for 30 and 60min. In response to 0.5 μ M of H₂O₂, we noted an up-regulation in the Cav-1 α protein expression at 30min as displayed in the represented Western Blot autoradiography film (Figure 19A). Indeed, densitometry analysis and quantification data suggest that Cav-1 α protein expression increased 5min post treatment with 0.1 μ M of H₂O₂ in that a 1.34-fold (\pm 0.18) increase was observed and quantified, but was determined to be statistically insignificant in comparison to the mock-treated *Lmna*^{-/-} MEFs (*P*-value>0.05) (Figure 19B) . On the contrary, we noticed a drop in the Cav-1 α protein expression in response to 0.5 μ M of H₂O₂ for 5min with a 0.67-fold (\pm 0.19) decrease that was not statistically different from the mock-treated control lamin A/C-deficient MEFs. After 15min of exposure to 0.1 μ M and 0.5 μ M of H₂O₂, the Cav-1 α protein expression levels normalized to GAPDH loading controls bounced back near baseline levels with a 0.89- and 1.04-fold (\pm 0.13 and \pm 0.16) respectively and were not determined to be statistically significant relative to their corresponding mock-treated controls (*P*-value>0.05). Cav-1 α protein expression levels normalized to GAPDH loading controls were induced in response to a 30min exposure to 0.5 μ M of H₂O₂. Specifically, we noted a 1.71-fold (\pm 0.26) increase in the Cav-1 α protein which was statistically different from the mock-treated control MEFs (*P*-value \leq 0.05). In addition, we also observed a decline in the translational levels of the Cav-1 α in response to 0.1 μ M of H₂O₂ for 30min with a 0.53-fold (\pm 0.1). The detected decrease was very close to significance (*P*-value=0.06). Nevertheless, a significant

decrease in the Cav-1 α protein level was later obtained 60min post exposure to 0.1 μ M of H₂O₂ with a 0.6-fold (± 0.14) (P -value ≤ 0.05). The response of the lamin A/C-deficient MEFs to a 60min treatment with 0.5 μ M of H₂O₂ was characterized by a minimal drop in the translational level of the Cav-1 α protein to a 1.18-fold (± 0.1) that was considered not significant in comparison to the mock-treated MEFs (P -value >0.05). Data represent mean fold change \pm SEM of four independent repeats.



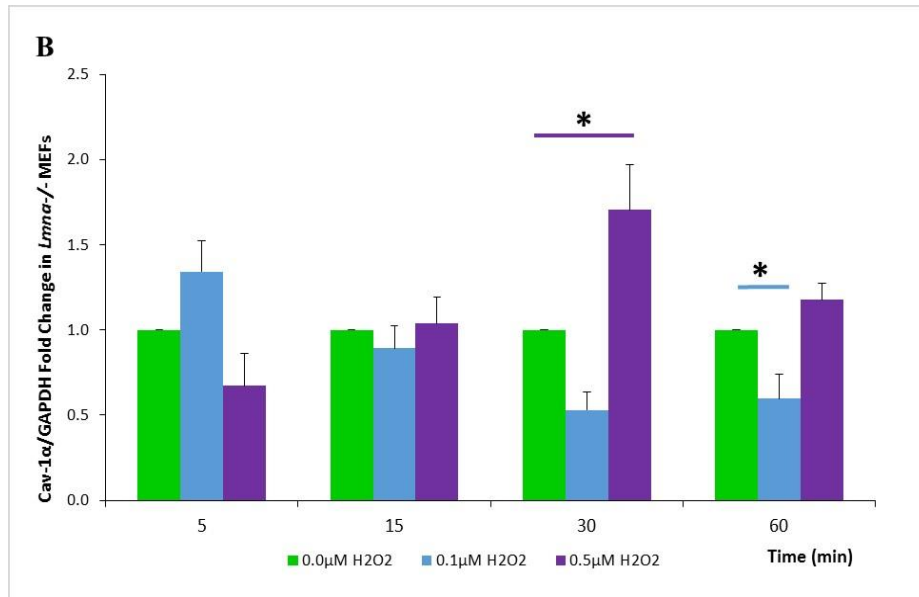


Figure 19| Cav-1 α protein expression in *Lmna*^{-/-} MEF cells (EDMD model) cultured at full confluence under H₂O₂-induced oxidative stress conditions for time increments of 5, 15, 30 and 60min. Data from Western Blot analysis (panel A; representative blot) and Image J quantification and analysis of the Cav-1 α densitometry signal normalized to that of the GAPDH loading control (panel B) show that there is a significant elevation in Cav-1 α protein in *Lmna*^{-/-} MEF cells following exposure to 0.5 μ M H₂O₂ for 30min and a significant reduction in Cav-1 α protein in *Lmna*^{-/-} MEF cells following exposure to 0.1 μ M H₂O₂ for 60min in comparison to mock-treated controls (0.0 μ M H₂O₂). Data represent mean fold change \pm SEM derived from 4 independent experiments. One asterisk represents a statistical significance ($P < 0.05$).

- d. Cav-1 α translational levels are not altered in *Lmna*^{-/-} MEF cells following exposure to 0.1 μ M and 0.5 μ M H₂O₂ for 1.5, 2, 4 and 6hrs in comparison to mock-treated controls (0.0 μ M H₂O₂).

We also tested any alterations in the Cav-1 α protein expression following exposure to 0.1 μ M and 0.5 μ M of H₂O₂ for 1.5, 2, 4 and 6hrs. Qualitative assessment was done by observing and comparing band intensities and thickness on autoradiography films subsequent to which band quantification and densitometry analysis occurred. Data suggest that lamin-A/C deficient MEFs exposed to two different concentrations of H₂O₂ for the four different time points did not show any differential expression in the Cav-1 α protein normalized to GAPDH loading control (Figure 20A).

Densitometry analysis using Image J suggests that *Lmna*^{-/-} MEFs exposed to 0.1 μ M and 0.5 μ M of H₂O₂ for 1.5hrs were not statistically different from the mock-treated controls in that a 1.23- and 1.13-fold (\pm 0.24 and \pm 0.34) change was detected (*P*-value>0.05) (Figure 20B). A similar response was obtained upon exposing the cells for 2hrs to both concentrations of H₂O₂. A 1.15- and 1.04-fold (\pm 0.18 and \pm 0.05) was noted in response to 0.1 μ M and 0.5 μ M of H₂O₂ respectively both of which were not determined to be significant in comparison to the mock-treated MEFs (0.0 μ M H₂O₂) (*P*-value>0.05). Cav-1 α normalized to GAPDH loading control stabilized to baseline levels with a 1.01-fold (\pm 0.07) in response to 0.5 μ M of H₂O₂ for 4hrs and was statistically insignificant relative to their corresponding mock-treated control (*P*-value>0.05). However, a slight drop in the translational level of Cav-1 α was detected with a 0.85-fold (\pm 0.17) decrease in response to a 4hr exposure to 0.1 μ M of H₂O₂ which was also found to be insignificant (*P*-value>0.05). After 6hrs of exposure to both concentrations of H₂O₂, we noted a stabilization in the Cav-1 α expression levels to near baseline with a 1.06- and 1.07-fold (\pm 0.19 and \pm 0.13), both of which were not statistically different from the mock-treated controls (*P*-value>0.05). Data represent mean fold change \pm SEM of three independent repeats.

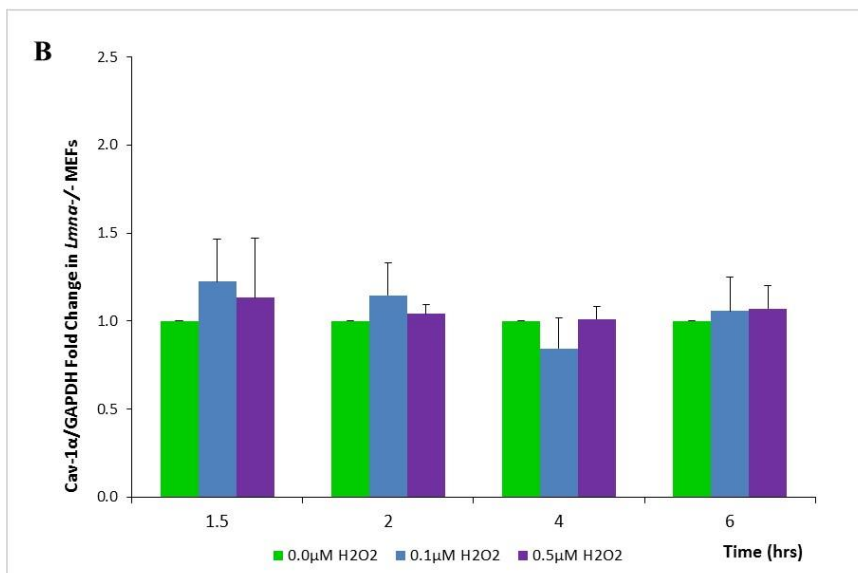
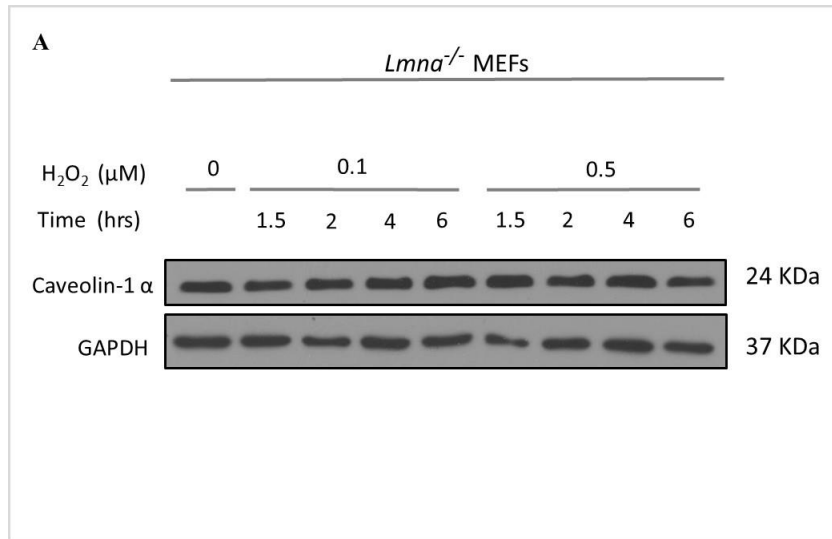


Figure 20| Cav-1 α protein expression in *Lmna*^{-/-} MEF cells (EDMD model) cultured at full confluence under H₂O₂-induced oxidative stress conditions for time increments of 1.5, 2, 4 and 6hrs. Data from Western Blot analysis (panel A; representative blot) show that immediate-early protein expression of Cav-1 α is not altered in *Lmna*^{-/-} MEF cells following exposure to 0.1 μ M or 0.5 μ M H₂O₂ for 1.5, 2, 4, and 6hrs in comparison to mock-treated controls (0.0 μ M H₂O₂). Image J quantification and analysis of the Cav-1 α densitometry signal normalized to that of the GAPDH loading control shows that there is no statistically significant difference in Cav-1 α protein expression in cells treated with the two different concentrations of H₂O₂ at the four different time points in comparison to the mock-treated control *Lmna*^{-/-} MEF cells (panel B). Data represent mean fold change \pm SEM derived from 3 independent experiments.

- e. Cav-1 α translational levels are reduced in *Lmna*^{N195K/N195K} MEF cells following exposure to 0.1 μ M and 0.5 μ M H₂O₂ for 5, 15, 30 and 60min in comparison to mock-treated controls (0.0 μ M H₂O₂).

Qualitative assessment of autoradiography Western Blot films generated from *Lmna*^{N195K/N195K} MEFs suggests that there exists a reduction in the protein expression of Cav-1 α normalized to GAPDH loading control following exposure to 0.1 μ M and 0.5 μ M of H₂O₂ along the 60min duration of the experiment (Figure 21A). As depicted in Figure 21B, the Cav-1 α protein expression decreased to 0.63- and 0.58-fold (\pm 0.03 and \pm 0.15) when compared to the mock-treated N195K control MEFs in response to 0.1 μ M and 0.5 μ M of H₂O₂ for 5min respectively (*P*-value<0.05). After 15min of exposure to both concentrations of H₂O₂, Cav-1 α protein expression remained constant in response to 0.1 μ M of H₂O₂ with a 0.61-fold (\pm 0.08) and was considered insignificant in comparison to the mock-treated control N195K MEFs (*P*-value>0.05); however, we were capable of detecting a more significant reduction in the Cav-1 α protein normalized to GAPDH with a 0.37-fold (\pm 0.16) decrease post exposure to 0.5 μ M of H₂O₂ (*P*-value<0.01). The response of Cav-1 α to 0.1 μ M and 0.5 μ M of H₂O₂ became roughly steady after 30min of treatment with a 0.57-fold (\pm 0.12) (*P*-value<0.05) and a 0.35-fold (\pm 0.12) (*P*-value<0.01) of that of the N195K MEF mock-treated control respectively. The protein expression of Cav-1 α was kept constant even after 1hr of treatment with 0.1 μ M of H₂O₂ whereby a 0.53-fold (\pm 0.14) was quantified relative to the mock-treated control (*P*-value<0.05). We also observed a slight elevation in the protein expression of Cav-1 α in that a 0.48-fold (\pm 0.03) increase was obtained in response to 0.5 μ M of H₂O₂ which was considered statistically different from the mock-treated control cells (*P*-value<0.01). Quantification densitometry data of Cav-1 α

normalized to GAPDH loading control is represented as mean fold change \pm SEM derived from three independent experiment.

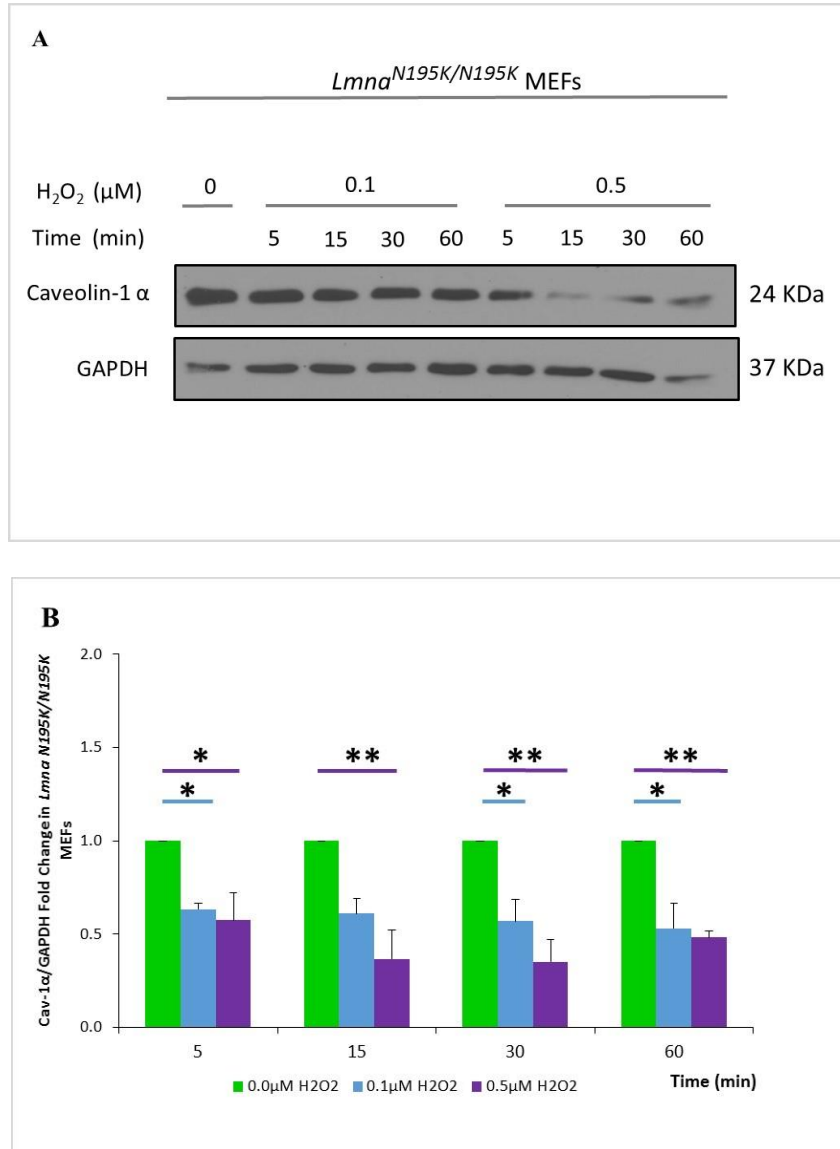


Figure 21| Cav-1 α protein expression in *Lmna*^{N195K/N195K} MEF cells (DCM model) cultured at full confluence under H₂O₂-induced oxidative stress conditions for time increments of 5, 15, 30 and 60min. Data from Western Blot analysis (panel A; representative blot) and Image J quantification and analysis of the Cav-1 α densitometry signal normalized to that of the GAPDH loading control (panel B) show that there is an immediate-early significant reduction in Cav-1 α protein in *Lmna*^{N195K/N195K} MEF cells following exposure to 0.1 μ M or 0.5 μ M H₂O₂ for 5, 15, 30, or 60min in comparison to mock-treated controls (0.0 μ M H₂O₂). Data represent mean fold change \pm SEM derived from 3 independent experiments. One asterisk represents a statistical significance ($P < 0.05$). Two asterisks represent a statistical significance ($P < 0.01$).

- f. Cav-1 α translational levels are not altered in *Lmna*^{N195K/N195K} MEF cells following exposure to 0.1 μ M and 0.5 μ M H₂O₂ for 1.5, 2, 4 and 6hrs in comparison to mock-treated controls (0.0 μ M H₂O₂).

Immediate-early protein expression of the Cav-1 α isoform normalized to GAPDH loading control shows no alterations in the translational level of Cav-1 α post exposure to both concentrations of H₂O₂ for 1.5, 2, 4 and 6hrs as indicated by the qualitative comparison of the autoradiography films (Figure 22A). Post exposure of *Lmna*^{N195K/N195K} MEFs to 0.1 μ M and 0.5 μ M of H₂O₂ for 1.5hrs, a 1.09- and 1.18-fold (\pm 0.03 and \pm 0.56) insignificant difference was detected by densitometry quantification respectively (P -value $>$ 0.05) (Figure 22B). A similar near baseline response of Cav-1 α was obtained after exposing the cells to 2hrs for 0.1 μ M and 0.5 μ M of H₂O₂ in that a 1.03- and 0.95-fold (\pm 0.07 and \pm 0.18) difference was measured relative to the mock-treated control *Lmna* N195K MEFs which was not determined to be statistically significant (P -value $>$ 0.05). We did not detect any alteration in the translational levels of Cav-1 α even after exposing the cells for 4hrs to both doses of H₂O₂ with a 0.88- and 0.94-fold (\pm 0.22 and \pm 0.09) difference in response to 0.1 μ M and 0.5 μ M of H₂O₂ respectively when compared to their corresponding mock-treated controls (P -value $>$ 0.05). A slight elevation in the expression levels of Cav-1 α was measured after 6hrs of exposing the cells to 0.1 μ M of H₂O₂ with a 1.11-fold (\pm 0.33) increase that was also found to be not statistically different from the mock-treated N195K control MEFs (Figure 22B). However, we obtained a minimal decrease in Cav-1 α protein expression normalized to GAPDH loading controls post exposure to 0.5 μ M of H₂O₂ for 6hrs with a 0.79-fold (\pm 0.16) (P -value $>$ 0.05). Quantification densitometry data of Cav-1 α normalized to GAPDH loading control is represented as mean fold change \pm SEM derived from three independent experiment.

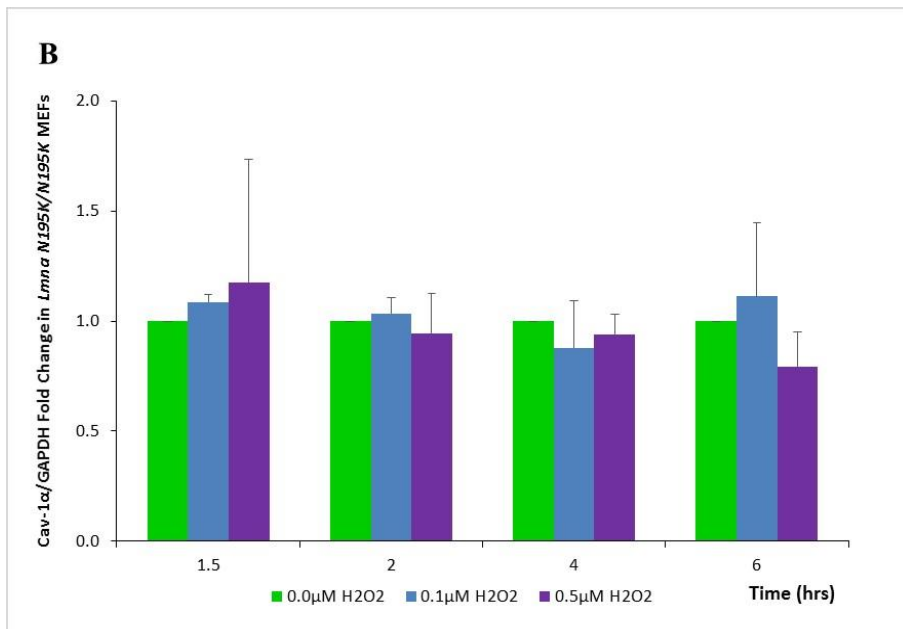
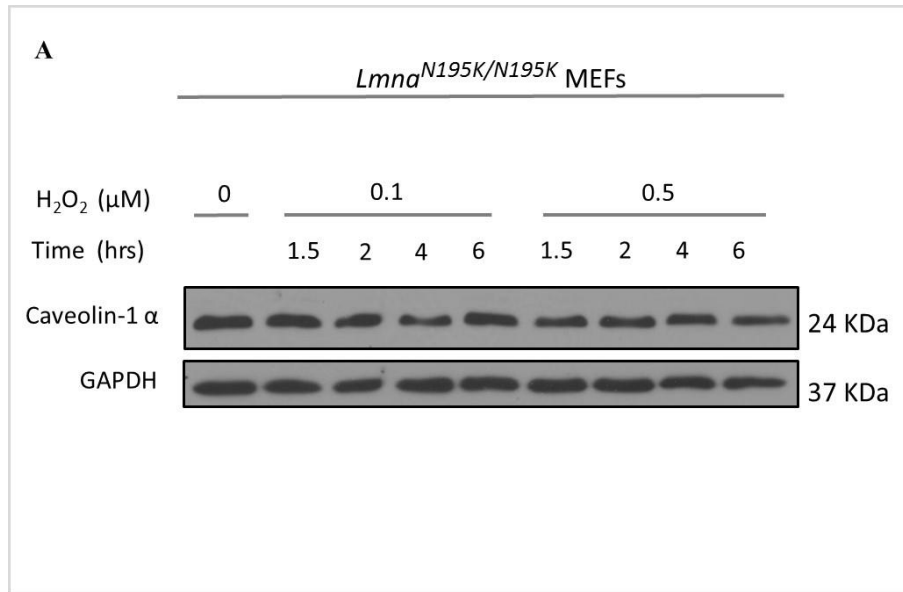


Figure 22| Cav-1 α protein expression in *Lmna*^{N195K/N195K} MEF cells (DCM model) cultured at full confluence under H₂O₂-induced oxidative stress conditions for time increments of 1.5, 2, 4 and 6hrs. Data from Western Blot analysis (panel A; representative blot) show that immediate-early protein expression of Cav-1 α is not altered in *Lmna*^{N195K/N195K} MEF cells following exposure to 0.1 μ M or 0.5 μ M H₂O₂ for 1.5, 2, 4, and 6hrs in comparison to mock-treated controls (0.0 μ M H₂O₂). Image J quantification and analysis of the Cav-1 α densitometry signal normalized to that of the GAPDH loading control shows that there is no statistically significant difference in Cav-1 α protein expression in cells treated with the two different concentrations of H₂O₂ at the four different time points in comparison to the mock-treated control *Lmna*^{N195K/N195K} MEF cells (panel B). Data represent mean fold change \pm SEM derived from 3 independent experiments.

3. *Cav-1 α* translational levels are not altered in Lamin A/C-deficient MEFs retrovirally transfected to express the LMNA WT or the mutant form that result in EDMD (E358K) and are significantly reduced in the mutant form (L530P) that results in EDMD in comparison to their control Lamin A/C-deficient MEFs expressing the mock retroviral vector without lamin A.

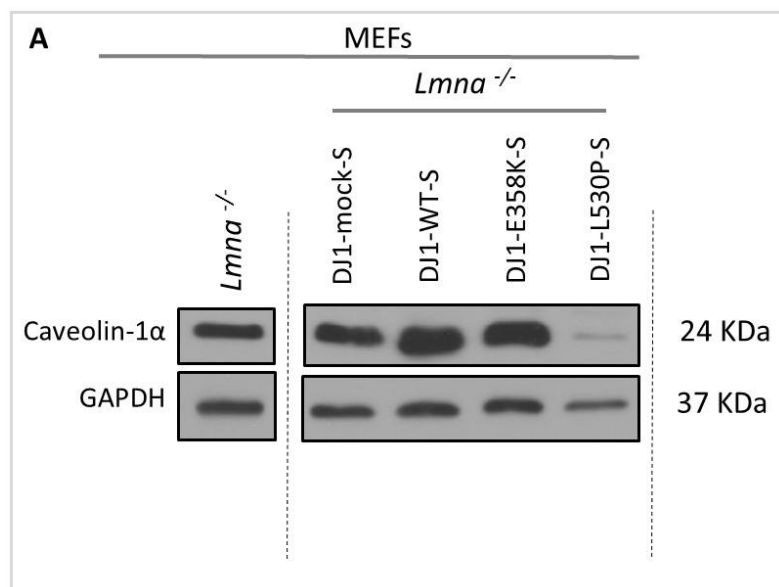
To further validate our hypothesis, we aimed at testing whether the retroviral expression of WT *LMNA* or mutant forms that result in EDMD in lamin A/C-deficient MEFs would affect the protein expression of Cav-1 α under baseline conditions. Accordingly, total cell lysates from *Lmna*^{-/-} MEFs genetically modified the *LMNA* WT (DJ1-WT-S) or mutant forms that result in EDMD (DJ1-E358K-S and DJ1-L530P-S) in comparison to their mock control (DJ1-mock-S) cells were extracted while ensuring consistency in cell density, spreading and confluency across tested samples and in independent repeats. Subsequently, SDS-PAGE and Western Blot densitometry quantification and analysis were done.

The protein expression level of Cav-1 α normalized to GAPDH loading controls is not altered in *Lmna*^{-/-} MEFs expressing the mock retroviral vector without lamin A, DJ1-mock-S, in comparison to its control *Lmna*^{-/-} MEFs as shown in Figure 23A. Densitometry quantification data suggest a non-significant difference in the translational levels of Cav-1 α normalized to GAPDH in that we obtained a 0.6-fold difference (\pm 0.23) in comparison to *Lmna*^{-/-} MEFs control (Figure 23B). Upon evaluating the expression of the Cav-1 α protein normalized to GAPDH between the *Lmna*^{-/-} MEFs retrovirally transfected to express the *LMNA* WT (DJ1-WT-S) or the mutant form that results in EDMD (DJ1-E358K-S) with the control *Lmna*^{-/-} MEFs expressing mock retroviral vector without lamin A, we did not obtain any significant difference in that a 1.49- and 1.73-fold (\pm 0.16 and \pm 0.67) change were measured respectively in

comparison to the *Lmna*^{-/-} MEFs DJ1-mock-S (*P*-value>0.05) (Figure 23C).

Nevertheless, densitometry analysis data suggest a significant reduction in the Cav-1 α protein normalized to GAPDH in *Lmna*^{-/-} MEFs genetically altered to express the mutant form that results in EDMD (DJ1-L530P-S) with a 0.13-fold decrease (\pm 0.06) relative to the control *Lmna*^{-/-} MEFs DJ1-mock-S (*P*-value<0.05) (Figure 23C).

Quantification densitometry data of Cav-1 α normalized to GAPDH loading control is represented as mean fold change \pm SEM derived from three independent experiment.



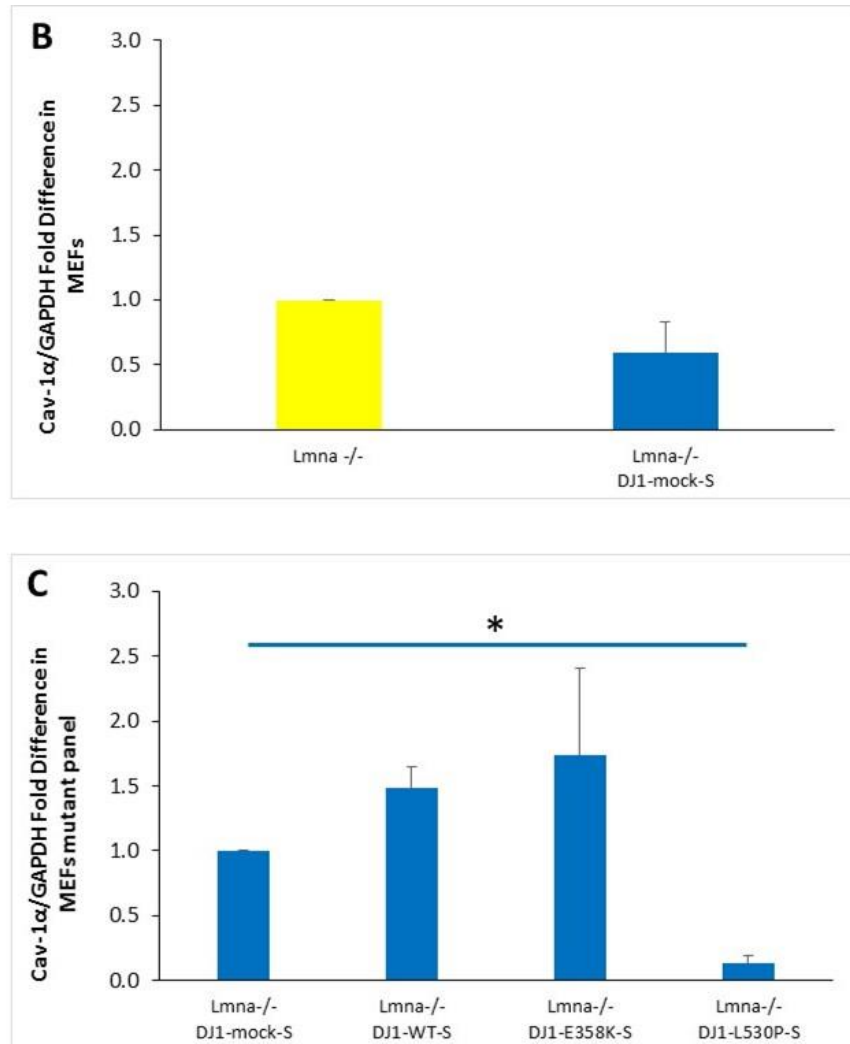


Figure 23| Mean fold change in Cav-1 α protein expression in lamin A/C-deficient MEFs retrovirally transfected to express the *LMNA* WT or mutant forms (E358K and L530P) that result in EDMD cultured at full confluence at baseline conditions. Panel A; representative blot. Image J quantification and analysis of the Cav-1 α densitometry signal normalized to that of the GAPDH loading control shows that there is no statistically significant difference in the Cav-1 α protein expression levels in lamin A/C-deficient MEFs expressing the mock vector without lamin A (*Lmna*^{-/-} MEFs DJ1-mock-S) in comparison to its control *Lmna*^{-/-} MEFs (panel B). Cav-1 α protein expression is not significantly different in the lamin A/C-deficient MEFs retrovirally transfected to express the *LMNA* WT or mutant form (E358K) that results in EDMD in comparison to their control lamin A/C-deficient MEFs expressing the mock vector without lamin A (*Lmna*^{-/-} MEFs DJ1-mock-S) (panel C). Cav-1 α translational levels are significantly reduced in lamin A/C-deficient MEFs retrovirally transfected to express the mutant form (L530P) that results in EDMD. Data represent mean fold difference \pm SEM in comparison to the controls *Lmna*^{-/-} MEFs (panel B) and *Lmna*^{-/-} MEFs (DJ1-mock-S) (panel C) derived from 3 independent experiments. One asterisk represents a statistical significance ($P < 0.05$).

4. ***Cav-1 α protein expression is differentially expressed in mouse embryo fibroblast (MEF) cell line derived from mice homozygous for the N195K mutant form (DCM phenotype), but not significantly altered in MEFs derived from mice either lacking A-type lamin expression or emerin expression (EDMD phenotype) in comparison to the wild-type (WT) controls under baseline conditions by immunofluorescence staining.***

To investigate potential alterations in the intracellular distribution and localization of Cav-1 α in *Lmna*^{+/+}, *Lmna*^{N195K/N195K}, *Lmna*^{-/-} and *Emd*^{-/-} MEFs under baseline conditions, we performed immunofluorescence staining of PFA fixed cells and stained the cells with Cav-1 α antibody. Using the same exposure time, we acquired nine image frames per slide for each of the above mentioned MEF cell lines. Subsequently, images were analyzed using Image J software whereby we did a relative semi-quantitative assessment of Cav-1 α per cell per frame by measuring the relative fluorescence intensity normalized to background between the various tested cell lines. The data indicates a significant increase in the protein expression of Cav-1 α in N195K MEFs with a 1.85-fold (\pm 0.29) in comparison to the control WT MEFs (*P*-value <0.05) (Figure 15B). A set of representative images are shown in figure 15A.

Immunofluorescence data, however, does not suggest any significant difference in the relative fluorescence intensity of Cav-1 α in lamin A/C- and Emd-deficient MEFs when compared to the WT control. Indeed, quantification of the relative fluorescence intensity in lamin A/C-deficient MEFs shows a 1.05-fold (\pm 0.06) insignificant difference relative to the WT controls (*P*-value >0.05). Similarly, a 0.85-fold (\pm 0.05) difference in the fluorescence intensity was quantified in Emd-deficient MEFs and was not determined to be statistically different from the WT MEFs (*P*-value >0.05) (Figure 15B). Results are represented as mean fold difference in the fluorescence intensity \pm SEM of three independent experiments.

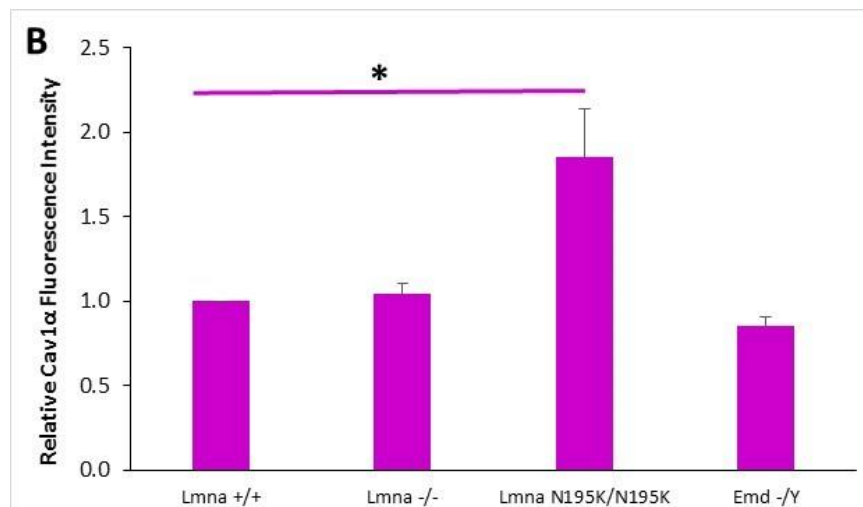
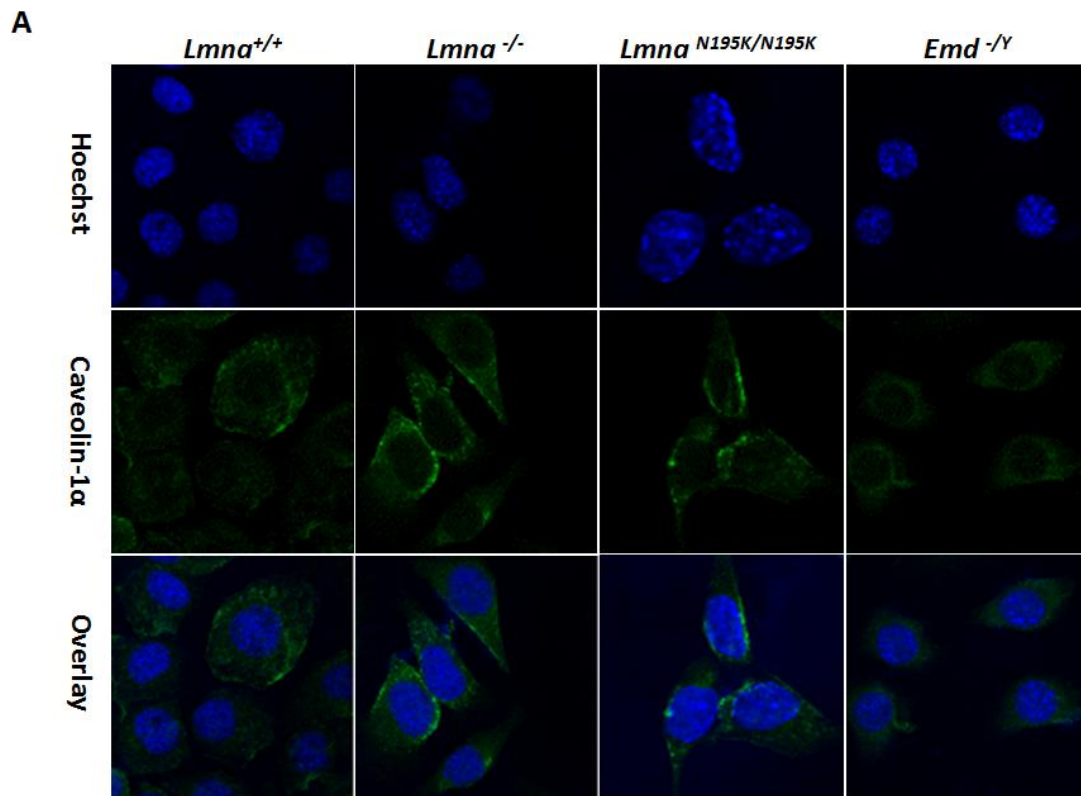


Figure 24 | Immunofluorescence staining and semi-quantitative analysis of Cav-1 α protein expression in *Lmna*^{-/-}, *Lmna*^{N195K/N195K} and *Emd*^{-/Y} mutant MEFs vs. control WT cells cultured at full confluence under baseline conditions. Panel A; representative confocal microscope images showing immunofluorescence staining of Cav-1 α in MEF cells deficient in A-type lamins and emerin and in MEF cells expressing the N195K mutant form in comparison to the WT MEF cells. Hoechst was used to stain the nuclei (uppermost panel). Images were acquired at 63x magnification. Semi-quantitative assessment of the relative fluorescence intensity of Cav-1 α reveals a significant increase in the Cav-1 α protein expression in *Lmna*^{N195K/N195K} MEFs relative to the WT cells (Panel B). Data represent mean \pm SEM derived from 3 independent repeats. One asterisk represents a statistical significance ($P < 0.05$).

C. Investigate potential alterations in protein expression and intracellular distribution of LKB1 under baseline conditions in mouse embryo fibroblast (MEF) cell lines derived from mice either lacking A-type lamin expression or emerin expression (EDMD phenotype), homozygous for the N195K mutant form (DCM phenotype) versus wild-type (WT) and in a panel of lamin A/C-deficient MEFs retrovirally transfected to express *LMNA* WT or mutant forms that result in EDMD (E358K, L530P).

1. *LKB1* protein expression is significantly elevated in *Lmna*^{-/-} MEFs (Lamin A/C null) but unaltered in *Lmna*^{N195K/N195K} MEFs and *Emd*^{-Y} MEFs (*Emd* null) under baseline conditions in comparison to *Lmna*^{+/+} control MEFs.

Western Blot densitometry qualitative and quantitative analysis pertaining to the expression of LKB1 protein normalized to GAPDH loading control under baseline conditions in the panel of MEF cells suggest a significant elevation in the LKB1 protein in *Lmna*^{-/-} MEFs with a 2.02-fold (± 0.35) when compared to the control WT MEFs (P -value < 0.05) (Figure 25 A & B). The data, however, does not indicate any significant difference in the LKB1 protein levels normalized to GAPDH loading control in *Lmna*^{N195K/N195K} and in *Emd*^{-Y} MEFs under baseline conditions and in comparison to the *Lmna* WT MEFs. As represented in Figure 15A, qualitative assessment of the autoradiography WB films does not show any change in the expression levels of LKB1 in both *Lmna* N195K and *Emd* null MEFs. Indeed, densitometry quantification data reveal a non-significant increase in LKB1 levels in *Lmna* N195K with a 1.32-fold (± 0.25) and in *Emd* null MEFs with a 1.54-fold (± 0.24) in comparison to *Lmna* WT MEFs (P -value > 0.05). Quantification densitometry data of LKB1 normalized to GAPDH loading control is represented as mean fold change \pm SEM derived from five independent experiment.

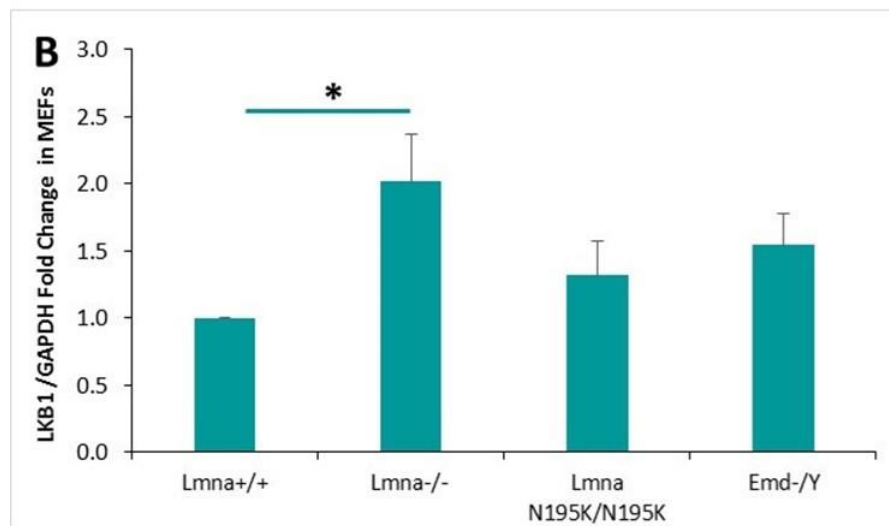
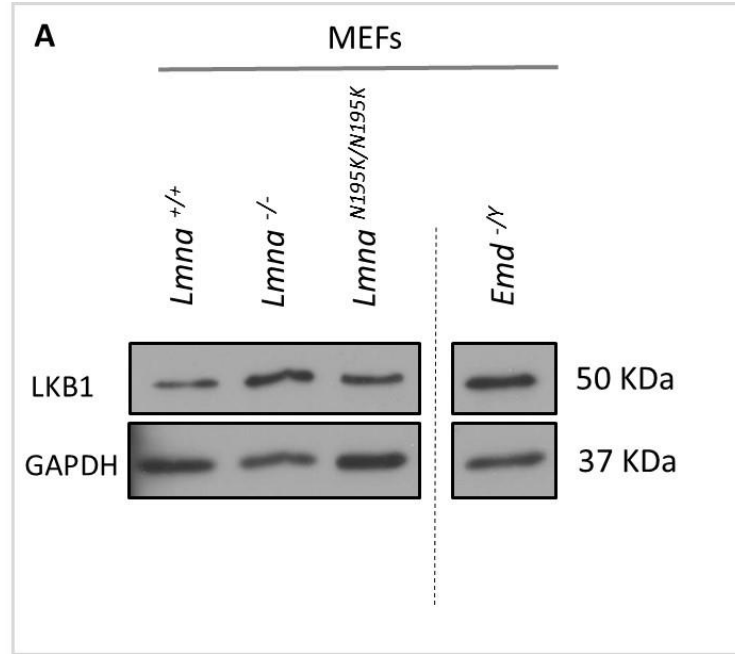


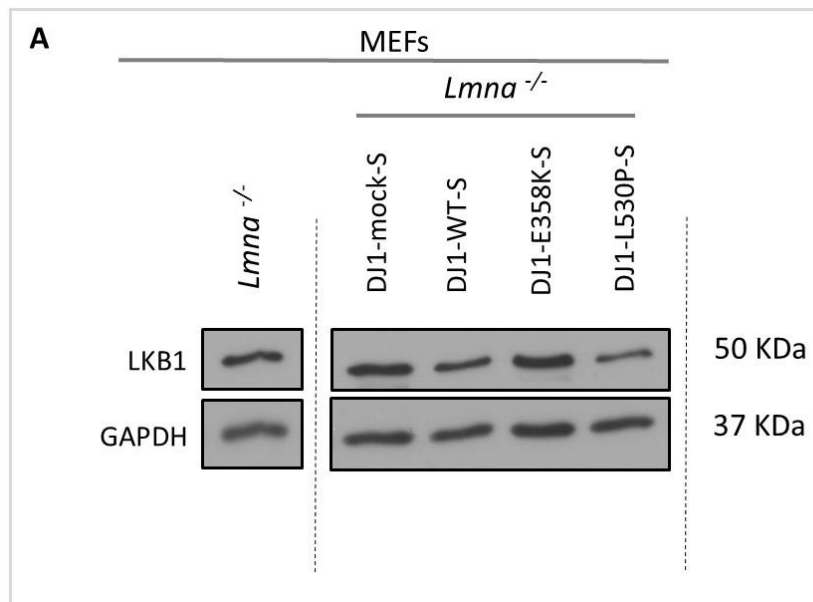
Figure 25| Western Blot analysis of LKB1 protein expression in *Lmna*^{-/-}, *Lmna*^{N195K/N195K} and *Emd*^{-Y} mutant MEFs vs. control WT cells cultured at full confluence under baseline conditions. Panel A; representative blot. Image J quantification and analysis of the LKB1 densitometry signal normalized to that of the GAPDH loading control shows that there is a significant up-regulation in LKB1 protein in *Lmna*^{-/-} cells in comparison to WT cells cultured under baseline conditions (panel B). The data suggest that there is an up-regulation in LKB1 protein expression in the other two mutant cell lines but it is not determined to be statistically significant. Data represent mean fold change ± SEM derived from 5 independent experiments. One asterisk represents a statistical significance ($P < 0.05$).

2. *LKB1* translational levels are not altered in Lamin A/C-deficient MEFs retrovirally transfected to express the LMNA WT or the mutant form that result in EDMD (E358K) and are significantly reduced in the mutant form (L530P) that results in EDMD in comparison to their control Lamin A/C-deficient MEFs expressing the mock retroviral vector without lamin A.

To further validate our hypothesis, we aimed at testing whether the retroviral expression of WT *LMNA* or *LMNA* mutant forms that result in EDMD in lamin A/C-deficient MEFs may plausibly affect the protein expression of Cav-1 α through altering the translational levels of *LKB1* under baseline conditions. Accordingly, total cell lysates from *Lmna*^{-/-} MEFs genetically modified the *LMNA* WT (DJ1-WT-S) or mutant forms that result in EDMD (DJ1-E358K-S and DJ1-L530P-S) in comparison to their mock control (DJ1-mock-S) cells were extracted while ensuring consistency in cell density, spreading and confluency across tested samples and in between independent repeats. This was followed by SDS-PAGE and Western Blot densitometry quantification and analysis.

The protein expression level of *LKB1* normalized to GAPDH loading control is not altered in *Lmna*^{-/-} MEFs expressing the mock retroviral vector without lamin A, DJ1-mock-S, in comparison to its control *Lmna*^{-/-} MEFs as shown in **Figure 26A**. Densitometry quantification data propose a non-significant difference in the translational levels of *LKB1* normalized to GAPDH in that we obtained a 1.29-fold difference (± 0.23) when compared to *Lmna*^{-/-} MEFs control (**Figure 26B**). Assessing the expression of the *LKB1* protein normalized to GAPDH between the *Lmna*^{-/-} MEFs genetically altered to express the *LMNA* WT (DJ1-WT-S) or the mutant form that results in EDMD (DJ1-E358K-S) with the control *Lmna*^{-/-} MEFs expressing mock retroviral vector without lamin A did not reveal any significant difference in that a 0.99- and 0.85-fold (± 0.23 and ± 0.3) change were measured respectively in comparison to

the *Lmna*^{-/-} MEFs DJ1-mock-S (*P*-value>0.05) (**Figure 26C**). On the contrary, densitometry analysis data suggest a significant reduction in the LKB1 protein normalized to GAPDH in *Lmna*^{-/-} MEFs genetically modified expressing the mutant form that results in EDMD (DJ1-L530P-S) with a 0.49-fold decrease (± 0.27) relative to the control *Lmna*^{-/-} MEFs DJ1-mock-S (*P*-value<0.05) (**Figure 26C**). Densitometry quantification data of LKB1 normalized to GAPDH loading control is represented as mean fold change \pm SEM derived from five independent repeats.



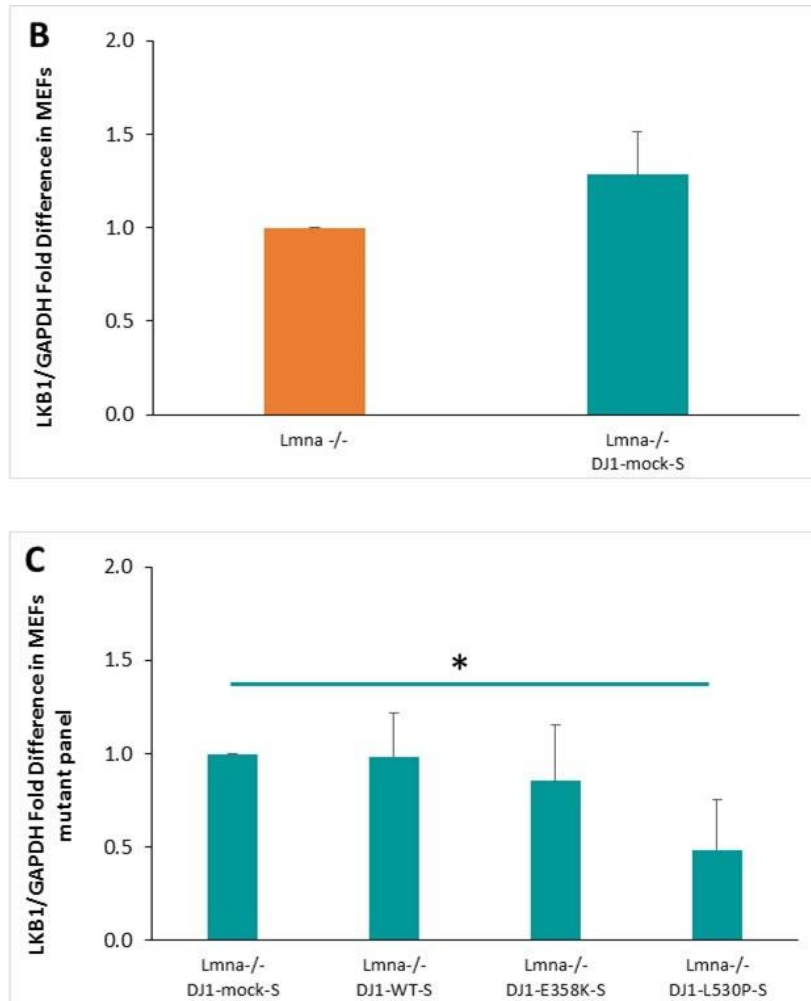


Figure 26| Mean fold change of LKB1 protein expression in lamin A/C-deficient MEFs retrovirally transfected to express the *LMNA* WT or mutant forms (E358K and L530P) that result in EDMD cultured at full confluence at baseline conditions. Panel A; representative blot. Image J quantification and analysis of the LKB1 densitometry signal normalized to that of the GAPDH loading control shows that there is no statistically significant difference in the LKB1 protein expression levels in lamin A/C-deficient MEFs expressing the mock vector without lamin A (*Lmna*^{-/-} MEFs DJ1-mock-S) in comparison to its control *Lmna*^{-/-} MEFs (panel B). LKB1 protein expression is not significantly different in the lamin A/C-deficient MEFs retrovirally transfected to express the *LMNA* WT or mutant form (E358K) that results in EDMD in comparison to their control lamin A/C-deficient MEFs expressing the mock vector without lamin A (*Lmna*^{-/-} MEFs DJ1-mock-S) (panel C). However, LKB1 translational levels are significantly reduced in lamin A/C-deficient MEFs retrovirally transfected to express the mutant form (L530P) that results in EDMD. Data represent mean fold difference \pm SEM in comparison to the controls *Lmna*^{-/-} MEFs (panel B) and *Lmna*^{-/-} MEFs (DJ1-mock-S) (panel C) derived from 5 independent experiments. One asterisk represents a statistical significance ($P < 0.05$).

CHAPTER IV

DISCUSSION

Laminopathies represent a group of genetic disorders manifested as diverse pathologies affecting a broad array of tissues including skeletal and cardiac muscle. They arise from mutations in the *LMNA* gene which encodes for the nuclear envelope (NE) proteins lamins A/C that anchor other NE proteins to the nuclear membrane. Many hypothesis have been postulated in an attempt to associate what is known about the NE functions with the disease phenotypes. In this study, we highlight the importance of the gene regulation hypothesis which proposes that mutations in the *LMNA* gene alter the normal gene expression profile either directly by interacting with chromatin, or indirectly by grossly disrupting protein-protein interactions. Since the localization of many INM proteins is dependent on lamins A/C, mutations in the *LMNA* gene may change the protein composition of the INM, the nucleoplasm and cytoplasm as well. Accordingly, different proteins may be displaced depending on whether their binding sites on the surface of lamins A/C are disrupted by mutations which ultimately explains the phenotypic diversity and the tissue specific impaired function in laminopathies. This has been broadly validated by several studies indicating the various lamin interacting partners including transcription factors and other signaling partners that function in a tissue specific manner. The interest in the gene regulation theory particularly in the pathogenesis of muscular laminopathies enabled us to focus our study on the mechanosensitive gene *Cav-1* as it plays fundamental roles in muscle repair and regeneration. Nevertheless, the choice of *Cav-1* was based on the finding that EDMD and DCM are manifested in mechanically strained tissues. As such, we rationalized that

the loss of lamins A/C or emerin, or mutations in the *LMNA* gene may affect the expression profile of Cav-1 at the transcriptional and translational levels thus contributing to the disease pathogenesis in EDMD and DCM. Real-Time PCR quantification data shows that *Cav-1α* transcript levels are reduced in *Lmna*^{-/-} MEFs in comparison to the WT controls. Interestingly, Cav-1α acts as negative regulator of proliferation and caveolin null MEFs show a hyper-proliferative phenotype. In addition, fibroblasts lacking functional A-type lamins show increased proliferation which may be explained in part by Cav-1α down-regulation. Moreover, our quantitative Real-Time PCR results suggest a significant elevation in the *Cav-1α* transcript levels in *Lmna*^{N195K/N195K} MEFs and *Emd*^{-Y} MEFs. Fibroblasts from emerin-deficient MEFs divide slowly *in vitro* under baseline conditions. The lower rate of proliferation observed in MEFs lacking emerin expression in comparison to the WT controls may be attributed in part to the elevated levels of Cav-1α. When probing for the total *Cav-1* pool (both α & β isoforms) at the transcriptional level, we detected a lower *Cav-1* transcript in lamin A/C-deficient MEFs in comparison to the wild-type controls, and an induction of total *Cav-1* transcript levels in N195K and Emd null MEFs. Any change in the total *Cav-1* pool reflects the status of the β isoform in the tested samples. Comparing the results obtained from investigating the expression of the *Cav-1α* transcript alone and total *Cav-1* pool at baseline conditions, suggests that in *Lmna*^{-/-} MEFs, the β isoform of *Cav-1* is not altered, yet the latter is minimally down-regulated in the *Emd*^{-Y} MEFs and slightly up-regulated in the N195K MEFs. Our next aim was to assess any putative alterations in the Cav-1α protein levels by Western Blot analysis under baseline conditions. Densitometry quantification results did not show any significant difference in the overall protein expression of Cav-1α between *Lmna*^{-/-}, *Lmna*^{N195K/N195K}, *Emd*^{-Y}

MEFs and their control *Lmna*^{+/+}. It is worth mentioning here that protein extracts from total cell lysates were prepared using standard RIPA lysis buffer which may not have released all caveolin-1 α proteins bound to caveolae via homo-oligomerization and hetero-oligomerization especially that caveolae and lipid raft microdomains are insoluble in non-ionic detergents at low temperature due to their abundance in cholesterol and sphingolipids. Consequently, our Western Blot results reveal existing protein expression differences primarily in the fraction of Cav-1 α protein that is more soluble in the protein extraction buffer used rather than the membrane bound fraction. A number of studies reported that Cav-1 α exists in multiple forms one of which is secreted into the medium overlaying cells. The fact that we could see a down-regulation of Cav-1 α at the transcriptional level and not at the protein level in *Lmna*^{-/-} MEFs may be in part explained by the fact that lamin A/C-deficient MEFs might compensate for the decreased gene expression by retaining Cav-1 α in the cells and decreasing its rate of secretion. Moreover, an up-regulation in the *Cav-1 α* transcript at the transcriptional level and not at the protein level as in *Lmna*^{N195K/N195K} and *Emd*^{-Y} MEFs suggests that the cells may be translating and secreting the protein. This can be further validated by quantification of the secreted form of the protein in the media overlaying the cells by Enzyme Linked Immunosorbent Assay (ELISA) to assess the abundance of Cav-1 α in media overlaying mutant cell lines relative to control WT cells. Nevertheless, it would be indispensable at this stage to test for differential Cav-1 α and/or total Cav-1 protein expression *in situ* in the mutant lines relative to the WT controls using cell-based ELISA kits that are commercially available. This would enable us to better interpret the data obtained from Western Blot analysis of protein expression in cell lysates. A second factor that may explain at least in part the results we obtained at the translational level

of Cav-1 α is the rate of turnover or the stability of the Cav-1 α mRNA; lower *Cav-1 α* transcript levels in *Lmna*^{-/-} MEFs may be counterbalanced by a delay in its breakdown at the protein level relative to the WT controls. However, the elevation in the *Cav-1 α* transcript levels in *Lmna*^{N195K/N195K} and *Emd*^{-Y} MEFs at baseline conditions which was not observed at the protein level may be attributed to its higher rate of turnover i.e. *Cav-1 α* transcript may have a shorter half-life in the two mutants *Lmna*^{N195K/N195K} and *Emd*^{-Y} MEFs in comparison to their control WT MEFs. Since Cav-1 is a lipid raft protein whose expression is very much affected by cell-cell contact and overall spreading and density of cells in tissue culture, we decided to assess whether there is any difference in the expression and distribution of the Cav-1 α protein in the three mutant MEFs in comparison to the WT controls by immunofluorescence staining while ensuring consistency in overall cell spreading and confluence across the four cell lines and the three independent repeats. Data suggest that the overall expression of Cav-1 α is significantly increased in *Lmna*^{N195K/N195K} MEFs relative to the control WT cells. No significant perturbation in the protein expression of Cav-1 α was observed in the lamin A/C-deficient and emerin-deficient MEFs in comparison to the WT control cells. The discrepancy obtained between the Western Blot and immunofluorescence data may be explained by differences in the membrane bound fraction of Cav-1 α in *Lmna*^{N195K/N195K} MEFs relative to their control WT MEFs which could not be detected by Western Blot due to the standard protein extraction technique used. We further aimed at validating our hypothesis in a panel of lamin A/C-deficient MEFs expressing the *LMNA* WT or mutant forms that result in EDMD (E358K and L530P) by retroviral transfection. We rationalized that the re-introduction of wild-type lamin A into lamin A/C-deficient MEFs by retroviral transfection would recapitulate the gene expression profile of Cav-

1 α in these MEFs relative to their mock controls transfected with a retroviral vector without lamin A. To our surprise, we found that retroviral transfection of lamin A/C-deficient MEFs with the mock vector (empty vector) that does not include lamin A led to a significant elevation in the transcript levels of *Cav-1* α and total *Cav-1* ($\alpha+\beta$) relative to their control *Lmna*^{-/-} MEFs. Caveolar/raft pathways have been extensively studied as clathrin-independent processes for endocytosis and infection of some viruses. During the early stages of infection, viruses inform the cells of their presence on cell surfaces allowing the latter to launch an endocytic response promoting viral entry into the cells. This fundamental event is mediated by activation of signaling cascades. Accordingly, many viruses associate with lipid rafts and caveolar domains to initiate intracellular signaling (Marsh & Helenius, 2006). It has been reported that signaling components involved in promoting the entry of viruses into the host cells include tyrosine kinases, raft lipids, dynamin 2, actin, Rho GTPases and caveolin-1 depending on the virus and the host cell type (Pelkmans et al., 2002). Therefore, the significant increase in the *Cav-1* transcript observed in the *Lmna*^{-/-} MEFs retro virally transfected with the mock vector may be possibly explained by the fact that viral infection may induce an increase in the caveolae and perhaps caveolin-1 at the plasma membrane for enhanced endocytosis and entry of viruses into the MEF cells. Despite the fact that this panel of MEF lines has been widely and successfully used in other research studies aiming at answering a broad array of biochemical and biomechanical questions relevant to these disease models particularly those related to nuclear fragility, it is worth mentioning that this panel of MEFs may not serve as a good model to study perturbations in the expression of signaling components downstream of caveolin-1. Our quantitative Real-Time PCR data revealed that the *Cav-1* gene expression profile was

restored upon the re-introduction of *LMNA* WT or *LMNA* E358K mutant form that results in EDMD; however, re-introducing the L530P mutant form of *LMNA* which also results in EDMD did not recapitulate the *Cav-1* transcript levels when compared to the mock control lamin A/C-deficient MEFs. This can be explained by the fact that this mutation in the lamin A protein may disrupt the binding of a transcription factor that is possibly required for the activation of *Cav-1* gene expression or at least may alter the binding of a protein that may affect directly or indirectly *Cav-1* expression. Indeed, L530 amino acid lies within the C-terminal domain particularly in the Ig-fold like domain of lamin A that is very well known in mediating protein-protein interactions. The leucine to proline mutation could result in conformational changes that may affect the surface structure of lamin A protein eventually altering the interaction between lamin A and the transcription factor for example. Interestingly, a previous study reported that L530P mutation in lamin A reduced the binding of the transcription factor Sterol- response element- binding protein1 (SREBP1) by 61%. This dramatic decrease in the interaction between lamin A in AD-EDMD with SREBP1 exceeded the loss of interactions between lamin A protein in FPLD mutations (reduced by 25-42%) which primarily affect the adipose tissue (Lloyd et al., 2002). This is supported by the finding that *LMNA* knock-out mice display features of loss of subcutaneous fat by ~ 4 weeks in addition to the EDMD phenotype (Sullivan et al., 1999). Intriguingly, the DNA regulatory sequence of SREBP1 known as the sterol regulatory element (SRE) like domain lies in the promoter region of the *Cav-1* gene (Bist et al., 1997). SREBP1 is a dual specificity transcription factor of the basic-helix-loop-helix-leucine zipper (bHLH-Zip) family which has been shown to be implicated in the independent regulation of cholesterol biosynthesis and adipogenesis (Lloyd et al., 2002). The binding of SREBP1

to the SRE in the promoter region of caveolin-1 is thought to inhibit caveolin-1 gene expression as reported by previous studies (Bist et al., 1997; Yuan et al., 2008). Other proteins that were reported to interact with the C-terminal domain and in the vicinity of the L530 amino acid position include actin, c-Fos, emerin and PKC α , all of which were previously shown to interact with caveolins either directly or indirectly (Ho & Lammerding, 2012). The observed increase at the transcriptional level of Cav-1 gene was not translated at the protein level in this panel of MEF cells. While comparing the protein expression of Cav-1 α in lamin A/C-deficient MEFs transfected with the empty vector (mock control) to their control lamin A/C-deficient MEFs, our Western Blot results did not show any significant difference in the protein expression of Cav-1 α . Likewise, the expression of Cav-1 α protein in lamin A/C-deficient MEFs genetically modified to express the *LMNA* WT or *LMNA* E358K mutant form that results in EDMD was not altered relative to the mock control lamin A/C-deficient MEFs transfected with the empty vector. The observed increase in *Cav-1* (both α & β) transcript levels was not reflected at the protein level possibly due to putative perturbations in the secreted form of Cav-1 α protein. In other words, lamin A/C-deficient MEFs expressing the *LMNA* WT or the E358K mutant form by retroviral transfection seem to secrete more of Cav-1 α to the media outside the cells in comparison to their mock control. The examined inconsistency in this panel of MEFs could also be attributed to a higher rate of turnover of *Cav-1 α* transcript. On the contrary, Cav-1 α protein level was significantly lower in lamin A/C-deficient MEFs genetically modified to express the *LMNA* L530P mutant form relative to its control. This can be explained in part by a decrease in the half-life of Cav-1 α post transcription and/or an elevation in the secreted pool of Cav-1 α . Further validation of putative modulations in Cav-1 α and/or total Cav-1 protein expression must

be done using cell-based ELISA kits. The role of caveolins in mechanotransduction has always been viewed as a downstream platform. In this study, however, we intended to investigate putative alterations in the protein expression of LKB1, an upstream kinase that was recently reported to influence caveolin-1 expression levels in an indirect manner (Zhang et al., 2014). Western Blot data suggest a significant rise in the protein expression of LKB1 in *Lmna*^{-/-} MEFs at baseline conditions in comparison to the WT controls. The protein expression of LKB1 was not altered in *Lmna*^{N195K/N195K} and *Emd*^{-/-} MEFs as displayed by our Western Blot experiments. LKB1 is a known upstream kinase of AMPK which once activated by LKB1, is known to inhibit the translocation of an RNA binding protein termed Human antigen R (HuR) from the nucleus to the cytoplasm through the regulation of importin- α 1, an adaptor protein involved in nuclear import (Wang et al., 2002). HuR is an RNA binding protein that regulates the stability of adenylate-uridylylate-rich element-containing transcripts primarily localized in the nucleus. In an attempt to better understand the regulation of caveolin-1 expression by LKB1, the 3' untranslated region (3'UTR) of Cav-1 mRNA was examined and found to possess 4 conserved adenylate-uridylylate-rich elements (Zhang et al., 2014). Accordingly, in the absence of AMPK activation, HuR can translocate from the nucleus to the cytoplasm where it binds to the 3'UTR of caveolin-1 mRNA enhancing its stability and, thus, resulting in elevated caveolin-1 protein levels. The increase in LKB1 protein levels in lamin A/C null MEFs may result in the activation of AMPK which in turn prevents HuR from binding to the 3'UTR of Cav-1 mRNA and stabilizing it. The reduction in *Cav-1* (both α & β) transcript levels obtained in lamin A/C null MEFs and not Cav-1 α protein levels favor this conclusion. Western Blot data suggest that in *Lmna*^{-/-} MEFs, *Cav-1* gene expression profile is in part

dependent on LKB1 signaling. Despite the consistency obtained in these results in the lamin A/C-deficient MEFs, we still have to confirm the involvement of AMPK in this signaling axis through assessing the phosphorylated forms of AMPK relative to the total AMPK levels in these MEFs under baseline conditions. Performing Western Blot on nuclear and cytosolic fractions of HuR and/or immunofluorescence staining to investigate intracellular localization of HuR between lamin A/C-deficient MEFs and their control WT cells would also provide better insight to its role in regulating the half-life of Cav-1 mRNA particularly in this context. On the other hand, LKB1 protein levels were not altered in *Lmna*^{N195K/N195K} and *Emd*^{-Y} MEFs relative to the WT controls implying that activated AMPK levels were not perturbed as well. The fact that we did not see any significant difference in the Cav-1 α protein despite the rise in *Cav-1* transcript suggests that alternative regulatory mechanisms independent of LKB1 may exist. Testing the expression of LKB1 in the panel of lamin A/C-deficient MEF cells expressing the *LMNA* WT or mutant forms that result in EDMD (E358K and L530P) by retroviral transfection revealed a significant decrease in LKB1 translational levels in the *LMNA* L530P relative to its mock control without detecting any significant difference in the *LMNA* WT or E358K mutant form. This did not correlate with the results observed at the translational level whereby we did not observe any change in the Cav-1 α protein in *LMNA* WT or E358K mutant form at baseline conditions further confirming our previous statement of assessing possible alterations in Cav-1 α and/or total Cav-1 *in situ* by cell-based ELISA. The decrease in LKB1 protein levels in *Lmna*^{-/-} MEFs genetically modified to express the *LMNA* L530P mutant was not reflected by an increase in the Cav-1 α protein pool which can be in part attributed to differences in the secreted Cav-

1 α protein or differences in Cav-1 α protein that we could not detect using the standard RIPA lysis buffer for extraction of proteins from total cell lysates.

Since patients suffering from laminopathies are more susceptible to oxidative stress and display higher levels of ROS, we evaluated the effect of H₂O₂-induced oxidative stress on the response of Cav-1 both at the transcriptional and translational levels in *Lmna*^{-/-}, *Lmna*^{N195K/N195K} MEFs in comparison to the WT control cells. We rationalized that the response of the two mutant cell lines at least at the transcriptional level would be different from that of the WT cells, given that the data obtained at baseline conditions suggested a higher pool of Cav-1 in *Lmna*^{N195K/N195K} and a lower pool in *Lmna*^{-/-} MEFs. Accordingly, we exposed the cells at full confluence to two doses of H₂O₂ namely, 0.1 μ M and 0.5 μ M for 5, 15, 30 and 60min. WT cells cultured at both 80% sub confluence and 100% full confluence did not respond to either doses of H₂O₂. Real-Time PCR data did not reveal any response of *Cav-1* (both α & β isoforms) to H₂O₂-induced oxidative stress. This was also reflected at the protein level whereby we did not detect any alteration in the soluble fraction of Cav-1 α in response to both doses of H₂O₂ for a timeline of 6hrs. The fact that WT cells did not respond to H₂O₂-induced oxidative stress can be in part attributed to them possessing a normal and functional nuclear lamina whereby redox responsive transcription factors may respond to a change in the cells' redox state ultimately activating genes involved in responding to oxidative stress. Nonetheless, the antioxidant enzymes in these cells may buffer the effect of H₂O₂-induced oxidative stress as reflected in the response of WT cells. This can also be attributed to the fact that the two depicted doses of H₂O₂ may not be close to the threshold concentration required to induce oxidative stress in WT cells; however, we decided to continue using these two concentrations as these stressed the two mutant cell

lines but did not induce apoptosis allowing us to detect alterations in the expression of Cav-1 from viable non-apoptotic cells. *Lmna*^{-/-} MEFs exposed to both doses of H₂O₂ displayed a rapid response at the transcriptional level characterized by an induction in both isoforms of *Cav-1*. The fast response seen in these cells is indicative of the reduced transcript levels of *Cav-1* at baseline conditions allowing the cells to activate gene transcription to generate the needed amount of protein at the time of H₂O₂ induction of oxidative stress. The protein expression of Cav-1 α in *Lmna*^{-/-} MEFs decreased after 5 min of exposure to 0.5 μ M of H₂O₂. At that same time point, the *Cav-1 α* transcript was significantly elevated suggesting that these MEFs respond to 0.5 μ M of H₂O₂ induced oxidative stress by rapidly secreting the protein. This response was also seen after 15min of H₂O₂ treatment. It is known that in response to oxidative stress, Cav-1 α gets phosphorylated and secreted into the media overlaying the cells for its proper functioning. Following exposure to 0.1 μ M of H₂O₂ for 15 min, we observed the same response in lamin A/C-deficient MEFs which was continuous over the 1hr timeline of H₂O₂ exposure. On the contrary, the protein expression of Cav-1 α post exposure to 0.5 μ M of H₂O₂ for 30min was shown to be significantly higher than the mock-treated control cells indicating that *Lmna*^{-/-} MEFs decreased protein secretion. Cav-1 α protein secretion was resumed after 1hr of exposure to 0.5 μ M of H₂O₂ in *Lmna*^{-/-} MEFs. In *Lmna*^{N195K/N195K} MEFs, we observed a slight delay in the *Cav-1* transcript induction at 15 min post induction of oxidative stress perhaps because these cells rely on the elevated levels of *Cav-1* transcript upfront at baseline conditions. Cav-1 α protein levels in *Lmna*^{N195K/N195K} MEFs were shown to be significantly reduced in response to H₂O₂-induced oxidative stress during the 60min exposure to both doses of H₂O₂ suggesting that the increase in the transcript level was not reflected at the protein level possibly

because Cav-1 α protein got secreted. It is known that in response to oxidative stress, Cav-1 α gets phosphorylated and secreted into the media overlaying the cells for its proper functioning. The significant reduction in the Cav-1 α protein as early as 5min post H₂O₂ exposure suggests that Cav-1 α gets rapidly phosphorylated and secreted into the media in *Lmna*^{N195K/N195K} MEFs. Nevertheless, after 1.5hrs of exposure to both doses of H₂O₂, Western Blot data propose that Cav-1 α protein bounces back to near baseline levels. The N195K MEFs may respond to the enhanced decrease in Cav-1 α protein post induction of oxidative stress for a timeline of 1hr by activating the translation of Cav-1 α transcript compensating for the secreted Cav-1 α post phosphorylation. Hence, it would be essential to check whether or not the phosphorylated form of Cav-1 α is differentially regulated following induction of stress in the two mutant cell lines versus the WT control under both baseline and oxidative stress conditions allowing us to better interpret our quantitative Real-Time PCR and Western Blots data. Our future aims also include investigating the effects of the loss of *LMNA* or *LMNA* mutations on the differential expression of total Cav-1 pool by Western Blot and immunofluorescence staining using a Cav-1 antibody specific for both isoforms. For a better assessment of the role of Cav-1 in EDMD, our future aims will also address modulations in the expression of Cav-1 under oxidative stress conditions in *Emd*^{-Y} MEFs. Furthermore, we intend to assess the translational levels of LKB1 protein under oxidative stress conditions as changes in protein levels of LKB1 may possibly explain the Western Blot results obtained in this study. Scanning electron microscopy (SEM) could also be employed to identify any structural changes particularly in the shape, the overall spreading and number of membrane caveolae between the mutant cell lines and the WT control. Considering that the laminopathies we are investigating are

those affecting striated muscle, it is imperative to investigate the expression of other caveolin proteins particularly caveolin-3 being the one exclusively expressed in muscle tissue. Any finding in this regard will have to be investigated *in vitro* in C2C12 myoblasts lacking A-type lamin expression or those expressing the N195K mutant form and further validated in skeletal and/or cardiac muscle tissue derived from an EDMD mouse model and/or a DCM mouse model. Ultimately, this further investigation will provide a better understanding of the mechanisms implicated in muscular laminopathies in a more relevant context.

Given the recent reports that caveolin-2 has a regulatory function in the nucleus subsequent to its insulin-induced targeting to the inner nuclear membrane and that numerous examples from the literature point out to a role of lamin A/C in gene regulation via regulating the activity of transcriptional factors, it would also be interesting to test by performing co-immunoprecipitation assays whether caveolins and A-type lamins interact/associate directly or indirectly. This would provide further insight into the intricate interplay between caveolins, lamin A/C, and laminopathies.

Studying the effects of specific lamin A/C mutations on the differential expression and localization of mechanosensitive genes such as *Cav-1* and *Cav-3* will unravel many clues related to the molecular and cell biology of muscular laminopathies. Advancement in this context will provide novel insights into putative mechanisms responsible for the phenotypic diversity of laminopathies. By that time, feasible therapies targeting the pathogenic consequences of lamin A/C mutations in muscular laminopathies will start to emerge.

REFERENCES

- Alessi, D. R., Sakamoto, K., & Bayascas, J. R. (2006). LKB1-dependent signaling pathways. *Annu. Rev. Biochem.*, *75*, 137–163.
- Allen, R.G., & Tresini, M. (2000). OXIDATIVE STRESS AND GENE REGULATION. *Free Radic. Biol. Med.*, *28*, 463–499.
- Andres, V., & Gonzalez, J. M. (2009). Role of A-type lamins in signaling, transcription, and chromatin organization. *J. Cell Biol.*, *187*, 945–957.
- Armulik, A., Abramsson, A., & Betsholtz, C. (2005). Endothelial/pericyte interactions. *Circ. Res.*, *97*, 512–523.
- Bengtsson, L., & Wilson, K. L. (2004). Multiple and surprising new functions for emerin, a nuclear membrane protein. *Curr. Opin. Cell Biol.*, *16*, 73–79.
- Bione, S., Maestrini, E., Rivella, S., Mancini, M., Regis, S., Romeo, G., & Toniolo, G. (1994). Identification of a novel X-linked gene responsible for Emery-Dreifuss muscular dystrophy. *Nat. Genet.*, *8*, 323–327.
- Bist, A., Fielding, P.E., & Fielding, C. J. (1997). Two sterol regulatory element-like sequences mediate up-regulation of caveolin gene transcription in response to low density lipoprotein free cholesterol. *Proc. Natl. Acad. Sci. U.S.A.*, *94*, 10693–10698.
- Bonne, G., Di Barletta, M.R., Varnous, S., Bécane, H.M., Hammouda, E.H., Merlini, L., ... Schwartz, K. (1999). Mutations in the gene encoding lamin A/C cause autosomal dominant Emery-Dreifuss muscular dystroph. *Nat. Genet.*, *21*(3), 285–288.
- Bossie, C.A. & Sanders, M. M. (1993). A cDNA from *Drosophila melanogaster* encodes a lamin C-like intermediate filament protein. *J. Cell Sci.*, *104*, 1263–1272.
- Broers, J.L., Hutchison, C.J., & Ramaekers, F. C. (2004). Laminopathies. *J. Pathol.*, *204*(4), 478–488.
- Broers, J.L., Peeters, E.A., Kuijpers, H.J., Endert, J., Bouten, C.V., Oomens, C.W., ... Ramaekers, F. C. (2004). Decreased mechanical stiffness in *LMNA*^{-/-} cells is caused by defective nucleo-cytoskeletal integrity: implications for the development of laminopathies. *Hum. Mol. Genet.*, *13*, 2567–2580.
- Bruno, C., Sotgia, F., Gazzero, E., Minetti, C., & Lisanti, M. P. (2007). *Caveolinopathies*. *GeneReviews*®.

- Burke, B., & Stewart, C. L. (2002). Life at the edge: the nuclear envelope and human disease. *Nat. Rev. Mol. Cell. Biol.*, 3(8), 575–585.
- Burke, B., & Stewart, C. L. (2013). The nuclear lamins: flexibility in function. *Nat. Rev. Mol. Cell. Biol.*, 14(1), 13–24.
- Capell, B. C., & Collins, F. S. (2006). Human laminopathies: nuclei gone genetically awry. *Nat. Rev. Genet.*, 7(12), 940–952.
- Chen, L., Lee, L., Kudlow, B.A., Santos, H.G.D., Sletvold, O., Shafeghati, Y., ... Oshima, J. (2003). LMNA mutations in atypical Werner's syndrome. *Lancet*, 362(9382), 440–445.
- Coffinier, C., Jung, H.J., Nobumori, C., Chang, S., Tu, Y., Barnes, R.H., ... Young, S. G. (2011). Deficiencies in lamin B1 and lamin B2 cause neurodevelopmental defects and distinct nuclear shape abnormalities in neurons. *Mol. Biol. Cell*, 22, 4683–4693.
- Cohen, A.W., Park, D.S., Woodman, S.E., Williams, T.M., Chandra, M., Shirani, J., ... Lisanti, M. P. (2003). Caveolin-1 null mice develop cardiac hypertrophy with hyperactivation of p42/44 MAP kinase in cardiac fibroblasts. *Am. J. Physiol. Cell Physiol.*, 284, C457–C474.
- Cohen, M., Lee, K. K., Wilson, K. L. & Gruenbaum, Y. (2001). Transcriptional repression, apoptosis, human disease and functional evolution of the nuclear lamina. *Trends Biochem. Sci.*, 26, 41–47.
- Collins, S. P., Reoma, J. L., Gamm, D. M., & Uhler, M. D. (2000). LKB1, a novel serine/threonine protein kinase and potential tumour suppressor, is phosphorylated by cAMP-dependent protein kinase (PKA) and prenylated in vivo. *Biochem. J.*, 680, 673–680.
- Constantinescu, D., Gray, H.L., Sammak, P.J., Schatten, G.P. & Csoka, A. B. (2006). Lamin A/C expression is a marker of mouse and human embryonic stem cell differentiation. *Stem Cells*, 24, 177–185.
- Dahl, K. N., Ribeiro, A. J. S., & Lammerding, J. (2008). Nuclear shape, mechanics, and mechanotransduction. *Circ. Res.*, 102(11), 1307–1318.
- Datta, K., Guan, T., & Gerace, L. (2009). NET37, a nuclear envelope transmembrane protein with glycosidase homology, is involved in myoblast differentiation. *J. Biol. Chem.*, 284(43), 29666–29676.
- De Sandre-Giovannoli, A., Chaouch, M., Kozlov, S., Vallat, J.M., Tazir, M., Kassouri, N., ... Lévy, N. (2002). Homozygous defects in LMNA, encoding lamin A/C nuclear-envelope proteins, cause autosomal recessive axonal neuropathy in human (Charcot-Marie-Tooth disorder type 2) and mouse. *Am. J. Hum. Genet.*, 70, 726–736.

- De Vos, W. H., Houben, F., Kamps, M., Malhas, A., Verheyen, F., Cox, J., ... Broers, J. L. V. (2011). Repetitive disruptions of the nuclear envelope invoke temporary loss of cellular compartmentalization in laminopathies. *Hum. Mol. Genet.*, *20*(21), 4175–4186.
- Dechat, T., Pflieger, K., Sengupta, K., Shimi, T., Shumaker, D. K., Solimando, L., & Goldman, R. D. (2008). Nuclear lamins : major factors in the structural organization and function of the nucleus and chromatin. *Genes Dev.*, *22*(312), 832–853.
- Denison, F.C., Hiscock, N.J., Carling, D., & Woods, A. (2009). Characterization of an Alternative Splice Variant of LKB1. *J. Biol. Chem.*, *284*(1), 67–76.
- Dittmer, T. a, & Misteli, T. (2011). The lamin protein family. *Genome Biol.*, *12*(5), 222.
- Dolinsky, V. W., Chan, A. Y. M., Robillard Frayne, I., Light, P. E., Des Rosiers, C., & Dyck, J. R. B. (2009). Resveratrol prevents the prohypertrophic effects of oxidative stress on LKB1. *Circulation*, *119*(12), 1643–1652.
- Drab, M., Verkade, P., Elger, M., Kasper, M., Lohn, M., Lauterbach, B., ... Kurzchalia, T. V. (2001). Loss of caveolae, vascular dysfunction, and pulmonary defects in caveolin-1 gene-disrupted mice. *Science*, *293*, 2449–2452.
- Engelman, J. A., Zhang, X., Galbiati, F., Volonte, D., Sotgia, F., Pestell, R. G., ... Lisanti, M. P. (1998). PROTEIN COMPLEXES ' 98 Molecular Genetics of the Caveolin Gene Family : Implications for Human Cancers , Diabetes , Alzheimer Disease , and Muscular Dystrophy. *Am. J. Hum.Genet.*, *63*, 1578–1587.
- Fabrini, R., Bocedi, A., Pallottini, V., Canuti, L., De Canio, M., Urbani, A., ... Ricci, G. (2010). Nuclear Shield: a multi-enzyme task-force for nucleus protection. *PLoS ONE.*, *5*, 1–11.
- Fairley, E.A., Kendrick-Jones, J., & Ellis, J. A. (1999). The Emery-Dreifuss muscular dystrophy phenotype arises from aberrant targeting and binding of emerin at the inner nuclear membrane. *J. Cell Sci.*, *112*, 2571–2582.
- Fang, P.-K., Solomon, K. R., Zhuang, L., Qi, M., McKee, M., Freeman, M. R., & Yelick, P. C. (2006). Caveolin-1 α and -1 β Perform Nonredundant Roles in Early Vertebrate Development. *Am. J. Pathol.*, *169*(6), 2209–2222.
- Fatkin, D., Otway, R., & Richmond, Z. (2010). Genetics of dilated cardiomyopathy. *Heart Failure Clinics*, *6*(2), 129–140.
- Favreau, C., Higuier, D., Courvalin, J.C., & Buendia, B. (2004). Expression of a mutant lamin A that causes Emery-Dreifuss muscular dystrophy inhibits in vitro differentiation of C2C12 myoblasts. *Mol. Cell Biol.*, *24*, 1481–1492.

- Fujimoto, T., Kogo, H., Nomura, R., & Une, T. (2000). Isoforms of caveolin-1 and caveolar structure. *J. Cell Sci.*, *113*, 3509–3517.
- Furukawa, K. & Hotta, Y. (1993). cDNA cloning of a germ cell specific lamin B3 from mouse spermatocytes and analysis of its function by ectopic expression in somatic cells. *EMBO J.*, *12*, 97–106.
- Furukawa, K., Inagaki, H. & Hotta, Y. (1994). Identification and cloning of an mRNA coding for a germ cell-specific A-type lamin in mice. *Exp. Cell Res.*, *212*, 426–430.
- Gan, R.-Y., & Li, H.-B. (2014). Recent progress on liver kinase B1 (LKB1): expression, regulation, downstream signaling and cancer suppressive function. *Int. J. Mol. Sci.*, *15*(9), 16698–16718.
- Gazzerro, E., Sotgia, F., Bruno, C., Lisanti, M. P., & Minetti, C. (2010). Caveolinopathies: from the biology of caveolin-3 to human diseases. *Eur. J. Hum. Genet.*, *18*(2), 137–145.
- Goldman, R.D., Gruenbaum, Y., Moir, R.D., Shumaker, D.K. & Spann, T. P. (2002). Nuclear lamins: Building blocks of nuclear architecture. *Genes Dev.*, *16*, 533–547.
- Gordon, L. B., Cao, K., & Collins, F. S. (2012). Progeria: translational insights from cell biology. *J. Cell Biol.*, *199*(1), 9–13.
- Grossman, E., Medalia, O., & Zwerger, M. (2012). Functional architecture of the nuclear pore complex. *Annu. Rev. Biophys.*, *41*, 557–584.
- Gruenbaum, Y., Margalit, A., Goldman, R. D., Shumaker, D. K., & Wilson, K. L. (2005). The nuclear lamina comes of age. *Nat. Rev. Mol. Cell Biol.*, *6*(1), 21–31.
- Gruenbaum, Y., Landesman, Y., Drees, B., Bare, J.W., Saumweber, H., & Paddy, M.R., ... Fisher, P. A. (1988). Drosophila nuclear lamin precursor Dm0 is translated from either of two developmentally regulated mRNA species apparently encoded by a single gene. *J. Cell Biol.*, *106*, 585–596.
- Guelen, L., Pagie, L., Brasset, E., Meuleman, W., Faza, M. B., Talhout, W., ... van Steensel, B. (2008). Domain organization of human chromosomes revealed by mapping of nuclear lamina interactions. *Nature*, *453*(7197), 948–951.
- Heessen, S., & Fornerod, M. (2007). The inner nuclear envelope as a transcription factor resting place. *EMBO Reports*, *8*(10), 914–9.
- Hnasko, R., & Lisanti, M. P. (2003). The Biology of Caveolae : Lessons from Caveolin Knockout Mice and Implications for Human Disease. *Mol. Interventions*, *3*(8), 445–464.

- Ho, C. Y., Jaalouk, D. E., Vartiainen, M. K., & Lammerding, J. (2013). Lamin A/C and emerin regulate MKL1-SRF activity by modulating actin dynamics. *Nature*, 497(7450), 507–511.
- Ho, C.Y., & Lammerding, J. (2012). Lamins at a glance. *J. Cell Sci.*, 125(9), 2087–2093.
- Holaska, J. M. (2008). Emerin and the nuclear lamina in muscle and cardiac disease. *Circ. Res.*, 103(1), 16–23.
- Holaska, J., Lee, K., Kowalski, A. & Wilson, K. (2003). Transcriptional repressor germ cell-less (GCL) and barrier-to-autointegration factor (BAF) compete for binding to emerin in vitro. *J. Biol. Chem.*, 278, 6969–6975.
- Hutchison, C. J. (2002). Lamins: building blocks or regulators of gene expression? *Nat. Rev. Mol. Cell Biol.*, 3(11), 848–858.
- Hutchison, C. J. (2011). The role of DNA damage in laminopathy progeroid syndromes. *Biochem. Soc. Trans.*, 39, 1715–1718.
- Hutchison, C. J., & Worman, H. J. (2004). A-type lamins : Guardians of the soma ? *Nat. Cell Biol.*, 6(11), 1062–1067.
- Ikeda, Y., Sato, K., Pimentel, D. R., Sam, F., Shaw, R. J., Dyck, J. R. B., & Walsh, K. (2009). Cardiac-specific deletion of LKB1 leads to hypertrophy and dysfunction. *J. Biol. Chem.*, 284(51), 35839–35849.
- Jaalouk, D. E., & Lammerding, J. (2009). Mechanotransduction gone awry. *Nat. Rev. Mol. Cell Biol.*, 10(1), 63–73.
- Jones, R.G., Plas, D.R., Kubek, S., Buzzai, M., Mu, J., Xu, Y., ... Thompson, C. B. (2005). AMP-Activated Protein Kinase Induces a p53-Dependent Metabolic Checkpoint. *Mol. Cell.*, 18, 283–293.
- Jung, H.J., Coffinier, C., Choe, Y., Beigneux, A.P., Davies, B.S., Yang, S.H., ... Fong, L. G. (2012). Regulation of prelamin A but not lamin C by miR-9, a brain-specific microRNA. *Proc. Natl. Acad. Sci. U.S.A.*, 109, E423–E431.
- Kim, Y., Sharov, A.A., McDole, K., Cheng, M., Hao, H., Fan, C.M., ... Zheng, Y. (2011). Mouse B-type lamins are required proper organogenesis but not by embryonic stem cells. *Science*, 334, 1706–1710.
- Kim, Y., Zheng, X. & Zheng, Y. (2013). Proliferation and differentiation of mouse embryonic stem cells lacking all lamins. *Cell Res.*, 23(12), 1420–1423.
- Kogo, H., Aiba, T., & Fujimoto, T. (2004). Cell Type-specific Occurrence of Caveolin-1 α and -1 β in the Lung Caused by Expression of Distinct mRNAs. *J. Biol. Chem.*, 279(24), 25574–25581.

- Korfali, N., Wilkie, G. S., Swanson, S. K., Srsen, V., Batrakou, D. G., Fairley, E. A. L., ... Schirmer, E. C. (2010). The leukocyte nuclear envelope proteome varies with cell activation and contains novel transmembrane proteins that affect genome architecture. *Molecular & Cellular Proteomics : MCP*, 9(12), 2571–2585.
- Lammerding, J., Fong, L. G., Ji, J. Y., Reue, K., Stewart, C. L., Young, S. G., & Lee, R. T. (2006). Lamins A and C but not lamin B1 regulate nuclear mechanics. *J. Biol. Chem.*, 281(35), 25768–25780.
- Lammerding, J., Schulze, P.C., Takahashi, T., Kozlov, S., Sullivan, T., Kamm, R.D., ... Lee, R. T. (2004). Lamin A/C deficiency causes defective nuclear mechanics and mechanotransduction. *J. Clin. Invest.*, 113, 370–378.
- Lander, H. M. (1997). An essential role for free radicals and derived species in signal transduction. *FASEB J.*, 11, 118–124.
- Lattanzi, G., Cenni, V., Marmioli, S., Capanni, C., Mattioli, E., Merlini, L., ... Mario Maraldi, N. (2003). Association of emerin with nuclear and cytoplasmic actin is regulated in differentiating myoblasts. *Biochem. Biophys. Res. Commun.*, 303(3), 764–770.
- Lee, K. K., Haraguchi, T., Lee, R. S., Koujin, T., Hiraoka, Y., & Wilson, K. L. (2001). Distinct functional domains in emerin bind lamin A and DNA-bridging protein BAF. *J. Cell Sci.*, 114, 4567–4573.
- Lee, J. & Schmid-Schonbein, G. W. (1995). Biomechanics of skeletal muscle capillaries: hemodynamic resistance, endothelial distensibility, and pseudopod formation. *Ann. Biomed. Eng.*, 23, 226–246.
- Li, W., Liu, P., Pilcher, B. K., & Anderson, R. G. W. (2001). Cell-specific targeting of caveolin-1 to caveolae, secretory vesicles, cytoplasm or mitochondria. *J. Cell Sci.*, 114, 1397–1408.
- Linke, K., & Jakob, U. (2003). Not every disulfide lasts for ever: disulfide bond formation as a redox switch. *Antioxid. Redox Signal.*, 5, 425–434.
- Liu, G.-H., Guan, T., Datta, K., Coppinger, J., Yates, J., & Gerace, L. (2009). Regulation of myoblast differentiation by the nuclear envelope protein NET39. *Mol. Cell. Biol.*, 29(21), 5800–5812.
- Liu, J., Rolef Ben-Shahar, T., Riemer, D., Treinin, M., Spann, P., Weber, K., ... Gruenbaum, Y. (2000). Essential roles for *Caenorhabditis elegans* lamin gene in nuclear organization, cell cycle progression, and spatial organization of nuclear pore complexes. *Mol. Biol. Cell*, 11(11), 3937–3947.
- Lloyd, D. J., Trembath, R. C., Shackleton, S., & Le, L. (2002). A novel interaction between lamin A and SREBP1: implications for partial lipodystrophy and other laminopathies. *Hum. Mol. Genet.*, 11(7), 769–778.

- Lloyd, D.J., Trembath, R.C., & Shackleton, S. (2002). A novel interaction between lamin A and SREBP1: implications for partial lipodystrophy and other laminopathies. *Hum. Mol. Genet.*, *11*, 769–777.
- Lombardi, M. L., & Lammerding, J. (2011). Keeping the LINC: the importance of nucleocytoskeletal coupling in intracellular force transmission and cellular function. *Biochem. Soc. Trans.*, *39*(6), 1729–34.
- Londesborough, A., Vaahtomeri, K., Tiainen, M., Katajisto, P., Ekman, N., Vallenius, T., & Makela, T. P. (2008). LKB1 in endothelial cells is required for angiogenesis and TGF- β -mediated vascular smooth muscle cell recruitment. *Development*, *135*(13), 2331–2338.
- Machiels, B.M., Zorenc, A.H., Endert, J.M., Kuijpers, H.J., Van Eys, G.J., Ramaekers, F.C. & Broers, J. L. (1996). An alternative splicing product of the lamin A/C gene lacks exon 10. *J. Biol. Chem.*, *271*, 9249–9253.
- Maraldi, N. M., Capanni, C., Cenni, V., Fini, M., & Lattanzi, G. (2011). Laminopathies and lamin-associated signaling pathways. *J. Cell. Biochem.*, *112*(4), 979–992.
- Marsh, M. & Helenius, A. (2006). Virus Entry: Open Sesame. *Cell*, *124*, 729–740.
- Mattout, A., Dechat, T., Adam, S.A., Goldman, R.D., Gruenbaum, Y. (2006). Nuclear lamins, diseases and aging. *Curr. Opin. Cell Biol.*, *18*(3), 335–341.
- Mazereeuw-Hautier, J., Wilson, L.C., Mohammed, S., Smallwood, D., Shackleton, S., Atherton, D.J. & Harper, J. I. (2007). Hutchinson-Gilford progeria syndrome: clinical findings in three patients carrying the G608G mutation in LMNA and review of the literature. *Br J Dermatol.*, *156*(6), 1308–1314.
- Meaburn, K. J., Cabuy, E., Bonne, G., Levy, N., Morris, G. E., Novelli, G., ... Bridger, J. M. (2007). Primary laminopathy fibroblasts display altered genome organization and apoptosis. *Aging Cell*, *6*(2), 139–153.
- Mehenni, H., Gehrig, C., Nezu, J., Oku, A., Shimane, M., Rossier, C., ... Antonarakis, S. E. (1998). Loss of LKB1 kinase activity in Peutz-Jeghers syndrome, and evidence for allelic and locus heterogeneity. *Am. J. Hum. Genet.*, *63*, 1641–1650.
- Melcon, G., Kozlov, S., Cutler, D. a, Sullivan, T., Hernandez, L., Zhao, P., ... Stewart, C. L. (2006). Loss of emerin at the nuclear envelope disrupts the Rb1/E2F and MyoD pathways during muscle regeneration. *Hum. Mol. Genet.*, *15*(4), 637–651.
- Meuleman, W., Peric-hupkes, D., Kind, J., Beaudry, J., Pagie, L., Kellis, M., ... Steensel, B. Van. (2013). Constitutive nuclear lamina – genome interactions are highly conserved and associated with A / T-rich sequence. *Genome Res.*, *23*, 270–280.

- Moir, R.D., Yoon, M., Khuon, S. & Goldman, R. D. (2000). Nuclear lamins A and B1: different pathways of assembly during nuclear envelope formation in living cells. *J. Cell Biol.*, *151*, 1155–1168.
- Monier, S., Dietzen, D.J., Hastings, W.R., Lublin, D.M. & Kurzchalia, T. V. (1996). Oligomerization of VIP21–caveolin in vitro is stabilized by long chain fatty acylation or cholesterol. *FEBS Lett.*, *388*, 143–149.
- Mounkes, L. C., Kozlov, S. V, Rottman, J. N., & Stewart, C. L. (2005). Expression of an LMNA-N195K variant of A-type lamins results in cardiac conduction defects and death in mice. *Hum. Mol. Genet.*, *14*(15), 2167–2180.
- Mounkes, L., Kozlov, S., Burke, B. & Stewart, C. L. (2003). The laminopathies: nuclear structure meets disease. *Curr. Opin. Genet. Dev.*, *13*(3), 223–230.
- Muchir, A., & Worman, H. J. (2004). The Nuclear Envelope and Human Disease. *Physiology (Bethesda)*, *19*(44), 309–314.
- Muchir, A., Bonne, G., van der Kooi, A.J., van Meegen, M., Baas, F., Bolhuis, P.A., ... Schwartz, K. (2000). Identification of mutations in the gene encoding lamins A/C in autosomal dominant limb girdle muscular dystrophy with atrioventricular conduction disturbances (LGMD1B). *Hum. Mol. Genet.*, *9*, 1453–1459.
- Noga, A. A., Soltys, C. L., Barr, A. J., Kovacic, S., Lopaschuk, G. D., & Dyck, J. R. (2007). Expression of an active LKB1 complex in cardiac myocytes results in decreased protein synthesis associated with phenylephrine-induced hypertrophy. *Am. J. Physiol. Heart Circ. Physiol.*, *292*, H1460–H1469.
- Novelli, G., Muchir, A., Sangiuolo, F., Helbling-leclerc, A., Apice, M. R. D., Massart, C., ... Merlini, L. (2002). Mandibuloacral Dysplasia Is Caused by a Mutation in LMNA -Encoding Lamin A/C. *Am. J. Hum. Genet.*, *71*, 426–431.
- Nowlan, N. C., Prendergast, P. J., & Murphy, P. (2008). Identification of mechanosensitive genes during embryonic bone formation. *PLoS Comput. Biol.*, *4*(12), e1000250.
- Ouchi, N., Shibata, R., & Walsh, K. (2005). AMP-activated protein kinase signaling stimulates VEGF expression and angiogenesis in skeletal muscle. *Circ. Res.*, *96*(8), 838–846.
- Padiath, Q.S., Saigoh, K., Schiffmann, R., Asahara, H., Yamada, T., Koeppen, A., ... Fu, Y. H. (2006). Lamin B1 duplications cause autosomal dominant leukodystrophy. *Nat. Genet.*, *38*, 1114–1123.
- Pajerowski, J.D., Dahl, K.N., Zhong, F.L., Sammak, P.J. & Discher, D. E. (2007). Physical plasticity of the nucleus in stem cell differentiation. *Proc. Natl. Acad. Sci. U.S.A.*, *104*, 15619–15624.

- Parton, R. G., & del Pozo, M. A. (2013). Caveolae as plasma membrane sensors, protectors and organizers. *Nat. Rev. Mol. Cell. Biol.*, *14*(2), 98–112.
- Parton, R. G., & Simons, K. (2007). The multiple faces of caveolae. *Nat. Rev. Mol. Cell. Biol.*, *8*(3), 185–194.
- Pederson, T. & Aebi, U. (2002). Actin in the nucleus: what form and what for? *J. Struct. Biol.*, *140*, 3–9.
- Pekovic, V., Gibbs-Seymour, I., Markiewicz, E., Alzoghaibi, F., Benham, A. M., Edwards, R., ... Hutchison, C. J. (2011). Conserved cysteine residues in the mammalian lamin A tail are essential for cellular responses to ROS generation. *Aging Cell*, *10*(6), 1067–1079.
- Pelkmans, L., Puntener, D., & Helenius, A. (2002). Local actin polymerization and dynamin recruitment in SV40-induced internalization of caveolae. *Science*, *296*, 535–539.
- Puckelwartz, M., & McNally, E. M. (2011). Emery-Dreifuss muscular dystrophy. *Handb. Clin. Neurol.*, *101*, 155–166.
- Razani, B., Wang, X.B., Engelman, J.A., Battista, M., Lagaud, G., Zhang, X.L., ... Lisanti, M. P. (2002). Caveolin-2-deficient mice show evidence of severe pulmonary dysfunction without disruption of caveolae. *Mol. Cell Biol.*, *22*, 2329–2344.
- Razani, B., Zhang, X. L., Bitzer, M., von Gersdorff, G., Böttinger, E.P., & Lisanti, M. P. (2001). Caveolin-1 regulates transforming growth factor (TGF)-beta/SMAD signaling through an interaction with the TGF-beta type I receptor. *J. Biol. Chem.*, *276*(9), 6727–6738.
- Roeber, R.-A., Weber, K. & Osborn, M. (1989). Differential timing of lamin A/C expression in the various organs of the mouse embryo and the young animal: a developmental study. *Development*, *105*, 365–378.
- Rowat, A. C., Jaalouk, D. E., Zwerger, M., Ung, W. L., Eydelnant, I. a, Olins, D. E., ... Lammerding, J. (2013). Nuclear envelope composition determines the ability of neutrophil-type cells to passage through micron-scale constrictions. *J. Biol. Chem.*, *288*(12), 8610–8618.
- Sapkota, G. P., Kieloch, A., Lizcano, J. M., Lain, S., Arthur, J. S., Williams, M. R., ... Alessi, D. R. (2001). Phosphorylation of the protein kinase mutated in Peutz-Jeghers cancer syndrome, LKB1/STK11, at Ser431 by p90(RSK) and cAMP-dependent protein kinase, but not its farnesylation at Cys(433), is essential for LKB1 to suppress cell vrowth. *J. Biol. Chem.*, *276*(22), 19469–19482.
- Sapkota, G.P., Deak, M., Kieloch, A., Morrice, N., Goodarzi, A.A., Smythe, C.,... Alessi, D. R. (2002). Ionizing radiation induces ataxia telangiectasia mutated

- kinase (ATM)-mediated phosphorylation of LKB1/STK11 at Thr-366. *Biochem. J.*, *368*, 507–516.
- Schirmer, E.C. & Foisner, R. (2007). Proteins that associate with lamins: Many faces, many functions. *Exp. Cell Res.*, *313*, 2167–2179.
- Sedding, D.G., Hermsen, J., Seay, U., Eickelberg, O., Kummer, W., Schwencke, C., ... Braun-Dullaeus, R. C. (2005). Caveolin-1 facilitates mechanosensitive protein kinase B (Akt) signaling in vitro and in vivo. *Circ. Res.*, *96*, 635–642.
- Shimi, T., & Goldman, R. D. (2014). Nuclear Lamins and Oxidative Stress in Cell Proliferation and Longevity. *Adv. Exp. Med. Biol.*, *773*, 415–430.
- Sieprath, T., Darwiche, R., & De Vos, W. H. (2012). Lamins as mediators of oxidative stress. *Biochem. Biophys. Res. Commun.*, *421*(4), 635–639.
- Sinha, B., Köster, D., Ruez, R., Gonnord, P., Bastiani, M., Abankwa, D., ... Nassoy, P. (2011). Cells respond to mechanical stress by rapid disassembly of caveolae. *Cell*, *144*(3), 402–413.
- Smart, E. J., Graf, G. A., Niven, M. A. M. C., Sessa, W. C., Engelman, J. A., Scherer, P. E., ... Lisanti, M. P. (1999). Caveolins, Liquid-Ordered Domains, and Signal Transduction. *Mol. Cell. Biol.*, *19*(11), 7289–7304.
- Smith, D.P., Spicer, J., Smith, A., Swift, S., & Ashworth, A. (1999). The mouse Peutz-Jeghers syndrome gene LKB1 encodes a nuclear protein kinase. *Hum. Mol. Genet.*, *8*, 1479–1485.
- Stahlhut, M., & Deurs, B. Van. (2000). Identification of Filamin as a Novel Ligand for Caveolin-1 : Evidence for the Organization of Caveolin-1 – associated Membrane Domains by the Actin Cytoskeleton. *Mol. Biol. Cell*, *11*, 325–337.
- Stewart, C. L., Roux, K. J., & Burke, B. (2007). Blurring the boundary: the nuclear envelope extends its reach. *Science*, *318*(5855), 1408–1412.
- Stewart, C. & Burke, B. (1987). Teratocarcinoma stem cells and early mouse embryos contain only a single major lamin polypeptide closely resembling lamin B. *Cell*, *51*, 383–392.
- Sullivan, T., Escalante-alcalde, D., Bhatt, H., Anver, M., Bhat, N., Nagashima, K., ... Burke, B. (1999). Loss of A-type Lamin Expression Compromises Nuclear Envelope Integrity Leading to Muscular Dystrophy. *J. Cell Biol.*, *147*(5), 913–919.
- Tesson, F., Saj, M., Uvaize, M.M., Nicolas, H., Płoski, R. & Bilińska, Z. (2014). Lamin A/C mutations in dilated cardiomyopathy. *Cardiol J.*, *21*(4), 331–342.

- Tiainen, M., Vaahtomeri, K., Ylikorkala, A., & Ma, T. P. (2002). Growth arrest by the LKB1 tumor suppressor :induction of p21WAF1/CIP1. *Hum. Mol. Genet.*, *11*(13), 1497–1504.
- Tiainen, M., Ylikorkala, A., & Mäkelä, T. M. (1999). Growth suppression by Lkb1 is mediated by a G1 cell cycle arrest. *Proc. Natl. Acad. Sci. U.S.A.*, *96*, 9248–9251.
- Vaahtomeri, K., & Mäkelä, T. P. (2011). Molecular mechanisms of tumor suppression by LKB1. *FEBS Letters*, *585*(7), 944–951.
- Van Berlo, J.H., de Voogt, W.G., van der Kooi, A.J., van Tintelen, J. P., & Bonne, G., Yaou, R.B., ... Pinto, Y. M. (2005). Meta-analysis of clinical characteristics of 299 carriers of LMNA gene mutations: do lamin A/C mutations portend a high risk of sudden death? *J. Mol. Med.*, *83*, 79–83.
- Verstraeten, V. L. R. M., Broers, J. L. V., Ramaekers, F. C. . . , & Van Steensel, M. A. M. (2007). The Nuclear Envelope , a Key Structure in Cellular Integrity and Gene Expression. *Curr. Med. Chem.*, *14*, 1231–1248.
- Volonte, D., Liu, Y., & Galbiati, F. (2005). The modulation of caveolin-1 expression controls satellite cell activation during muscle repair. *FASEB J.*, *19*(2), 237–239.
- Wagner, N. & Krohne, G. (2007). LEM-domain proteins: New insights into lamin-interacting proteins. *Int. Rev. Cytol.*, *261*, 1–46.
- Wang, W., Fan, J., Yang, X., Fürer-galban, S., Silanes, I. L. De, Kobbe, C. Von, ... Gorospe, M. (2002). AMP-Activated Kinase Regulates Cytoplasmic HuR. *Mol. Cell. Biol.*, *22*(10), 3425–3436.
- Williams, T. M., & Lisanti, M. P. (2004). Protein family review The caveolin proteins. *Genome Biol.*, *5*(3), 1–8.
- Worman, H. J., & Courvalin, J.-C. (2005). Nuclear envelope, nuclear lamina, and inherited disease. *Int. Rev. Cytol.*, *246*(05), 231–279.
- Worman, H. J., Fong, L. G., Muchir, A., & Young, S. G. (2009). Laminopathies and the long strange trip from basic cell biology to therapy. *J.Clin. Invest.*, *119*(7), 1825–1836.
- Xie, L., Frank, P. G., Lisanti, M. P., & Sowa, G. (2010). Endothelial cells isolated from caveolin-2 knockout mice display higher proliferation rate and cell cycle progression relative to their wild-type counterparts. *Am. J. Physiol.-Cell Physiol.*, *298*(3), C693–C701.
- Yang, S.H., Chang, S.Y., Yin, L., Tu, Y., Hu, Y., Yoshinaga, Y., ... Young, S. G. (2011). An absence of both lamin B1 and lamin B2 in keratinocytes has no effect on cell proliferation or the development of skin and hair. *Hum. Mol. Genet.*, *20*, 3537–3544.

- Ylikorkala, A., Rossi, D. J., Korsisaari, N., Luukko, K., Alitalo, K., Henkemeyer, M., & Ma, T. P. (2001). Vascular Abnormalities and Deregulation of VEGF in Lkb1 - Deficient Mice. *Science*, 293, 1323–1327.
- Yu, J., Bergaya, S., Murata, T., Alp, I. F., Bauer, M. P., Lin, M. I., ... Sessa, W. C. (2006). Direct evidence for the role of caveolin-1 and caveolae in mechanotransduction and remodeling of blood vessels. *J. Clin. Invest.*, 116(5), 1284–1291.
- Yuan, H.Y., Kuang, S.Y., Zheng, X., Ling, H.Y., Yang, Y.B., Yan, P.K., ... Liao, D. F. (2008). Curcumin inhibits cellular cholesterol accumulation by regulating SREBP-1/caveolin-1 signaling pathway in vascular smooth muscle cells. *Acta Pharmacol Sin.*, 29(5), 555–563.
- Zastrow, M.S., Vlcek, S. & Wilson, K. L. (2004). Proteins that bind A-type lamins: Integrating isolated clues. *J. Cell Sci.*, 117, 979–987.
- Zhang, W., Wang, Q., Wu, Y., Moriasi, C., Liu, Z., Dai, X., ... Zou, M.-H. (2014). Endothelial cell-specific liver kinase B1 deletion causes endothelial dysfunction and hypertension in mice in vivo. *Circulation*, 129(13), 1428–1439.
- Zhao, Y., Liu, Y., Stan, R., Fan, L., Gu, Y., Dalton, N., ... Chien, K. R. (2002). Defects in caveolin-1 cause dilated cardiomyopathy and pulmonary hypertension in knockout mice. *Proc. Natl. Acad. Sci. U.S.A.*, 99(17), 11375–11380.
- Zwergler, M., Jaalouk, D. E., Lombardi, M. L., Isermann, P., Mauermann, M., Dialynas, G., ... Lammerding, J. (2013). Myopathic lamin mutations impair nuclear stability in cells and tissue and disrupt nucleo-cytoskeletal coupling. *Hum. Mol. Genet.*, 22(12), 2335–2349.